

Orbital ordering phenomena in d - and f -electron systems

Takashi Hotta

Advanced Science Research Center, Japan Atomic Energy Agency
Tokai, Ibaraki 319-1195, Japan

E-mail: hotta.takashi@jaea.go.jp

Abstract. In recent decades, novel magnetism of d - and f -electron compounds has been discussed very intensively both in experimental and theoretical research fields of condensed matter physics. It has been recognized that those material groups are in the same category of strongly correlated electron systems, while the low-energy physics of d - and f -electron compounds has been separately investigated rather in different manners. One of common features of both d - and f -electron systems is certainly the existence of active orbital degree of freedom, but in f -electron materials, due to the strong spin-orbit interaction in rare-earth and actinide ions, the physics seems to be quite different from that of d -electron systems. In general, when the number of internal degrees of freedom and relevant interactions is increased, it is possible to obtain rich phase diagram including large varieties of magnetic phases by using several kinds of theoretical techniques. However, we should not be simply satisfied with the reproduction of rich phase diagram. It is believed that more essential point is to seek for a simple principle penetrating complicated phenomena in common with d - and f -electron materials, which opens the door to a new stage in orbital physics. In this sense, it is considered to be an important task of this article to explain common features of magnetism in d - and f -electron systems from a microscopic viewpoint, using a key concept of orbital ordering, in addition to the review of the complex phase diagram of each material group. As a typical d -electron complex material exhibiting orbital order, first we focus on perovskite manganites, in which remarkable colossal magnetoresistance effect has been intensively studied. The manganites provide us a good stage to understand that a simple mechanism works for the formation of complex spin, charge, and orbital ordering. We also explain intriguing striped charge ordering on the orbital-ordered background in nickelates and the effect of orbital ordering to resolve spin frustration in geometrically frustrated e_g electron systems. Note that orbital ordering phenomena are also found in t_{2g} electron systems. Here we review recent advances in the understanding of orbital ordering phenomenon in Ca_2RuO_4 . Next we discuss another spin-charge-orbital complex system such as f -electron compound. After the detailed explanation of the construction of microscopic models on the basis of a j - j coupling scheme, we introduce a d -electron-like scenario to understand novel magnetism in some actinide compounds with the HoCoGa_5 -type tetragonal crystal structure. Finally, we show that complicated multipole order can be understood from the spin-orbital model on the basis of the j - j coupling scheme. As a typical material with multipole order, we pick up NpO_2 which has been believed to exhibit peculiar octupole order. Throughout this review, it is emphasized that the same orbital physics works both in d - and f -electron complex materials in spite of the difference between d and f orbitals.

Contents

1	Introduction	3
2	Model Hamiltonian for d-electron systems	8
2.1	Crystalline electric field effect	8
2.2	Coulomb interactions	13
2.3	Electron-phonon interactions	19
2.4	Electron hopping	22
2.5	Intersite interaction term	24
2.6	Summary	25
3	Orbital physics in manganites	25
3.1	Concept of double-exchange	26
3.2	Topological aspects of orbital ordering	28
3.2.1	A simplified model	28
3.2.2	Band-insulating state	29
3.2.3	Topological number	33
3.2.4	Stability of zigzag structure	37
3.2.5	Summary	38
3.3	Spin, charge, and orbital ordering	39
3.3.1	Effect of Coulomb interaction	39
3.3.2	$x=0$	41
3.3.3	$x=0.5$	45
3.3.4	$x>0.5$	49
3.3.5	$x<0.5$	52
3.4	Summary	55
4	Orbital physics in other d-electron materials	55
4.1	e_g electron systems	55
4.2	t_{2g} electron systems	62
4.3	Geometrically frustrated systems	65
5	Model Hamiltonian for f-electron systems	69
5.1	LS vs. j - j coupling schemes	70
5.2	Local f -electron state	71
5.3	Local f -electron term in the j - j coupling scheme	77
5.4	Level scheme in the j - j coupling scheme	81
5.5	Model Hamiltonian	85
5.6	Γ_8 model	87

<i>Orbital ordering phenomena in d- and f-electron systems</i>	3
6 Orbital physics in f-electron systems	89
6.1 Spin and orbital structure of actinide compounds	89
6.1.1 U-115	93
6.1.2 Np-115	95
6.2 Multipole ordering	98
7 Conclusions	103

1. Introduction

It has been widely recognized that orbital degree of freedom plays a key role in understanding of novel magnetism observed in transition metal oxides [1, 2, 3, 4]. A typical material of such spin-charge-orbital complex is the manganese oxide, exhibiting remarkable colossal magneto-resistance (CMR) phenomena [5]. In the recent decade, the study of manganites has been one of the most important areas of research in condensed matter physics. In one word, the CMR effect is considered to occur when the manganite ground-state changes from insulating to ferromagnetic (FM) metallic, after a small magnetic field is applied. Based on the concept of two-phase competition, the CMR behavior has been successfully qualitatively reproduced in computational simulations, for instance, employing resistor-network models [6]. In the two phases, the appearance of the FM metallic phase in manganites has been usually rationalized by the so-called double-exchange (DE) mechanism [7], based on a strong Hund’s rule coupling between mobile e_g electrons and localized t_{2g} spins. On the other hand, the insulating phase in manganites is basically understood by the coupling between degenerate e_g electrons and Jahn-Teller (JT) distortions of the MnO_6 octahedra [3, 4], leading to the various types of charge and/or orbital orders observed experimentally.

The rich phase diagram of manganites has been revealed due to competition and interplay among spin, charge, and orbital degrees of freedom, but a recent trend is to unveil further new phases both from experimental and theoretical investigations. A typical example can be found in the undoped perovskite manganite, RMnO_3 with rare earth ion R, which is the mother compound of CMR manganites. For $\text{R}=\text{La}$, it has been understood clearly that the A-type antiferromagnetic (AF) phase appears [8, 9] with the C-type ordering of $(3x^2-r^2)$ - and $(3y^2-r^2)$ -orbitals [10]. Here “A-type” denotes a layered antiferro structure with ferro-order in the ab plane and antiferro-order along the c axis, while “C-type” indicates a chain-type antiferro structure with antiferro-order in the ab plane and ferro-order along the c axis [8]. See Fig. 8(a) for each structure. Theoretically, the A-type ordering has been explained by using several kinds of techniques [11, 12, 13, 14, 15, 16, 17, 18, 19, 20, 21, 22, 23, 24, 25, 26, 27]. By substituting La by alkaline earth ions such as Sr and Ca, holes are effectively doped into e_g -electron band and due to the DE mechanism, the FM metallic phase appears with its concomitant CMR effect. Most of the discussion in manganites has centered on the many phases induced by doping with holes the A-type AF state, at different values of

their bandwidths. In this framework, it is implicitly assumed that the undoped material is always in the A-type AF state.

However, recently, a new AF phase has been reported as the ground state in the undoped limit for R=Ho [28, 29]. This phase is called the “E-type” spin structure following the standard notation in this context [8]. See Fig. 9(b) for the E-type spin structure. It is surprising that a new phase can be still found even in the undoped material, previously considered to be well understood. In addition, the nature of the states obtained by lightly doping this E-phase is totally unknown, and new phenomena may be unveiled experimentally in the near future. This is believed to open an exciting new branch of investigations in manganites [30, 31], since novel phases appear to be hidden in the vast parameter space of these compounds. A clear example has been recently provided by the prediction of a FM charge-ordered (CO) phase at $x=1/2$ [32, 33], which may have been found experimentally [34, 35]. These facts indicate the importance of both experimental and theoretical efforts to unveil new phases in manganites, in addition to the explanation of the complex phases already observed. Such efforts have also been made to find new phases in other transition metal oxides, for instance, ruthenates and nickelates, as we will see later in this article. Concerning RMnO₃ with hexagonal structure, quite recently, “multiferroics” has been another keyword to understand exotic magnetic phenomena emerging from the multi-phase competition [36]. We believe that it is useful to review the nature of spin, charge, and orbital ordered phases of manganites and other transition metal oxides from a unified viewpoint, even though it is true that more work remains to be done to fully understand transition metal oxides, in particular, unusual magneto-transport properties of manganese oxides and appearance of unconventional superconductivity.

A trend to seek for new magnetic as well as superconducting phases has been also found in the *f*-electron system, which is another type of spin-charge-orbital complex [37, 38]. Among so many kinds of *f*-electron materials, in recent years, *f*-electron compounds with HoCoGa₅-type tetragonal crystal structure, frequently referred to as “115”, have been intensively investigated both in experimental and theoretical research fields of condensed matter physics. Such vigorous activities are certainly motivated by “high” temperature superconductivity observed in some 115 compounds. First, unconventional superconductivity has been found in Ce-based 115 compounds, CeTIn₅ (T=Rh, Ir, and Co). A surprising point is that CeCoIn₅ exhibits the superconducting transition temperature $T_c=2.3\text{K}$ [39], which was the highest among yet observed for heavy fermion materials at ambient pressure when it was discovered. On the other hand, CeIrIn₅ shows $T_c=0.4\text{K}$ [40] which is much less than that of CeCoIn₅. Note that CeRhIn₅ is antiferromagnet with a Néel temperature $T_N=3.8\text{K}$ at ambient pressure, while under high pressure, it becomes superconducting with $T_c=2.1\text{K}$ [41].

After the discovery of superconductivity in Ce-115, the rapid expansion of the research frontier to transuranium systems has been accelerated by the discovery of superconductivity of Pu-based 115 compounds, PuTGa₅ (T=Co and Rh). It has been reported that T_c of PuCoGa₅ is 18.5K [42, 43], which is amazingly high value even

compared with other well-known intermetallic compounds. The coefficient of electronic specific heat γ is estimated as $\gamma=77\text{mJ/mol}\cdot\text{K}^2$, moderately enhanced relative to that for normal metals, suggesting that PuCoGa_5 should be heavy-fermion superconductor. In PuRhGa_5 , superconductivity has been also found [44]. Although the value of $T_c=8.7\text{K}$ is lower than that of PuCoGa_5 , it is still high enough compared with other heavy-fermion superconductors. Quite recently, high quality single crystal PuRhGa_5 has been synthesized [45] and the Ga-NQR measurement has revealed that *d*-wave superconductivity is realized in PuRhGa_5 [46]. The Ga-NMR measurement of PuCoGa_5 is consistent with this conclusion [47]. PuIrGa_5 has been also synthesized, but it is considered to be paramagnetic at ambient pressure. At least up to now, there is no indication of superconductivity even under the pressure of 9.5GPa down to 1.4K [48].

Besides such high temperature superconductivity of Ce-115 and Pu-115 compounds, interesting magnetic properties have been reported for UTGa_5 , where T is a transition metal ion. For several transition metal ions T, UTGa_5 are AF metals or Pauli paramagnets [49, 50, 51, 52, 53, 54, 55, 56, 57, 58, 59, 60]. Among them, neutron scattering experiments have revealed that UNiGa_5 exhibits the G-type AF phase, while UPdGa_5 and UPtGa_5 have the A-type AF state [56, 60]. See Fig. 33 for the magnetic structure. Note that G-type indicates a three-dimensional Néel state [8]. On the other hand, for UTGa_5 with T=Co, Rh, Ir, Fe, Ru, and Os, magnetic susceptibility is almost independent of temperature, since these are Pauli paramagnets. It is quite interesting that the magnetic structure is different for U-115 compounds which differ only by the substitution of transition metal ions.

Recently, Np-115 compounds NpTGa_5 (T=Fe, Co, Rh, and Ni) have been also synthesized and several kinds of physical quantities have been successfully measured [61, 62, 63, 64, 65, 66, 67, 68, 69, 70]. In particular, the de Haas-van Alphen (dHvA) effect has been observed in NpNiGa_5 [62], which is the first observation of dHvA signal in transuranium compounds. Quite recently, dHvA measurement has been also successfully performed in plutonium compound PuIn_3 over beyond several kinds of difficulties [71]. For NpCoGa_5 and NpRhGa_5 , the dHvA oscillations have been also detected and plural number of cylindrical Fermi surfaces are found [64, 65]. For NpFeGa_5 , the magnetic moment at Fe site has been suggested in neutron scattering experiments [66] and it has been also detected by ^{57}Fe Mössbauer spectroscopy [68]. The magnetic structure of Np-115 compounds also depends sensitively on transition metal ion [66, 69, 70]: G-AF for NpNiGa_5 , A-AF for NpCoGa_5 and NpRhGa_5 , and C-AF for NpFeGa_5 . See Fig. 33 for the magnetic structure. Note also that in the neutron scattering experiment for NpNiGa_5 , the signal suggesting the G-AF grows, after the FM transition occurs [66]. This G-AF structure is due to canted magnetic moments of Np ions. It is characteristic of U-115 and Np-115 compounds that the magnetic properties are sensitive to the choice of transition metal ions.

The appearance of several kinds of AF states in U-115 and Np-115 compounds reminds us of the magnetic phase diagram of CMR manganites. Thus, we envisage a scenario to understand the complex magnetic structure of actinide compounds based on

an orbital degenerate model similar to that of manganites. However, one must pay due attention to the meanings of “spin” and “orbital” in *f*-electron systems. Since they are tightly coupled with each other through a strong spin-orbit interaction, distinguishing them is not straightforward in comparison with *d*-electron systems. This point can create serious problems when we attempt to understand microscopic aspects of magnetism and superconductivity in *f*-electron compounds. Thus, it is necessary to carefully define the terms “orbital” and “spin” for *f* electrons in a microscopic discussion of magnetism and superconductivity in *f*-electron compounds.

From a conceptual viewpoint, in general, *f* electrons are more localized in comparison with *d* electrons, but when we turn our attention from $4f$ to $5f$, electronic properties are changed gradually from localized to itinerant nature, leading to rich phenomena which have been recently investigated intensively. In this sense, it has been also highly requested to push forward the microscopic research on *f* electron systems. However, in sharp contrast to *d* electron systems, the existence of strong spin-orbit coupling has been a problem to develop a theoretical study in the same level as *d*-electron research.

In order to overcome such problems, it has been recently proposed to employ a *j-j* coupling scheme to discuss microscopic aspects of magnetism and superconductivity of *f*-electron systems [72, 73], on the basis of the relativistic band-structure calculation results [74, 75, 76, 77, 78, 79, 80, 81]. There are a couple of advantages of the *j-j* coupling scheme. First, it is quite convenient for the inclusion of many-body effects using standard quantum-field theoretical techniques, since individual *f*-electron states are clearly defined. In contrast, in the *LS* coupling scheme we cannot use such standard techniques, since Wick’s theorem does not hold. Second we can, in principle, include the effects of valence fluctuations. In some uranium compounds, the valence of the uranium ion is neither definitely U^{3+} nor U^{4+} , indicating that the *f*-electron number takes a value between 2 and 3. In the *j-j* coupling scheme this is simply regarded as the average number of *f* electron per uranium ion.

As we will discuss later in detail, with the use of the *j-j* coupling scheme, it is possible to establish the microscopic Hamiltonian for *f*-electron systems. In particular, under crystalline electric field of cubic symmetry, the *f*-electron model on the basis of the *j-j* coupling scheme can be reduced to the orbital degenerate model, which is equivalent to the e_g electron Hubbard model [72]. The common microscopic model for *d*- and *f*-electron compounds is a simple explanation for the appearance of magnetic structure in common with manganites and actinide 115 compounds, as actually analyzed by using numerical calculations [82, 83]. In order to understand unconventional superconductivity of Ce-115 and Pu-115 materials, the orbital degenerate model has been also analyzed with the use of a fluctuation-exchange approximation to include effectively spin and orbital fluctuations [84, 85, 86]. A possible scenario for odd-parity triplet superconductivity induced by the Hund’s rule interaction has been discussed based on the orbital degenerate model on the non-Bravais lattice such as honeycomb lattice [87, 88]. Novel magnetism and exotic superconductivity of filled skutterudite

materials [89, 90] have been discussed by using the microscopic model on the basis of the j - j coupling scheme [91, 92, 93, 94]. We would like to emphasize that the same orbital physics should work between d - and f -electron systems, after the application of the j - j coupling scheme to f -electron materials. This is an important clue to establish the unified picture, which penetrates complex phenomena both in d - and f -electron compounds.

Another advantage of the model on the basis of the j - j coupling is that it is possible to develop a microscopic theory for multipole ordering of f -electron materials. Recently, ordering of high-order multipole such as octupole has been intensively discussed for $\text{Ce}_x\text{La}_{1-x}\text{B}_6$ [95, 96, 97, 98, 99, 100, 101, 102, 103, 104] and for NpO_2 [105, 106, 107, 108, 109, 110, 111, 112, 113] to reconcile experimental observations which seem to contradict one another at first glance. Very recently, a possibility of octupole ordering has been also proposed for $\text{SmRu}_4\text{P}_{12}$ [114, 115]. Here we note that spin and orbital degrees of freedom correspond to dipole and quadrupole moment, respectively. The microscopic aspects of octupole ordering has not been discussed satisfactorily in the context of electronic models. Rather, phenomenological theories have been developed under the assumption that octupole ordering occurs. Note that direct detection of octupole ordering is very difficult, since the octupole moment directly couples to neither a magnetic field nor lattice distortions. However, those phenomenological theories have successfully explained several experimental facts consistently, e.g., induced quadrupole moments in octupole ordered states in $\text{Ce}_x\text{La}_{1-x}\text{B}_6$ [96, 100, 101] and NpO_2 [107, 110]. On the other hand, it has been highly required to proceed to microscopic theory, in order to understand the origin of multipole ordering in f -electron systems over beyond the phenomenological level.

Concerning this issue, recently, it has been clearly shown that the model based on the j - j coupling scheme also works for the explanation of octupole ordering [113, 116, 117, 118, 119]. It is possible to obtain the multipole interaction from the f -electron model, by applying the same procedure to derive the orbital-dependent superexchange interaction in d -electron systems. Namely, we can provide the microscopic basis for multipole interaction. It is also possible to show the stability of octupole ordered phase depending on the lattice structure. In this scenario, octupole is the combined degree of freedom of spin and orbital. In another word, octupole is considered to be characterized by the anisotropic spin densities. Thus, the difference in anisotropic up- and down-spin densities naturally provide the magnetic moment of octupole. It is one of progresses in orbital physics that higher-order multipole can be also understood in the context of spin and orbital ordering phenomena.

In this article, in Sec. 2, we review the construction of the microscopic models for d -electron systems in detail. Then, we arrive at three kinds of Hamiltonians, depending on the active orbitals, which are (i) e_g -electron doubly degenerate model, (ii) t_{2g} -electron triply degenerate model, and (iii) e_g -orbital double-exchange model coupled with t_{2g} localized spins. In Sec. 3, in order to explain the orbital ordering in manganites, we focus on the theoretical results on the model (iii). In particular, the topological aspects

of orbital ordering will be discussed in detail. Then, we explain characteristic features of orbital ordering depending on hole doping x in subsections for $x=0.0$, $x=0.5$, $x>0.5$, and $x<0.5$. In Sec. 4, we discuss the results of models (i) and (ii), by introducing nickelates and ruthenates as typical materials, respectively. In Sec. 5, we will move on to the model construction for *f*-electron materials with the use of the *j-j* coupling scheme. We will explain the spirit of the *j-j* coupling scheme in detail, in comparison with the *LS* coupling scheme. Then, we establish the orbital degenerate model for *f*-electron systems. In Sec. 6, we will show theoretical results on the microscopic model for *f*-electron systems. We will explain possible orbital ordering of 115 compounds and octupole ordering of NpO_2 from a microscopic viewpoint. Finally, in Sec. 7, we will summarize this article.

2. Model Hamiltonian for *d*-electron systems

Before proceeding to the description of theoretical results on orbital ordering phenomena in *d*-electron compounds, first it is necessary to define the model Hamiltonian for *d*-electron systems. The model should be composed of three parts as

$$H = H_{\text{kin}} + H_{\text{loc}} + H_{\text{inter-site}}, \quad (1)$$

where H_{kin} expresses the kinetic term of *d* electrons, H_{loc} denotes the local term for *d* electrons, and $H_{\text{inter-site}}$ indicates the inter-site interaction among *d* electrons, which is not fully included by the combination of H_{kin} and H_{loc} . Among them, the local term H_{loc} includes three important ingredients, written as

$$H_{\text{loc}} = H_{\text{CEF}} + H_{\text{el-el}} + H_{\text{el-ph}}, \quad (2)$$

where H_{CEF} is the crystalline electric field (CEF) term, $H_{\text{el-el}}$ denotes the Coulomb interactions among *d* electrons, and $H_{\text{el-ph}}$ indicates the coupling term between *d* electrons and lattice distortions. The full Hamiltonian includes several competing tendencies and couplings, but as shown below, the essential physics can be obtained using relatively simple models, deduced from the complicated full Hamiltonian.

2.1. Crystalline electric field effect

In order to construct the model Hamiltonian for *d*-electron systems, let us start our discussion at the level of the atomic problem, in which just one electron occupies a certain orbital in the $3d$ shell of a transition metal ion. In the next subsection, we will include the effect of Coulomb interactions among *d* electrons. For an isolated ion, a five-fold degeneracy exists for the occupation of the $3d$ orbitals, but this degeneracy is partially lifted by the CEF potential from anions surrounding the transition metal ion. Since it is the electrostatic potential field acting on one electron state even in the complicated crystal structure, the CEF potential should be, in any case, given in the second-quantized form as

$$H_{\text{CEF}} = \sum_{\mathbf{i}, \sigma, m, m'} A_{m, m'} d_{\mathbf{i}m\sigma}^\dagger d_{\mathbf{i}m'\sigma}, \quad (3)$$

where $d_{i m \sigma}$ is the annihilation operator for a d -electron with spin σ in the m -orbital at site \mathbf{i} , $m(=-2, \dots, 2)$ is the z -component of angular momentum $\ell(=2)$, and $A_{m,m'}$ is the coefficient of the CEF potential, depending on the crystal structure and the angular momentum.

The explicit form of $A_{m,m'}$ has been analyzed in detail by the ligand field theory. Here we briefly explain the derivation of $A_{m,m'}$ by following the procedure of Hutchings [120, 121]. The CEF potential is given by the sum of electro-static potential from anions surrounding the transition metal ion, written by

$$V_{\text{CEF}}(\mathbf{r}) = \sum_i \frac{Ze^2}{|\mathbf{R}_i - \mathbf{r}|}, \quad (4)$$

where Z is the valence of anion, e is elementary electric charge, \mathbf{R}_i denotes the position of i -th anion, and \mathbf{r} indicates the position of $3d$ electron around the nucleus of transition metal ion. Then, the CEF coefficient is evaluated by

$$A_{m,m'} = \int d\mathbf{r} \Psi_{nlm}^*(\mathbf{r}) V_{\text{CEF}}(\mathbf{r}) \Psi_{nlm'}(\mathbf{r}), \quad (5)$$

where $\Psi_{nlm}(\mathbf{r})$ is the wavefunction of d electron, expressed as

$$\Psi_{nlm}(\mathbf{r}) = R_{n\ell}(r) Y_{\ell m}(\theta, \varphi), \quad (6)$$

with $\mathbf{r}=(r, \theta, \varphi)$ in the polar coordinate. Here $R_{n\ell}(r)$ is the radial wavefunction and $Y_{\ell m}$ is the spherical harmonics, which are obtained by solving the Schrödinger equation for the hydrogen-like potential problem. Note that n denotes the principal quantum number. In the actual situation, $|\mathbf{r}|$ is in the order of Bohr radius, while $|\mathbf{R}_i|$ is related to the lattice constant which is in the order of several angstroms. Thus, it is convenient to expand V_{CEF} in terms of $|\mathbf{r}|/|\mathbf{R}_i|$ as

$$V_{\text{CEF}}(\mathbf{r}) = \sum_i \frac{Ze^2}{R_i} \sum_{k=0}^{\infty} \sum_{m=-k}^k \frac{4\pi}{2k+1} \left(\frac{r}{R_i}\right)^k Y_{km}(\theta, \varphi) Y_{km}^*(\theta_i, \varphi_i), \quad (7)$$

where $\mathbf{R}_i=(R_i, \theta_i, \varphi_i)$ in the polar coordinate.

For further calculations, it is necessary to set the actual crystal structure. As a typical example, in this review article, we pick up the perovskite structure composed of MO_6 octahedron, in which transition metal ion M is surrounded by six oxygen ions, as shown in Fig. 1. To make the situation general, we set the different values, a and b , for the size of octahedron in the xy plane and along the z axis, respectively. The positions of oxygen ions are, then, given by $\mathbf{R}_1=(a/2, 0, 0)$, $\mathbf{R}_2=(0, -a/2, 0)$, $\mathbf{R}_3=(-a/2, 0, 0)$, $\mathbf{R}_4=(0, a/2, 0)$, $\mathbf{R}_5=(0, 0, b/2)$, and $\mathbf{R}_6=(0, 0, -b/2)$. For the case of $a = b$, the cubic symmetry is maintained, while for the case of $a \neq b$, the system is in the tetragonal symmetry. After some algebraic calculations using the explicit form of the wavefunction for d electrons, a general form for $A_{m,m'}$ is given by

$$\begin{aligned} A_{m,m'} = & -\frac{\langle r^2 \rangle}{a^2} \frac{2Ze^2}{a} \left[1 - \left(\frac{a}{b}\right)^3 \right] c^{(2)}(2m, 2m') \delta_{m,m'} \\ & + \frac{\langle r^4 \rangle}{a^4} \frac{2Ze^2}{a} \left[\frac{3}{4} + \left(\frac{a}{b}\right)^5 \right] c^{(4)}(2m, 2m') \delta_{m,m'} \end{aligned}$$

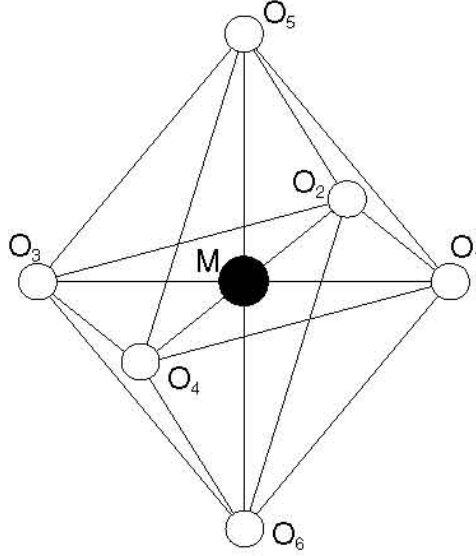


Figure 1. MO_6 octahedron at site i . The position of the i -th oxygen ion labeled by O_i is \mathbf{R}_i . The size of the octahedron is specified by a and b , which are given by $a=|\mathbf{R}_1 - \mathbf{R}_3|=|\mathbf{R}_2 - \mathbf{R}_4|$ and $b=|\mathbf{R}_5 - \mathbf{R}_6|$, respectively. See the maintext for the definitions of \mathbf{R}_i .

$$+ \frac{\langle r^4 \rangle}{a^4} \frac{Ze^2}{a} \sqrt{\frac{35}{8}} c^{(4)}(2m, 2m') \delta_{m-m', \pm 4}, \quad (8)$$

where $\delta_{m,m'}$ is the Kronecker's delta, $\langle r^k \rangle$ is given by

$$\langle r^k \rangle = \int_0^\infty r^k |R_{3d}(r)|^2 r^2 dr, \quad (9)$$

and $c^{(k)}(\ell m, \ell' m')$ is the so-called Gaunt coefficient [122, 123], defined by

$$c^{(k)}(\ell m, \ell' m') = \sqrt{\frac{4\pi}{2k+1}} \int \sin \theta d\theta d\varphi Y_{\ell m}^*(\theta, \varphi) Y_{k m-m'}(\theta, \varphi) Y_{\ell' m'}(\theta, \varphi). \quad (10)$$

The non-zero values for the Gaunt coefficients have been tabulated in the standard textbook [124]. By consulting with the table for the Gaunt coefficient, we explicitly obtain $A_{m,m'}$ as

$$\begin{aligned} A_{2,2} &= A_{-2,-2} = 2A_{20} + A_{40}, \\ A_{1,1} &= A_{-1,-1} = -A_{20} - 4A_{40}, \\ A_{0,0} &= -2A_{20} + 6A_{40}, \\ A_{2,-2} &= A_{-2,2} = A_{44}, \end{aligned} \quad (11)$$

where

$$\begin{aligned} A_{20} &= \frac{2}{7} \frac{Ze^2}{a} \frac{\langle r^2 \rangle}{a^2} \left[1 - \left(\frac{a}{b} \right)^3 \right], \\ A_{40} &= \frac{1}{6} \frac{Ze^2}{a} \frac{\langle r^4 \rangle}{a^4} \left[\frac{3}{7} + \frac{4}{7} \left(\frac{a}{b} \right)^5 \right], \\ A_{44} &= \frac{5}{6} \frac{Ze^2}{a} \frac{\langle r^4 \rangle}{a^4}. \end{aligned} \quad (12)$$

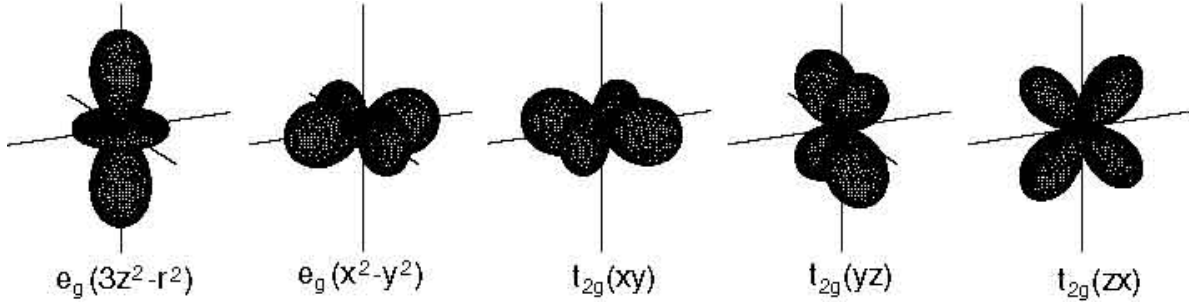


Figure 2. Views for *d*-electron orbitals.

Note that $A_{20}=0$ and $A_{44}=5A_{40}$ for the cubic case ($a=b$).

For instructive purpose, here we have shown a part of tedious calculations to determine CEF potential, but for actual purpose, it is more convenient to consult with the table of Hutchings, in which all possible CEF parameters have been listed for arbitrary angular momentum J (both integer and half-integer). For the *d*-electron case, we can simply refer the results for $J=2$ in the Hutchings table [120]. For instance, in the tetragonal CEF as discussed above, we easily obtain

$$\begin{aligned}
 A_{2,2} &= A_{-2,-2} = 6B_2^0 + 12B_4^0, \\
 A_{1,1} &= A_{-1,-1} = -3B_2^0 - 48B_4^0, \\
 A_{0,0} &= -6B_2^0 + 72B_4^0, \\
 A_{2,-2} &= A_{-2,2} = 12B_4^4,
 \end{aligned} \tag{13}$$

where B_n^m with integers n and m is the so-called CEF parameter, traditionally used in the ligand field theory. It is easy to express the CEF parameters B_n^m by using ours as $B_2^0 = A_{20}/3$, $B_4^0 = A_{40}/12$, and $B_4^4 = A_{44}/12$. Note again that $B_2^0=0$ and $B_4^4=5B_4^0$ for the cubic case. In actuality, we do not estimate the CEF parameters purely theoretically, but they are determined from the fitting of experimental results such as magnetic susceptibility and specific heat at high temperatures.

For a cubic case ($a=b$), the five-fold degeneracy in *d* orbital is lifted into doubly-degenerate e_g -orbitals ($d_{x^2-y^2}$ and $d_{3z^2-r^2}$) and triply-degenerate t_{2g} -orbitals (d_{xy} , d_{yz} , and d_{zx}). The shape of each orbital is illustrated in Fig. 2. The eigenenergy for e_g -orbitals is given by

$$\varepsilon_{3z^2-r^2} = \varepsilon_{x^2-y^2} = 6A_{40} = 72B_4^0 = \frac{Ze^2 \langle r^4 \rangle}{a a^4}, \tag{14}$$

while for t_{2g} orbitals, we obtain

$$\varepsilon_{xy} = \varepsilon_{yz} = \varepsilon_{zx} = -4A_{40} = -48B_4^0 = -\frac{2}{3} \frac{Ze^2 \langle r^4 \rangle}{a a^4}. \tag{15}$$

Then, the CEF term can be written as

$$H_{\text{CEF}} = \sum_{\mathbf{i}, \sigma, \gamma} \varepsilon_{\gamma} d_{\mathbf{i}\gamma\sigma}^{\dagger} d_{\mathbf{i}\gamma\sigma}, \tag{16}$$

where $d_{i\gamma\sigma}$ is the annihilation operator for a *d*-electron with spin σ in the γ -orbital at site i . The energy difference between those two levels is usually expressed as $10Dq$ in the traditional notation in the ligand field theory. It is explicitly written as

$$10Dq = 10A_{40} = 120B_4^0 = \frac{5}{3} \frac{Ze^2}{a} \frac{\langle r^4 \rangle}{a^4}. \quad (17)$$

Let us try to estimate theoretically the value of $10Dq$. For the purpose, it is convenient to transform the above equation into

$$10Dq = \frac{10Z}{3} \frac{e^2}{2a_B} \left(\frac{a_B}{a}\right)^5 \frac{\langle r^4 \rangle}{a_B^4}, \quad (18)$$

where a_B denotes the Bohr radius ($a_B=0.529\text{\AA}$). Note that $Z=2$ for O^{2-} ion and $e^2/(2a_B)=1$ Ryd.=13.6 eV. By using the solution of the hydrogen-like potential problem, we obtain $\langle r^4 \rangle/a_B^4=25515/Z_M^4$, where Z_M denotes the atomic number of transition metal atom. For instance, if we simply set $Z_M=25$ for manganese and $a=2\text{\AA}$ as a typical value for perovskite structure, we obtain $10Dq=7.7\text{meV}$, which is very small compared with the observed value, since $10Dq$ is found to be in the order of eV in actual transition metal oxides. In fact, the estimation by Yoshida suggests that $10Dq$ is about $10000\text{-}15000\text{cm}^{-1}$ (remember that $1\text{ eV} = 8063\text{ cm}^{-1}$) [125]. The electrostatic contribution obtained in the above naive estimation is considered to be much smaller than the observed CEF splitting.

Here note that the energy level for the t_{2g} -orbitals is lower than that for e_g -orbitals for perovskite structure. Qualitatively this can be intuitively understood as follows: The energy difference originates in the Coulomb interaction between the $3d$ electrons and the oxygen ions surrounding transition metal ion. As shown in Fig. 2, while the wave-functions of the e_g -orbitals are extended along the direction of the bond between transition metal ion and oxygen ions, those in the t_{2g} -orbitals avoid this direction. Thus, an electron in t_{2g} -orbitals is not heavily influenced by the Coulomb repulsion due to the negatively charged oxygen ions, and the energy level for t_{2g} -orbitals is lower than that for e_g -orbitals.

For a tetragonal case with $a < b$, as observed in cuprates, we find the splitting of each degenerate orbital. The e_g orbital is split into a_{1g} ($3z^2 - r^2$) and b_{1g} ($x^2 - y^2$) orbitals, of which eigen energies are, respectively, given by

$$\varepsilon_{3z^2-r^2} = 6\tilde{D}q - \frac{4}{7} \frac{Ze^2}{a} \frac{\langle r^2 \rangle}{a^2} \left[1 - \left(\frac{a}{b}\right)^3\right] - \frac{5}{21} \frac{Ze^2}{a} \frac{\langle r^4 \rangle}{a^4} \left[1 - \left(\frac{a}{b}\right)^5\right], \quad (19)$$

and

$$\varepsilon_{x^2-y^2} = 6\tilde{D}q + \frac{4}{7} \frac{Ze^2}{a} \frac{\langle r^2 \rangle}{a^2} \left[1 - \left(\frac{a}{b}\right)^3\right] + \frac{5}{21} \frac{Ze^2}{a} \frac{\langle r^4 \rangle}{a^4} \left[1 - \left(\frac{a}{b}\right)^5\right], \quad (20)$$

where $\tilde{D}q$ is defined as

$$\tilde{D}q = \frac{1}{6} \frac{Ze^2}{a} \frac{\langle r^4 \rangle}{a^4} \left[\frac{2}{3} + \frac{1}{3} \left(\frac{a}{b}\right)^5\right]. \quad (21)$$

On the other hand, t_{2g} orbital is split into e_g degenerate (yz and zx) and b_{2g} (xy) orbitals, of which eigen energies are, respectively, given by

$$\varepsilon_{yz} = \varepsilon_{zx} = -4\tilde{D}q - \frac{2}{7} \frac{Ze^2}{a} \frac{\langle r^2 \rangle}{a^2} \left[1 - \left(\frac{a}{b}\right)^3\right] + \frac{10}{63} \frac{Ze^2}{a} \frac{\langle r^4 \rangle}{a^4} \left[1 - \left(\frac{a}{b}\right)^5\right], \quad (22)$$

and

$$\varepsilon_{xy} = -4\tilde{D}q + \frac{4}{7} \frac{Ze^2 \langle r^2 \rangle}{a a^2} \left[1 - \left(\frac{a}{b} \right)^3 \right] - \frac{20}{63} \frac{Ze^2 \langle r^4 \rangle}{a a^4} \left[1 - \left(\frac{a}{b} \right)^5 \right]. \quad (23)$$

Note that also for the tetragonal case, the CEF term is written as Eq. (16).

The splitting in the tetragonal case with $a < b$ is intuitively understood from the shape of orbitals, on the basis of the point that the energy difference originates in the Coulomb interaction between the $3d$ electrons and the oxygen ions surrounding transition metal ion. While the wave-function of the $3z^2-r^2$ orbital is extended along the z -direction, x^2-y^2 orbital shape is extended in the x - y plane. Since apical oxygens move to the z -direction for the case of $a < b$, the energy loss for $3z^2-r^2$ orbital becomes small, indicating that the $3z^2-r^2$ orbital is lower. Concerning the splitting of t_{2g} orbitals, we note that xy orbital is extended in the xy plane, while yz and zx orbitals have some extension along z axis. Then, for $a < b$, the penalty from the electrostatic potential would be smaller for yz and zx , compared with that for xy . Then, we intuitively consider that the energy level for xy orbital is higher than those for yz and zx orbitals.

2.2. Coulomb interactions

Now we include the effect of Coulomb interactions among d electrons in the level of atomic problem. In the localized ion system, the Coulomb interaction term among d -electrons is generally given by

$$H_{\text{el-el}} = \frac{1}{2} \sum_{\mathbf{i}} \sum_{m_1, m_2, m_3, m_4} \sum_{\sigma_1 \sigma_2} I_{m_1 m_2, m_3 m_4}^d d_{\mathbf{i} m_1 \sigma_1}^\dagger d_{\mathbf{i} m_2 \sigma_2}^\dagger d_{\mathbf{i} m_3 \sigma_2} d_{\mathbf{i} m_4 \sigma_1}, \quad (24)$$

where the Coulomb matrix element among d electrons I^d is expressed as

$$I_{m_1 m_2, m_3 m_4}^d = \int \int d\mathbf{r}_1 d\mathbf{r}_2 \Psi_{32m_1}^*(\mathbf{r}_1) \Psi_{32m_2}^*(\mathbf{r}_2) g_{12} \Psi_{32m_3}(\mathbf{r}_2) \Psi_{32m_4}(\mathbf{r}_1). \quad (25)$$

Here $g_{12} = g(|\mathbf{r}_1 - \mathbf{r}_2|)$ is the screened Coulomb interaction, which can be expanded in spherical harmonics

$$g_{12} = g(|\mathbf{r}_1 - \mathbf{r}_2|) = \sum_{\ell, m} g_\ell(r_1, r_2) Y_{\ell m}(\theta_1, \phi_1) Y_{\ell m}(\theta_2, \phi_2), \quad (26)$$

with $\mathbf{r}_1 = (r_1, \theta_1, \phi_1)$ and $\mathbf{r}_2 = (r_2, \theta_2, \phi_2)$ in the polar coordinate. The complicated integrals can be partly performed and the result is given by using the Gaunt coefficients as

$$I_{m_1 m_2, m_3 m_4}^d = \delta_{m_1 + m_2, m_3 + m_4} \sum_{k=0, 2, 4} c^{(k)}(m_1, m_3) c^{(k)}(m_4, m_2) F_d^k. \quad (27)$$

Note that the sum is limited by the Wigner-Eckart theorem to $k=0, 2$, and 4 . Here we define F_d^k , which is the radial integral for the k -th partial wave, called Slater integral or Slater-Condon parameter [126, 127], given by

$$F_d^k = \int_0^\infty r_1^2 dr_1 \int_0^\infty r_2^2 dr_2 R_{3d}^2(r_1) R_{3d}^2(r_2) g_k(r_1, r_2). \quad (28)$$

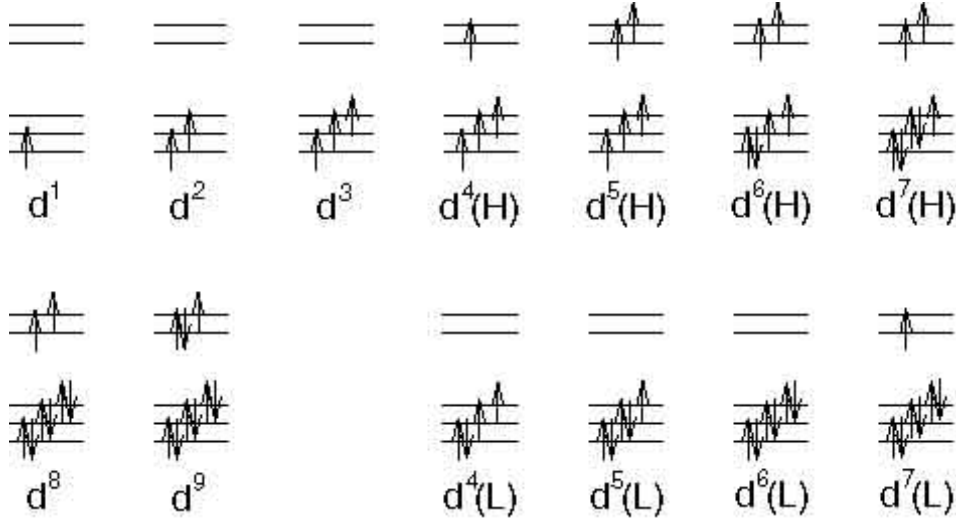


Figure 3. Configurations of d^n electrons for $n=1\sim 9$. For $n=4\sim 7$, we show both the high- and low-spin states.

By using Slater-Condon parameters, it is more convenient to define Racah parameters, given by

$$\begin{aligned}
 A &= F_d^0 - F_d^4/9, \\
 B &= (9F_d^2 - 5F_d^4)/441, \\
 C &= 5F_d^4/63,
 \end{aligned}
 \tag{29}$$

where A , B , and C are Racah parameters [123]. All possible Coulomb integrals are expressed by these Racah parameters [128]. In usual, the Racah parameters are determined from the experimental results in the high-energy region.

By diagonalizing $H_{\text{CEF}} + H_{\text{el-el}}$, let us discuss d^n -electron configuration under the cubic CEF, where the superscript n denotes the local d -electron number. It is possible to obtain analytic result partly, but most of the solutions can be obtained only numerically. As summarized in Fig. 3, the results are understood from the electron configuration obtained by accommodating n electrons in e_g and t_{2g} orbitals due to the competition between the CEF splitting $10Dq$ and the Hund's rule interaction. For $n=1$, we find 6-fold degenerate ground state, originating from the three t_{2g} orbitals with spin degree of freedom. For $n=2$, 9-fold degeneracy is found in the ground state. When we accommodate a couple of electrons among three t_{2g} orbitals, there are three possibilities for the formation of total spin $S=1$ between two of three orbitals. Since each spin $S=1$ has three degenerate states with $S_z=-1, 0$, and $+1$, in total we obtain 9-fold degeneracy. For $n=3$, 4-fold degeneracy is found in the ground state. Now three t_{2g} electrons form $S=3/2$ spin due to Hund's rule, which have four degenerate states with $S_z=\pm 3/2$ and $\pm 1/2$.

For the case of $n=4$, we find two types of ground states, depending on the balance between $10Dq$ and Coulomb interaction. For small $10Dq$, 10-fold degeneracy is observed in the ground state, while the degeneracy is changed to 9-fold for large $10Dq$. These

are high- and low-spin states, labeled by “H” and “L”, respectively. In the high-spin configuration, due to the strong Hund’s rule interaction, total spin $S=2$ is formed, but we consider that one electron is added to the d^3 configuration. The fourth electron should be accommodated in e_g sector, which provide an extra double degeneracy. Since $S=2$ state include five degenerate states with $S_z=\pm 2, \pm 1$, and 0, in total we obtain 10-fold degeneracy. The eigen energy for $d^4(\text{H})$ is exactly given by $E[d^4(\text{H})]=6A - 21B - 72B_4^0$. On the other hand, for the low-spin state, we consider that all four electrons are included among t_{2g} orbitals to gain the CEF potential energy. Namely, $S=1$ spin is formed in the t_{2g} sector, leading to 9-fold degeneracy as in the case of d^2 . The energy for $d^4(\text{L})$ can be obtained only numerically, but in the limit of infinite $10Dq$, the energy is asymptotically given by $E[d^4(\text{L})]=6A - 15B + 5C - 192B_4^0$. Due to the comparison of two energies, we obtain a rough condition for the change of the spin state as $6B + 5C > 10Dq$, which indicates clearly that the high-spin state is chosen when the Hund’s rule interaction is stronger than the effect of CEF potential.

In the high-spin state for $n=4$, as observed in Mn^{3+} ion, three electrons are accommodated in the t_{2g} orbitals, while one electron exists in the e_g orbital. In such a case, it is necessary to treat both t_{2g} and e_g electrons in the same model Hamiltonian. On the other hand, if the low-spin state for $n=4$ is favored due to the large CEF potential, it is enough to consider only the t_{2g} orbital, as in the cases of $n=1\sim 3$. In fact, for $4d$ electron systems, the effect of CEF potential becomes strong due to the large ion radius. For instance, in ruthenates, Ru^{4+} ion includes four $4d$ electrons, which form the low-spin state with $S=1$, as deduced from the AF phase of Ca_2RuO_4 .

For $n=5$, we find 6-fold degeneracy in the region of small $10Dq$. This is originating from the high-spin $S=5/2$ state with $S_z=\pm 5/2, \pm 3/2$ and $\pm 1/2$, in which each orbital is occupied by one electron. For very large $10Dq$, the ground state degeneracy is still six, but the wavefunction is drastically changed in this low-spin $S=1/2$ state. It is understood that five electrons (or one hole) occupies the t_{2g} orbitals. Namely, there are three kinds of $S=1/2$ state, leading to six-fold degeneracy in total. In principle, the intermediate spin state with $S=3/2$ is possible, but the region for the intermediate state seems to be very limited in the parameter space.

For $n=6$, the ground state for small $10Dq$ has 15-fold degeneracy. This is the high-spin $S=2$ state, in which two electrons in the e_g sector, while four electrons in the t_{2g} section. As shown in the configuration of $d^6(\text{H})$ in Fig. 3, there are three possibility for down spin electron in the t_g orbitals. Namely, there are three kinds of $S=2$ states, leading to 15-fold degeneracy in total. For large $10Dq$, we obtain the singlet ground state, which is the low-spin state with $S=0$, in which t_{2g} orbitals are fully occupied by six electrons.

For $n=7$, the high-spin state in the region of small $10Dq$ has 12-fold degeneracy, by accommodating two electrons in the e_g and five electrons in the t_{2g} orbitals. As shown in the configuration of $d^7(\text{H})$ in Fig. 3, there are three possibility for one hole in the t_g orbitals. Thus, there are three kinds of $S=3/2$ states, leading to 12-fold degeneracy in total. In the low-spin state, on the other hand, the ground state degeneracy is four. It

is easily understood, when we put one more electron in the e_g orbital in addition to the $d^6(L)$ configuration.

Both for $n=8$ and 9, since t_{2g} orbitals are fully occupied and thus, active orbital is e_g . For $n=8$, the ground state with $S=1$ composed of a couple of e_g electrons is triply degenerate. For $n=9$, we find one hole in the e_g orbitals, there are four fold degeneracy in the ground state. Note that for $n=9$, when the tetragonal CEF effect is strong enough, as actually found in perovskite copper oxides, only $x^2 - y^2$ orbital becomes active.

In general, it is necessary to consider all five orbitals in the Hamiltonian for the complete analysis of electronic properties of transition metal oxides, even if the full Hamiltonian includes several competing tendencies and couplings. However, the essential physics can be frequently obtained even using relatively simple models, by focusing on the active orbital, emerging out of the competition between the CEF potential and the Coulomb interaction. In this sense, we immediately arrive at two possibilities: One is t_{2g} model for the cases of $d^1 \sim d^3$ and $d^4(L) \sim d^6(L)$. Another is e_g model for the cases of $d^7(L)$, d^8 , and d^9 . For other cases, it is necessary to consider both e_g and t_{2g} orbitals in the same Hamiltonian simultaneously. However, for the cases of $d^4(H)$, it is possible to define a simplified model, which will be explained later for Mn^{3+} ion with the high-spin state.

For the purpose to express the above models, it is convenient to simplify the Coulomb interaction term in a qualitatively correct form, since the representation using Racah parameters are exact, but too complicated for further analysis. Under the cubic CEF potential, as described in the previous subsection, two e_g and three t_{2g} orbitals provide appropriate basis. Then, the Coulomb interaction term should be expressed as

$$H_{el-el} = \frac{1}{2} \sum_{\mathbf{i}} \sum_{\gamma_1 \gamma_2 \gamma_3 \gamma_4} \sum_{\sigma_1 \sigma_2} \tilde{I}_{\gamma_1 \sigma_1, \gamma_2 \sigma_2; \gamma_3 \sigma_2, \gamma_4 \sigma_1} d_{\mathbf{i} \gamma_1 \sigma_1}^\dagger d_{\mathbf{i} \gamma_2 \sigma_2}^\dagger d_{\mathbf{i} \gamma_3 \sigma_2} d_{\mathbf{i} \gamma_4 \sigma_1}, \quad (30)$$

where the modified Coulomb matrix element \tilde{I} is given by the proper combination of the original one I^d . Note that the orbital index γ denotes e_g and t_{2g} orbitals, which are defined by linear combination of the original d -electron orbitals labeled by m .

By using the modified Coulomb matrix element, it is useful to define the so-called ‘‘Kanamori parameters’’, U , U' , J , and J' [129]. Among them, U is the intra-orbital Coulomb interaction, given by

$$U_\gamma = \tilde{I}_{\gamma\sigma, \gamma\sigma'; \gamma\sigma', \gamma\sigma}, \quad (31)$$

with $\sigma \neq \sigma'$. U' is the inter-orbital Coulomb interaction, expressed by

$$U'_{\gamma, \gamma'} = \tilde{I}_{\gamma\sigma, \gamma'\sigma'; \gamma'\sigma', \gamma\sigma}, \quad (32)$$

with $\gamma \neq \gamma'$. J is the inter-orbital exchange interaction, leading to the Hund’s rule coupling, written as

$$J_{\gamma, \gamma'} = \tilde{I}_{\gamma\sigma, \gamma'\sigma'; \gamma\sigma', \gamma'\sigma}, \quad (33)$$

with $\gamma \neq \gamma'$. Finally, J' is the pair-hopping amplitude between different orbitals, given by

$$J'_{\gamma, \gamma'} = \tilde{I}_{\gamma\sigma, \gamma'\sigma'; \gamma'\sigma', \gamma'\sigma}, \quad (34)$$

γ	γ'	$U'_{\gamma,\gamma'}$	$J_{\gamma,\gamma'}$
xy, yz, zx	xy, yz, zx	$A-2B+C$	$3B+C$
$x^2-y^2, 3z^2-r^2$	$x^2-y^2, 3z^2-r^2$	$A-4B+C$	$4B+C$
xy	x^2-y^2	$A+4B+C$	C
xy	$3z^2-r^2$	$A-4B+C$	$4B+C$
yz, zx	x^2-y^2	$A-2B+C$	$3B+C$
yz, zx	$3z^2-r^2$	$A+2B+C$	$B+C$

Table 1. Expressions for U' and J by using Racah parameters A , B , and C . Note that $U=A+4B+3C$ for each orbital. For more information, see Refs. [128] and [129].

with $\gamma \neq \gamma'$ and $\sigma \neq \sigma'$.

In Table. 1, we list the values for possible Kanamori parameters. Here we have four comments on the relation among Kanamori parameters. (i) A relation $J=J'$ holds, which is simply due to the fact that each of the parameters above is given by an integral of the Coulomb interaction sandwiched with appropriate orbital wave functions. Analyzing the form of those integrals the equality between J and J' can be deduced. (ii) For completeness, we explicitly show the orbital indices for the definition of Kanamori parameters. In fact, as found in Table. 1, the inter-orbital Coulomb interactions between e_g and t_{2g} orbitals depend on the kind of orbitals, while there is no orbital dependence in Coulomb interactions among e_g or t_{2g} orbitals. (iii) We point out that among e_g or t_{2g} orbitals, another relation $U=U'+J+J'$ holds in any combination of orbitals. This relation is needed to recover the rotational invariance in orbital space. (iv) Since the largest energy scale among the Kanamori parameters is U , the orbitals are not doubly occupied by both up- and down-spin electrons. Thus, only one electron can exist in each orbital of the degenerate e_g or t_{2g} sector. Furthermore, in order to take advantage of J , the spins of electrons point along the same direction. This is the so-called ‘‘Hund’s rule’’.

Then, for the case with active e_g orbital degree of freedom, we can define the Coulomb interaction term as

$$\begin{aligned}
H_{\text{el-el}}^{e_g} = & U \sum_{\mathbf{i},\gamma} n_{\mathbf{i}\gamma\uparrow} n_{\mathbf{i}\gamma\downarrow} + U' \sum_{\mathbf{i}} n_{\mathbf{ia}} n_{\mathbf{ib}} \\
& + J \sum_{\mathbf{i},\sigma,\sigma'} d_{\mathbf{ia}\sigma}^\dagger d_{\mathbf{ib}\sigma'}^\dagger d_{\mathbf{ia}\sigma} d_{\mathbf{ib}\sigma'} + J' \sum_{\mathbf{i}} (d_{\mathbf{ia}\uparrow}^\dagger d_{\mathbf{ia}\downarrow}^\dagger d_{\mathbf{ib}\downarrow} d_{\mathbf{ib}\uparrow} + \text{h.c.}), \quad (35)
\end{aligned}$$

where the subscripts, a and b, denote $x^2 - y^2$ and $3z^2 - r^2$ orbitals, respectively, $n_{\mathbf{i}\gamma\sigma} = d_{\mathbf{i}\gamma\sigma}^\dagger d_{\mathbf{i}\gamma\sigma}$, and $n_{\mathbf{i}\gamma} = \sum_{\sigma} n_{\mathbf{i}\gamma\sigma}$. As easily understood from Table. 1, we find $U'=A-4B+C$ and $J=4B+C$ for e_g orbital.

On the other hand, for the case with active t_{2g} orbital, the Coulomb interaction term is expressed by

$$H_{\text{el-el}}^{t_{2g}} = U \sum_{\mathbf{i},\gamma} n_{\mathbf{i}\gamma\uparrow} n_{\mathbf{i}\gamma\downarrow} + \frac{U'}{2} \sum_{\mathbf{i},\gamma \neq \gamma'} n_{\mathbf{i}\gamma} n_{\mathbf{i}\gamma'}$$

$$+ \frac{J}{2} \sum_{\mathbf{i}, \sigma, \sigma'} \sum_{\gamma \neq \gamma'} d_{\mathbf{i}\gamma\sigma}^\dagger d_{\mathbf{i}\gamma'\sigma'}^\dagger d_{\mathbf{i}\gamma\sigma} d_{\mathbf{i}\gamma'\sigma} + \frac{J'}{2} \sum_{\mathbf{i}, \gamma \neq \gamma'} d_{\mathbf{i}\gamma\uparrow}^\dagger d_{\mathbf{i}\gamma\downarrow}^\dagger d_{\mathbf{i}\gamma\downarrow} d_{\mathbf{i}\gamma\uparrow}, \quad (36)$$

where γ and γ' run in the t_{2g} orbitals, $U'=A-2B+C$, and $J=3B+C$.

Next we consider the more complicated case, in which the Coulomb interaction term is not expressed only among e_g or t_{2g} orbitals. A typical situation can be found in the high-spin state of d^4 configuration, which is relevant to manganites in the cubic perovskite structure. Due to the Hund's rule, tetravalent manganese ion includes three d electrons to form $S=3/2$ in the t_{2g} orbitals. By adding one more electron to Mn^{4+} with three up-spin t_{2g} -electrons, let us consider the configuration for the Mn^{3+} ion. As mentioned above, there are two possibilities due to the balance between the crystalline-field splitting and the Hund's rule coupling, but in $3d$ electron system such as manganites, the high-spin state is realized, since the Hund's rule coupling dominates over $10Dq$.

In order to simplify the model without loss of essential physics, it is reasonable to treat the three spin-polarized t_{2g} -electrons as a localized "core-spin" expressed by \mathbf{S}_i at site \mathbf{i} , since the overlap integral between t_{2g} and oxygen p orbital is small compared with that between e_g and p orbitals. Moreover, due to the large value of the total spin $S=3/2$, it is usually approximated by a classical spin. This approximation has been tested by using computational techniques [130, 131]. Thus, the effect of Coulomb interaction between e_g and t_{2g} electrons can be effectively included by the strong Hund's rule coupling between the e_g -electron spin and localized t_{2g} -spins, given by

$$H_{\text{Hund}} = -J_H \sum_{\mathbf{i}} \mathbf{s}_i \cdot \mathbf{S}_i, \quad (37)$$

where $\mathbf{s}_i = \sum_{\gamma\alpha\beta} d_{\mathbf{i}\gamma\alpha}^\dagger \sigma_{\alpha\beta} d_{\mathbf{i}\gamma\beta}$, $J_H (>0)$ is the Hund's rule coupling between localized t_{2g} -spin and mobile e_g -electron, and $\sigma = (\sigma_x, \sigma_y, \sigma_z)$ are the Pauli matrices. The magnitude of J_H is considered to be of the order of J . Here note that \mathbf{S}_i is normalized as $|\mathbf{S}_i|=1$. Thus, the direction of the classical t_{2g} -spin at site \mathbf{i} is defined as

$$\mathbf{S}_i = (\sin \theta_i \cos \phi_i, \sin \theta_i \sin \phi_i, \cos \theta_i), \quad (38)$$

by using the polar angle θ_i and the azimuthal angle ϕ_i .

Note that the effect of the Coulomb interaction is not fully taken into account only by H_{Hund} , since there remains the direct electrostatic repulsion between e_g -electrons. Then, by further adding the e_g electron interaction term, we obtain the Coulomb interaction term for $d^4(\text{H})$ configuration as

$$H_{\text{el-el}}^{\text{DE}} = H_{\text{Hund}} + H_{\text{el-el}}^{e_g}. \quad (39)$$

Here we use "DE" in the superscript for the Hamiltonian, which is the abbreviation of "double exchange". We will explain later the reason why we use "DE", in the section explaining the result for manganites.

2.3. Electron-phonon interactions

Another important ingredient in the model Hamiltonian for transition metal oxides is the lattice distortion coupled to e_g or t_{2g} electrons. In particular, the orbital degeneracy is lifted by the Jahn-Teller distortion. It is difficult to explain all possible types of electron-phonon coupling term, but here we explain the coupling between degenerate e_g orbital and the distortion of the octahedron, since later we will focus on the magnetic properties of manganites in the perovskite structure. The coupling of the same type of distortions of octahedron to t_{2g} orbitals is also discussed in this subsection.

The basic formalism for the study of electrons coupled to Jahn-Teller modes has been set up by Kanamori [132]. He focused on cases where the electronic orbitals are degenerate in the undistorted crystal structure, as in the case of manganese ion in an octahedron of oxygens. As explained by Kanamori, the Jahn-Teller effect in this context can be simply stated as follows. When a given electronic level of a cluster is degenerate in a structure of high symmetry, this structure is generally unstable, and the cluster will present a distortion toward a lower symmetry ionic arrangement [133]. In the case of Mn^{3+} , which is orbitally doubly degenerate when the crystal is undistorted, a splitting will occur when the crystal is distorted. The distortion of the MnO_6 octahedron is “cooperative” since once it occurs in a particular octahedron, it will affect the neighbors. The basic Hamiltonian to describe the interaction between electrons and Jahn-Teller modes was written by Kanamori. In the adiabatic approximation, it is given in the form of

$$H_{\text{JT}} = g \sum_{\mathbf{i}} (Q_{2\mathbf{i}} \tau_{x\mathbf{i}} + Q_{3\mathbf{i}} \tau_{z\mathbf{i}}) + k_{\text{JT}} \sum_{\mathbf{i}} (Q_{2\mathbf{i}}^2 + Q_{3\mathbf{i}}^2)/2, \quad (40)$$

where g is the coupling constant between the e_g -electrons and distortions of the MnO_6 octahedron, $Q_{2\mathbf{i}}$ and $Q_{3\mathbf{i}}$ are normal modes of vibration of the oxygen octahedron that remove the degeneracy between the electronic levels, and k_{JT} is the spring constant for the Jahn-Teller mode distortions. We note that the sign of g depends on the kind of ion and electron configuration. The pseudospin operators are defined as

$$\tau_{x\mathbf{i}} = \sum_{\sigma} (d_{\mathbf{ia}\sigma}^{\dagger} d_{\mathbf{ib}\sigma} + d_{\mathbf{ib}\sigma}^{\dagger} d_{\mathbf{ia}\sigma}), \quad \tau_{z\mathbf{i}} = \sum_{\sigma} (d_{\mathbf{ia}\sigma}^{\dagger} d_{\mathbf{ia}\sigma} - d_{\mathbf{ib}\sigma}^{\dagger} d_{\mathbf{ib}\sigma}). \quad (41)$$

In the expression of H_{JT} , a $\tau_{y\mathbf{i}}$ -term does not appear for symmetry reasons, since it belongs to the A_{2u} representation. The non-zero terms should correspond to the irreducible symmetric representations of $E_g \times E_g$, namely, E_g and A_{1g} . The former representation is expressed by using the pseudo spin operators $\tau_{x\mathbf{i}}$ and $\tau_{z\mathbf{i}}$ as discussed here, while the latter, corresponding to the breathing mode, is discussed later.

Following Kanamori, $Q_{2\mathbf{i}}$ and $Q_{3\mathbf{i}}$ are explicitly given by

$$Q_{2\mathbf{i}} = (X_{1\mathbf{i}} - X_{3\mathbf{i}} - Y_{2\mathbf{i}} + Y_{4\mathbf{i}})/\sqrt{2}, \quad (42)$$

and

$$Q_{3\mathbf{i}} = (2Z_{5\mathbf{i}} - 2Z_{6\mathbf{i}} - X_{1\mathbf{i}} + X_{3\mathbf{i}} - Y_{2\mathbf{i}} + Y_{4\mathbf{i}})/\sqrt{6}, \quad (43)$$

where $X_{\mu i}$, $Y_{\mu i}$, and $Z_{\mu i}$ are the displacement of oxygen ions from the equilibrium positions along the x -, y -, and z -direction, respectively. Explicitly, they are included in the positions of oxygen ions as $\mathbf{R}_{1i}=(a/2+X_{1i}, 0, 0)$, $\mathbf{R}_{2i}=(0, -a/2+Y_{2i}, 0)$, $\mathbf{R}_{3i}=(-a/2+X_{3i}, 0, 0)$, $\mathbf{R}_{4i}=(0, a/2+Y_{4i}, 0)$, $\mathbf{R}_{5i}=(0, 0, a/2+Z_{5i})$, and $\mathbf{R}_{6i}=(0, 0, -a/2+Z_{6i})$. Here we consider the deformation of octahedron from the cubic case. The convention for the labeling μ of coordinates is shown in Fig. 1.

In order to solve the local Jahn-Teller problem, it is convenient to scale the phononic degrees of freedom as

$$Q_{2i} = (g/k_{\text{JT}})q_{2i}, \quad Q_{3i} = (g/k_{\text{JT}})q_{3i}, \quad (44)$$

where g/k_{JT} is the typical length scale for the Jahn-Teller distortion, which is of the order of 0.1 Å, namely, a few percent of the lattice constant. When the Jahn-Teller distortion is expressed in the polar coordinate as

$$q_{2i} = q_i \sin \xi_i, \quad q_{3i} = q_i \cos \xi_i, \quad (45)$$

the ground state is easily obtained as $(-\sin[\xi_i/2]d_{i\alpha\sigma}^\dagger + \cos[\xi_i/2]d_{i\beta\sigma}^\dagger)|0\rangle$ with the use of the phase ξ_i . The corresponding eigenenergy is given by $-E_{\text{JT}}$, where E_{JT} is the static Jahn-Teller energy, defined by

$$E_{\text{JT}} = g^2/(2k_{\text{JT}}). \quad (46)$$

Note here that the ground state energy is independent of the phase ξ_i . Namely, the shape of the deformed isolated octahedron is not uniquely determined in this discussion. In the Jahn-Teller crystal, the kinetic motion of e_g electrons, as well as the cooperative effect between adjacent distortions, play a crucial role in lifting the degeneracy and fixing the shape of the local distortion.

To complete the electron-phonon coupling term, it is necessary to consider the breathing mode distortion, coupled to the local electron density as

$$H_{\text{br}} = g \sum_{\mathbf{i}} Q_{1i} n_{\mathbf{i}} + k_{\text{br}} \sum_{\mathbf{i}} Q_{1i}^2/2, \quad (47)$$

where $n_{\mathbf{i}} = \sum_{\gamma,\sigma} d_{i\gamma\sigma}^\dagger d_{i\gamma\sigma}$ and the breathing-mode distortion Q_{1i} is given by

$$Q_{1i} = (X_{1i} - X_{3i} + Y_{2i} - Y_{4i} + Z_{5i} - Z_{6i})/\sqrt{3}, \quad (48)$$

and k_{br} is the associated spring constant. Note that, in principle, the coupling constants of the e_g electrons with the Q_1 , Q_2 , and Q_3 modes could be different from one another. For simplicity, here it is assumed that those coupling constants take the same value. On the other hand, for the spring constants, a different notation for the breathing mode is introduced, since the frequency for the breathing mode distortion has been found experimentally to be different from that for the Jahn-Teller mode. This point will be briefly discussed later. Note also that the Jahn-Teller and breathing modes are competing with each other. As it was shown above, the energy gain due to the Jahn-Teller distortion is maximized when one electron exists per site. On the other hand, the breathing mode distortion energy is proportional to the total number of e_g electrons per site, since this distortion gives rise to an effective on-site attraction between electrons.

By combining the Jahn-Teller mode and breathing mode distortions, the electron-phonon term for the e_g model is summarized as

$$H_{\text{el-ph}}^{e_g} = H_{\text{JT}} + H_{\text{br}}. \quad (49)$$

This expression depends on the parameter $\beta = k_{\text{br}}/k_{\text{JT}}$, which regulates which distortion, the Jahn-Teller or breathing mode, plays a more important role. This point will be discussed in a separate subsection.

When we simply ignore buckling and rotational modes and consider only the Jahn-Teller-type distortions of octahedron, the electron-lattice coupling for t_{2g} orbitals is given by [134]

$$H_{\text{el-ph}}^{t_{2g}} = g \sum_{\mathbf{i}} (Q_{z\mathbf{i}} n_{\mathbf{i}xy} + Q_{x\mathbf{i}} n_{\mathbf{i}yz} + Q_{y\mathbf{i}} n_{\mathbf{i}zx}) + (k_{\text{JT}}/2) \sum_{\mathbf{i}} (Q_{2\mathbf{i}}^2 + Q_{3\mathbf{i}}^2), \quad (50)$$

where $Q_{x\mathbf{i}} = (-1/2)Q_{3\mathbf{i}} + (\sqrt{3}/2)Q_{2\mathbf{i}}$, $Q_{y\mathbf{i}} = (-1/2)Q_{3\mathbf{i}} - (\sqrt{3}/2)Q_{2\mathbf{i}}$, and $Q_{z\mathbf{i}} = Q_{3\mathbf{i}}$. Later we will consider the effect of this type of electron-phonon coupling on the magnetic structure of t_{2g} electron systems.

Let us now consider the cooperative effect. Although we have not explicitly mentioned thus far, the distortions at each site are *not* independent, since all oxygens are shared by neighboring MnO_6 octahedra, as easily understood by the explicit expressions of $Q_{1\mathbf{i}}$, $Q_{2\mathbf{i}}$, and $Q_{3\mathbf{i}}$ presented before. A direct and simple way to consider such cooperative effect is to determine the oxygen positions $X_{1\mathbf{i}}$, $X_{4\mathbf{i}}$, $Y_{2\mathbf{i}}$, $Y_{5\mathbf{i}}$, $Z_{3\mathbf{i}}$, and $Z_{6\mathbf{i}}$, by using computational method such as the Monte Carlo simulations and numerical relaxation techniques. To reduce the burden on the numerical calculations, for instance, the displacements of oxygen ions are assumed to be along the bond direction between nearest neighboring manganese ions. In other words, the displacement of the oxygen ion perpendicular to the Mn-Mn bond, i.e., the buckling mode, is usually ignored. As shown later, even in this simplified treatment, several interesting results have been obtained for the spin, charge, and orbital ordering in manganites.

Rewriting Eqs. (42), (43), and (48) in terms of the displacement of oxygens from the equilibrium positions, we express the distortions as

$$\begin{aligned} Q_{1\mathbf{i}} &= (\Delta_{x\mathbf{i}} + \Delta_{y\mathbf{i}} + \Delta_{z\mathbf{i}})/\sqrt{3}, \\ Q_{2\mathbf{i}} &= (\Delta_{x\mathbf{i}} - \Delta_{y\mathbf{i}})/\sqrt{2}, \\ Q_{3\mathbf{i}} &= (2\Delta_{z\mathbf{i}} - \Delta_{x\mathbf{i}} - \Delta_{y\mathbf{i}})/\sqrt{6}, \end{aligned} \quad (51)$$

where $\Delta_{\mathbf{ai}}$ is given by

$$\Delta_{\mathbf{ai}} = u_{\mathbf{i}}^{\mathbf{a}} - u_{\mathbf{i}-\mathbf{a}}^{\mathbf{a}}, \quad (52)$$

with $u_{\mathbf{i}}^{\mathbf{a}}$ being the displacement of oxygen ion at site \mathbf{i} from the equilibrium position along the \mathbf{a} -axis. In the *cooperative* treatment, the $\{u\}$'s are directly optimized in the numerical calculations [25, 26]. On the other hand, in the *non-cooperative* calculations, $\{Q\}$'s are treated instead of the $\{u\}$'s. In the simulations, variables are taken as $\{Q\}$'s or $\{u\}$'s, depending on the treatments of lattice distortion.

Finally, we briefly comment on the effect of macroscopic distortion. In the above treatment, we assume the cubic symmetry for the equilibrium positions of oxygens,

γ	γ'	$E_{\gamma,\gamma'}$
$x^2 - y^2$	$x^2 - y^2$	$(3/4)(\ell^2 - m^2)^2(dd\sigma) + [\ell^2 + m^2 - (\ell^2 - m^2)^2](dd\pi)$
$3z^2 - r^2$	$3z^2 - r^2$	$[n^2 - (\ell^2 + m^2)/2]^2(dd\sigma) + 3n^2(\ell^2 + m^2)(dd\pi)$
$x^2 - y^2$	$3z^2 - r^2$	$(\sqrt{3}/2)(\ell^2 - m^2)[n^2 - (\ell^2 + m^2)/2](dd\sigma) + \sqrt{3}n^2(m^2 - \ell^2)(dd\pi)$
xy	xy	$3\ell^2m^2(dd\sigma) + (\ell^2 + m^2 - 4\ell^2m^2)(dd\pi)$
xy	yz	$3\ell m^2n(dd\sigma) + \ell n(1 - 4m^2)(dd\pi)$
xy	zx	$3\ell^2mn(dd\sigma) + mn(1 - 4\ell^2)(dd\pi)$

Table 2. Expressions for hopping amplitude between d orbitals. As for details, see Ref. [135]. We use a direction cosine as (ℓ, m, n) for the direction of hopping from γ to γ' orbitals. We show the contributions from the hoppings through σ - and π -bonds.

but in actuality, the crystal structure is frequently deviated from the cubic symmetry. Although we cannot determine the stable crystal structure in the present treatment, the effect of macroscopic distortions is included as offset values for the distortions, which are given by

$$\begin{aligned}
Q_1^{(0)} &= (\delta L_x + \delta L_y + \delta L_z)/\sqrt{3}, \\
Q_2^{(0)} &= (\delta L_x - \delta L_y)/\sqrt{2}, \\
Q_3^{(0)} &= (2\delta L_z - \delta L_x - \delta L_y)/\sqrt{6},
\end{aligned} \tag{53}$$

where $\delta L_{\mathbf{a}} = L_{\mathbf{a}} - L$, the non-distorted lattice constants are $L_{\mathbf{a}}$, and $L = (L_x + L_y + L_z)/3$. Note that $L_{\mathbf{a}}$ is determined from the experimental results. By adding $Q_{\mu}^{(0)}$ in the right-hand side of $Q_{\mu\mathbf{i}}$ in Eq. (51), it is possible to consider the effect of the deviation from the cubic symmetry

2.4. Electron hopping

In previous subsections, we have discussed the local electron state due to CEF potential and Coulomb interaction. We have also considered an additional electron-phonon coupling term. Since the possible local terms have been completed, let us consider the intersite effect in the next step. In actual materials, there are several kinds of intersite effects. Among them, we consider the electron hopping between adjacent d electron orbitals. For transition metal oxides, such a hopping process occurs through the oxygen ion, but in the formalism, it is enough to consider the direct hopping d -electron orbitals. Effect of oxygen will be discussed later.

Fortunately, the hopping amplitudes have been already evaluated and tabulated for any combination of electron orbitals. We can simply consult with the table of Slater-Koster integral [135], which is the general scheme for the overlap integral between adjacent electron orbitals. The kinetic term for e_g or t_{2g} electrons is expressed in a common form as

$$H_{\text{kin}}^{\Gamma} = \sum_{\mathbf{i}, \mathbf{a}, \sigma} \sum_{\gamma, \gamma'} t_{\gamma\gamma'}^{\mathbf{a}} d_{\mathbf{i}\gamma\sigma}^{\dagger} d_{\mathbf{i}+\mathbf{a}\gamma'\sigma}, \tag{54}$$

where Γ is the irreducible representation, \mathbf{a} is the vector connecting nearest-neighbor sites, and $t_{\gamma\gamma'}^{\mathbf{a}}$ is the nearest-neighbor hopping amplitude between γ - and γ' -orbitals along the \mathbf{a} -direction.

For the cubic lattice composed of transition metal ion, we consider the three axis directions, $\mathbf{x}=(1,0,0)$, $\mathbf{y}=(0,1,0)$, and $\mathbf{z}=(0,0,1)$. Then, $t_{\gamma\gamma'}^{\mathbf{a}}$ for e_g orbital is given in a 2×2 matrix form as

$$t^{\mathbf{x}} = t_1 \begin{pmatrix} 3/4 & -\sqrt{3}/4 \\ -\sqrt{3}/4 & 1/4 \end{pmatrix}, \quad (55)$$

for x -direction,

$$t^{\mathbf{y}} = t_1 \begin{pmatrix} 3/4 & \sqrt{3}/4 \\ \sqrt{3}/4 & 1/4 \end{pmatrix}, \quad (56)$$

for y -direction, and

$$t^{\mathbf{z}} = t_1 \begin{pmatrix} 0 & 0 \\ 0 & 1 \end{pmatrix}, \quad (57)$$

for z -direction, where $t_1=(dd\sigma)$ and $(dd\sigma)$ is one of Slater integrals [135]. It should be noted that the signs in the hopping amplitudes between different orbitals are different between x - and y -directions.

On the other hand, for t_{2g} orbitals, we obtain the hopping amplitudes in a 3×3 matrix form as

$$t^{\mathbf{x}} = t_2 \begin{pmatrix} 1 & 0 & 0 \\ 0 & 0 & 0 \\ 0 & 0 & 1 \end{pmatrix}, \quad (58)$$

for x -direction,

$$t^{\mathbf{y}} = t_2 \begin{pmatrix} 1 & 0 & 0 \\ 0 & 1 & 0 \\ 0 & 0 & 0 \end{pmatrix}, \quad (59)$$

for y -direction, and

$$t^{\mathbf{z}} = t_2 \begin{pmatrix} 0 & 0 & 0 \\ 0 & 1 & 0 \\ 0 & 0 & 1 \end{pmatrix}, \quad (60)$$

for z -direction, where $t_2=(dd\pi)$.

Now let us consider explicitly the effect of oxygen orbitals. Since oxygen ion is placed in the middle of transition metal ions in the cubic perovskite, the main hopping process should occur via oxygen $2p$ orbitals. Thus, the d -electron hopping can be expressed by $(pd\sigma)$ or $(pd\pi)$, which is the overlap integral between d and p orbitals, divided by the energy difference between d and p orbitals. It is possible to calculate the d -electron hopping via oxygen $2p$ orbitals, by consulting again the Slater-Koster table for the overlap integral between d and p orbitals. However, due to

the symmetry argument, we easily understand that the form of hopping amplitude is invariant, after the redefinition of $t_1 = -(dp\sigma)^2/(\varepsilon_p - \varepsilon_d)$ and $t_2 = -(dp\pi)^2/(\varepsilon_p - \varepsilon_d)$ for e_g and t_{2g} electron cases, respectively, where ε_d and ε_p are the energy levels for *d* and *p* electrons, respectively.

We have considered the nearest neighbor hopping, but in actuality, it is necessary to consider higher neighbors in order to reproduce the Fermi surface observed in the experiments such as de Haas-van Alphen measurements. However, there is no essential difficulty for the consideration of higher neighbors by consulting the Slater-Koster table.

2.5. Intersite interaction term

In the previous subsections, we have considered the local term and kinetic motion of *d* electrons. Of course, due to the combination of these terms, intersite interaction terms effectively appear. In particular, in the strong-coupling limit, orbital-dependent superexchange terms can be obtained, leading to the complex magnetic structure with orbital ordering. Such effects are considered automatically, as long as we consider the problem within the electronic model.

However, in the model for the high-spin state of d^4 electron configuration, it is necessary to explicitly add an extra term between localized t_{2g} spin. As explained above, due to the Hund's rule coupling between e_g and t_{2g} interaction, we can easily understand that e_g electrons can move smoothly without any energy loss, if spins of e_g and t_{2g} are in the same direction. Namely, in order to gain the kinetic energy of e_g , t_{2g} spins array ferromagnetically. This is a simple explanation for the appearance of ferromagnetism in the orbital degenerate system, in particular, in manganites. However, there should exist AF intersite coupling between neighboring t_{2g} spins due to the superexchange interaction, given by

$$H_{\text{inter-site}}^{\text{AF}} = J_{\text{AF}} \sum_{\langle \mathbf{i}, \mathbf{j} \rangle} \mathbf{S}_i \cdot \mathbf{S}_j, \quad (61)$$

where $\langle \mathbf{i}, \mathbf{j} \rangle$ denotes the pair of nearest neighbor sites and J_{AF} is the AF coupling between neighboring t_{2g} spins. This term should be added to the model for manganites. As we will explain later, the competition between FM tendency to gain kinetic energy and AF energy to gain magnetic energy is a possible source of complex magnetic structure in manganites.

In addition to the effective coupling among localized spins, sometimes we consider another intersite effect originating from long-range Coulomb interaction, even if it is screened in actual materials. In order to include such effect in an effective manner, we also add

$$H_{\text{inter-site}}^{\text{C}} = V \sum_{\langle \mathbf{i}, \mathbf{j} \rangle} n_i n_j, \quad (62)$$

where V denotes the nearest-neighbor Coulomb interaction. Since V has a tendency to stabilize the charge ordering, there occurs competition between striped spin order

and bipartite charge ordering. This is another source of complex spin-charge-orbital ordering.

2.6. Summary

We have completed the preparation of all components for the model Hamiltonian. As a short summary of this section, we show three types of model Hamiltonians due to the appropriate combination of several terms.

For the system with active e_g or t_{2g} orbital degree of freedom, we can consider the orbital degenerate model, expressed in a common form as

$$H_\Gamma = H_{\text{kin}}^\Gamma + H_{\text{el-el}}^\Gamma + H_{\text{el-ph}}^\Gamma + H_{\text{inter-site}}^C, \quad (63)$$

where Γ denotes e_g or t_{2g} . Note that the inter-site Coulomb interaction term is explicitly added here, but depending on the nature of the problem, this term may be ignored.

For the case of $d^4(\text{H})$ in which both e_g and t_{2g} orbitals are included, we can define the following model:

$$H_{\text{DE}} = H_{\text{kin}}^{e_g} + H_{\text{el-el}}^{\text{DE}} + H_{\text{el-ph}}^{e_g} + H_{\text{inter-site}}^{\text{AF}} + H_{\text{inter-site}}^C. \quad (64)$$

This expression is believed to define an appropriate starting model for manganites, but unfortunately, it is quite difficult to solve such a Hamiltonian. In order to investigate further the properties of manganites, further simplifications are needed. This point will be discussed in detail in the next section.

3. Orbital physics in manganites

In the complicated phase diagram for manganites, there appear so many magnetic phases. A key issue to understand such richness is the competition between itinerant and localized tendencies contained in manganites. As mentioned in the model construction, e_g electrons can gain the kinetic energy when the background t_{2g} spins array ferromagnetically, leading to a metallic FM phase in manganites. On the other hand, in order to gain magnetic energy between localized t_{2g} spins, there occurs AF phase with insulating tendency. In one word, the competition between FM metallic and AF insulating phases is the origin of complex phase diagram of manganites.

As we will review very briefly in the next subsection, the metallic tendency has been discussed in the concept of double exchange for a long time, and the essential point has been considered to be well understood. However, the tendency toward insulating phase has not been satisfactorily understood, mainly due to the complexity of multi-degrees of freedom such as spin, charge, and orbital. In particular, ‘‘orbital ordering’’ is the remarkable feature, characteristic to manganites with active e_g orbital. In this section, spin, charge, and orbital structure for the typical hole doping in the phase diagram of manganites is focused by stressing the importance of orbital ordering.

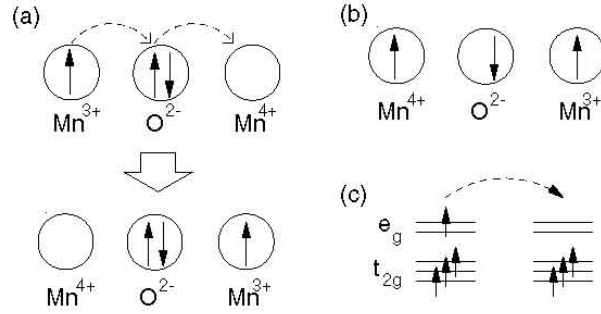


Figure 4. (a) Sketch of the double exchange mechanism which involves two Mn ions and one O ion. (b) The intermediate state of the process (a). (c) The mobility of e_g -electrons improves if the localized spins are polarized.

3.1. Concept of double-exchange

Since the historical review of theoretical and experimental works on manganites have been found in some articles and textbooks, we simply refer literatures such as Refs. [3, 4, 5, 6]. However, it is instructive to mention here the meaning of “double exchange” (DE), which is important basic concept for manganites, by following the previous review article [3].

In the earth stage of the research on manganites, it was the task to clarify the qualitative aspects of the experimentally discovered relation between transport and magnetic properties, namely the increase in conductivity upon the polarization of the spins. The concept of “double exchange” was proposed by Zener [7] as a way to allow for charge to move in manganites by the generation of a spin polarized state. The DE process has been historically explained in two somewhat different ways. Originally, Zener considered the explicit movement of electrons, as shown in Fig. 4(a). This process is schematically written as $\text{Mn}_1^{3+}\text{O}_{2\uparrow,3\downarrow}\text{Mn}^{4+} \rightarrow \text{Mn}^{4+}\text{O}_{1\uparrow,3\downarrow}\text{Mn}_2^{3+}$ [136], where 1, 2, and 3 label electrons that belong either to the oxygen between manganese, or to the e_g -level of the Mn-ions. In this process, there are two simultaneous motions involving electron 2 moving from the oxygen to the right Mn-ion, and electron 1 from the left Mn-ion to the oxygen. This is the origin of the name of “double exchange”.

The second way to visualize DE processes was presented in detail by Anderson and Hasegawa [137], and it involves a second-order process in which the two states described above go from one to the other using an intermediate state $\text{Mn}_1^{3+}\text{O}_{3\downarrow}\text{Mn}_2^{3+}$, as shown in Fig. 4(b). In this context, the effective hopping for the electron to move from one Mn-site to the next is proportional to the square of the hopping involving the *p*-oxygen and *d*-manganese orbitals (t_{pd}). Following Anderson and Hasegawa, let us consider a two-site problem, in which one itinerant electron with hopping amplitude t between sites 1 and 2 is coupled with localized spin \mathbf{S} at each site. The coupling is assumed to be ferromagnetic and the magnitude is defined as J . For $t=0$, the local ground state is labelled by $S+1/2$ with the energy of $-JS$ per site, while the excited state is specified as $S-1/2$ with the energy of $J(S+1)$ per site. For $t \neq 0$ with $t \ll J$, as observed

in manganese ions, the effective hopping amplitude t_{eff} is in proportion to the overlap integral between $|S+1/2, S, S_0\rangle$ and $|S, S+1/2, S_0\rangle$, where $|S_1, S_2, S_0\rangle$ indicates the state with spin S_i at site i and total spin S_0 . Note that S_0 is composed of two localized spins and one itinerant spin. The overlap integral is evaluated as $\langle S+1/2, S, S_0 | S, S+1/2, S_0 \rangle = 2(S+1)W(S, 1/2, S_0, S; S+1/2, S+1/2)$, where W is the so-called Racah coefficient for the combination of three spins. By using some relations for the Racah coefficient [138], we obtain $|t_{\text{eff}}/t| = (S_0 + 1/2)/(2S + 1)$.

For $S=1/2$, we can intuitively understand the meaning of the reduction factor. When the two localized spins are parallel, we obtain $S_0=3/2$ due to the large J and the reduction factor is unity. This is understood by the fact that the local triplet formed by the large J is not destroyed in the course of electron hopping motion. However, when the two localized spins are anti-parallel, $S_0=1/2$ and the reduction factor is $1/2$. In this case, it is necessary to reconstruct the local triplet state after the hopping of electron, leading to the effective reduction of the electron hopping. For the case of large S , the localized spins are considered classical. When we define an angle θ between nearest-neighbor ones, the above overlap integral is easily evaluated by rotating the itinerant electron basis so as to be parallel to the localized spin direction. Then, we obtain $t_{\text{eff}} = t \cos(\theta/2)$, as shown by Anderson and Hasegawa. If $\theta=0$ the hopping is the largest, while if $\theta=\pi$, corresponding to an AF background, then the hopping cancels.

Note that the oxygen linking the Mn-ions is crucial to understand the origin of the word “double” in this process. Nevertheless, the majority of the theoretical work carried out in the context of manganites simply forgets the presence of the oxygen and uses a manganese-only Hamiltonian. It is interesting to observe that FM states appear in this context even without the oxygen. It is clear that the electrons simply need a polarized background to improve their kinetic energy, as shown in Fig. 4(c), in similar ways as the Nagaoka phase is generated in the one-band Hubbard model at large U/t . This tendency to optimize the kinetic energy is at work in a variety of models and the term double-exchange appears unnecessary. However, in spite of this fact, it has become customary to refer to virtually any FM phase found in manganese models as “DE induced” or “DE generated”, forgetting the historical origin of the term. In this review, a similar convention will be followed, namely the credit for the appearance of FM phases will be given to the DE mechanism, although a more general and simple kinetic-energy optimization is certainly at work. This is also the reason why we have used the abbreviation “DE” in the model for manganites.

Early theoretical work on manganites carried out by Goodenough [139] explained many of the features observed in the neutron scattering experiments on $\text{La}_{1-x}\text{Ca}_x\text{MnO}_3$ by Wollan and Koehler [8], notably the appearance of the A-type AF phase at $x=0$ and the CE-type phase at $x=0.5$. The approach of Goodenough was based on the notion of “semicovalent exchange”. Analyzing the various possibilities for the orbital directions and generalizing to the case where Mn^{4+} ions are also present, Goodenough arrived to the A- and CE-type phases of manganites very early in the theoretical study of these compounds. In this line of reasoning, note that the Coulomb interactions are important

to generate Hund-like rules and the oxygen is also important to produce the covalent bonds. The lattice distortions are also quite relevant in deciding which of the many possible states minimizes the energy. However, it is interesting to observe that in more recent theoretical work described below in this review, both the A- and CE-type phases can be generated without the explicit appearance of oxygens in the models and also without including long-range Coulomb terms.

3.2. Topological aspects of orbital ordering

In Sec. 2, we have already set the model Hamiltonian for manganites H_{DE} . Before proceeding to the exhibition of the theoretical results on this model, we explain the essential point of manganites from a purely theoretical viewpoint. We believe that it is an important issue to establish a simple principle penetrating the complicated phenomena.

3.2.1. A simplified model In order to extract the essential feature of manganites, let us define a minimal model, since H_{DE} is still a complex model. We note that there exist two important ingredients which should be kept even in the minimal model. One is the existence of orbital degree of freedom and another is a competition between FM metallic and AF insulating tendencies. In order to minimize the model by keeping these two issues, first we simply ignore the interaction terms, $H_{\text{el-el}}^{e_g}$, $H_{\text{el-ph}}^{e_g}$, and $H_{\text{inter-site}}^C$. Second, we take an infinite limit of the Hund's rule coupling, J_{H} , between e_g electron and t_{2g} spins. Then, the direction of e_g -electron spin perfectly follows that of t_{2g} spin. We can suppress the spin index, if we define the spinless operator at each site in which the spin direction is fixed as that of t_{2g} spin at each site. Namely, the model is virtually expressed by using spinless operators with orbital degree of freedom. Then, we obtain a simplified double-exchange model as

$$H = - \sum_{\mathbf{i}, \mathbf{a}, \gamma, \gamma'} D_{\mathbf{i}, \mathbf{i}+\mathbf{a}} t_{\gamma, \gamma'}^{\mathbf{a}} c_{\mathbf{i}\gamma}^{\dagger} c_{\mathbf{i}+\mathbf{a}\gamma'} + J_{\text{AF}} \sum_{\langle \mathbf{i}, \mathbf{j} \rangle} S_{\mathbf{i}}^z S_{\mathbf{j}}^z, \quad (65)$$

where $c_{\mathbf{i}\gamma}$ is the annihilation operator for spinless d electron in the γ orbital at site \mathbf{i} , the hopping amplitudes are given in Eqs. (55), (56), and (57), where $t_1 = -t_0$ with $t_0 = (pd\sigma)^2 / (\varepsilon_p - \varepsilon_d)$, and $D_{\mathbf{i}, \mathbf{j}}$ is the so-called double-exchange factor, given by

$$D_{\mathbf{i}, \mathbf{j}} = \cos(\theta_{\mathbf{i}}/2) \cos(\theta_{\mathbf{j}}/2) + \sin(\theta_{\mathbf{i}}/2) \sin(\theta_{\mathbf{j}}/2) e^{-i(\phi_{\mathbf{i}} - \phi_{\mathbf{j}})}. \quad (66)$$

Here $\theta_{\mathbf{i}}$ and $\phi_{\mathbf{i}}$ denote the polar and azimuthal angles of t_{2g} spin at site \mathbf{i} , respectively. This factor expresses the change of hopping amplitude due to the difference in angles between t_{2g} -spins at sites \mathbf{i} and \mathbf{j} . Note that the effective hopping in this case is a complex number (Berry phase), contrary to the real number widely used in a large number of previous investigations. As for the effect of the Berry phase in the case of the one-orbital DE model, readers should refer Ref. [140].

Furthermore, when we assume the Ising t_{2g} spins, the double-exchange factor $D_{\mathbf{i}, \mathbf{j}}$ denotes 0 or 1 depending on the spin configuration. Namely, $D_{\mathbf{i}, \mathbf{j}} = 1$ for FM t_{2g} spin

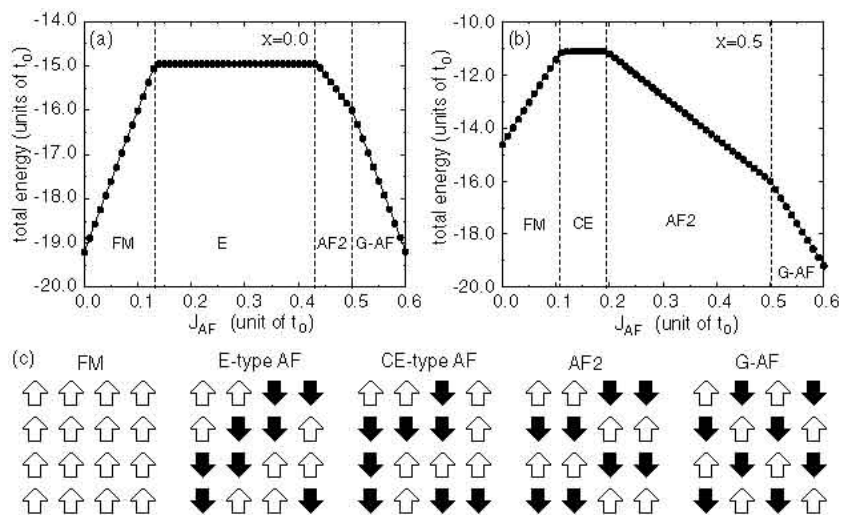


Figure 5. Ground-state energy vs. J_{AF} for (a) $x=0.0$ and (b) $x=0.5$ of a simplified model. The unit cell is taken as a 4×4 lattice. (c) Schematic views for spin structure of FM, E-type AF, CE-type AF, AF2, and G-AF phases.

pair at sites \mathbf{i} and \mathbf{j} , while $D_{\mathbf{i},\mathbf{j}}=0$ for AF pair. One may feel that the model seems to be oversimplified, but as will see later, we can grasp an essential point of complex phases of manganites, since the competition between FM metallic and AF insulating natures is correctly included in this model.

3.2.2. Band-insulating state First let us consider two limiting situations, $J_{AF}=0$ and $J_{AF} \gg t_0$. For simplicity, a two-dimensional (2D) square lattice is taken here. For $J_{AF}=0$, it is easy to understand the appearance of FM metallic phase, since the Hamiltonian includes only the kinetic term of electrons in this limit. On the other hand, for $J_{AF} \gg t_0$, AF insulating phase should appear due to the magnetic energy gain. Then, what happens for intermediate value of J_{AF} ? Naively thinking, it is possible to consider the mixture of FM and AF regions, in order to gain both kinetic and magnetic energies. For instance, we can consider the C-type AF phase, in which one-dimensional (1D) FM chains are antiferromagnetically coupled with each other. However, there is no special reason to fix the shape of the FM region as straight 1D chain. It may be possible to have zigzag shape for the FM region.

In order to determine the optimal shape of the FM region, we perform simple simulations for magnetic structure in the 2D lattice [141]. Since the model does not include explicit many-body interaction among e_g electrons, we can solve the problem on the periodic lattice composed of an appropriate unit cell such as 4×4 cluster. Namely, we prepare all possible patterns for t_{2g} spin configuration and evaluate the ground state energy on each magnetic structure by changing the value of J_{AF} . Note that the calculations have been done on the momentum space by introducing the Bloch phase factor at the boundary.

The results for $x=0.0$ and 0.5 are shown in Figs. 5(a) and 5(b), where x denotes hole doping from the case of quarter filling, i.e., one electron per site with two orbitals. Note that $x=0.0$ corresponds to the case in which all sites are occupied by trivalent manganese ions, while $x=0.5$ indicates the situation in which half of the sites are occupied by Mn^{4+} . For $x=0.0$, there are four regions in Fig. 5(a). As mentioned above, we obtain 2D FM phase at $J_{\text{AF}}=0$, while for large J_{AF} , the G-AF phase appears, as expected. In the intermediate region, we observe the striped spin phase, characterized by zigzag FM path, as shown in Fig. 5(c). This structure is just the E-type AF phase. Note that the magnetic energy is cancelled in the E-type phase, since the numbers of FM and AF bonds are exactly equal. We also find a narrow window for another AF phase, called ‘‘AF2’’, between the E-type and G-type AF phases. In the present context, the appearance of this phase is not important.

For $x=0.5$, as shown in Fig. 5(b), the situation looks similar with the case of $x=0.0$, but among four magnetic phases, the spin structure in the region labeled by ‘‘CE’’ differs from that of the E-type phase at $x=0.0$. Namely, the period of the zigzag is different from that for $x=0.0$, as shown in Fig. 5(c). We emphasize here that the spin structure in the intermediate coupling is composed of a bundle of spin FM chains, each with the zigzag geometry, and with AF interchain coupling. This is just the CE-type AF phase. Note that the magnetic energy is also cancelled, since the numbers of FM and AF bonds are exactly equal in the CE-type phase.

Now we consider the reason why such complicated structure appears. For the time being, let us discuss what happens if the zigzag geometry of CE- or E-type is assumed, and how it compares with a straight line. A straightforward way is to calculate the energy band for the e_g electron system on the zigzag 1D path, since e_g electrons can move only in the FM region in the simplified model due to the double exchange factor. First we consider the C-type AF phase characterized by straight 1D path, even though it is not the ground state. As shown in Sec. 2, the hopping amplitudes of e_g electrons depend on the direction, but as easily checked by a diagonalization of 2×2 matrix, due to the cubic symmetry, the energy band does not depend on the chain direction. Then, by choosing the hopping direction along the z -axis, we easily obtain $E_k=0$ and $-2t_0 \cos k$, since there is non-zero hopping amplitude only between $3z^2 - r^2$ orbitals along this direction.

To solve the present one-body problem in the zigzag 1D case, unit cells are defined as shown in Figs. 6(a) and 6(b), in which the hopping amplitudes change with a period of two or four lattice spacings for E- and CE-type structure, respectively, since the hopping direction changes as $\{\dots, x, y, x, y, \dots\}$ and $\{\dots, x, x, y, y, \dots\}$ along the zigzag chain, with $t_{\mu\nu}^x = -t_{\mu\nu}^y$ for $\mu \neq \nu$ according to the values of the hopping amplitudes discussed before. This difference in sign, i.e., the phase change, is essential for this problem. To make this point clear, it is useful to transform the spinless e_g -electron operators by using

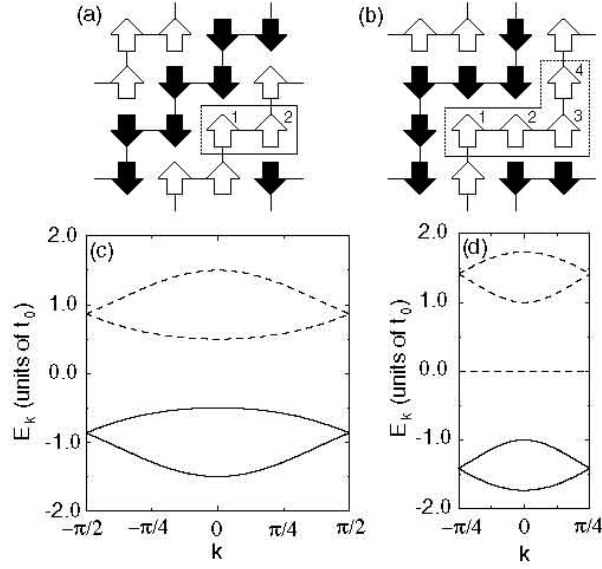


Figure 6. Definition of the unit cell for (a) E-type and (b) CE-type 1D zigzag chain. Momentum is defined along the zigzag chain. Energy band structure for (c) E-type and (d) CE-type structure. Solid and broken curves denote occupied and unoccupied bands, respectively. Note that the flat band in (d) has four-fold degeneracy.

a unitary matrix as

$$\begin{pmatrix} \alpha_i \\ \beta_i \end{pmatrix} = \frac{1}{\sqrt{2}} \begin{pmatrix} 1 & i \\ 1 & -i \end{pmatrix} \begin{pmatrix} c_{ia} \\ c_{ib} \end{pmatrix}. \quad (67)$$

After simple algebra, H_{kin} is rewritten as

$$H_{\text{kin}} = -t_0/2 \sum_{\mathbf{i}, \mathbf{a}} (\alpha_{\mathbf{i}}^\dagger \alpha_{\mathbf{i}+\mathbf{a}} + \beta_{\mathbf{i}}^\dagger \beta_{\mathbf{i}+\mathbf{a}} + e^{i\phi_{\mathbf{a}}} \alpha_{\mathbf{i}}^\dagger \beta_{\mathbf{i}+\mathbf{a}} + e^{-i\phi_{\mathbf{a}}} \beta_{\mathbf{i}}^\dagger \alpha_{\mathbf{i}+\mathbf{a}}), \quad (68)$$

where the phase $\phi_{\mathbf{a}}$ depends only on the hopping direction, and it is given by $\phi_{\mathbf{x}} = -\phi$, $\phi_{\mathbf{y}} = \phi$, and $\phi_{\mathbf{z}} = \pi$, with $\phi = \pi/3$. Note that the e_g -electron picks up a phase change when it moves between different neighboring orbitals. In this expression, the effect of the change of the local phase is correctly included in the Hamiltonian.

Here we solve the problem in the E-type structure. Details of the solutions of the CE-type structure have found in the previous review [3]. To introduce the momentum k along the zigzag chain, the Bloch's phase $e^{\pm ik}$ is added to the hopping term between adjacent sites. Then, the problem is reduced to finding the eigenvalues of a 4×4 matrix, given by

$$\hat{h} \begin{pmatrix} \psi_{\alpha 1} \\ \psi_{\beta 1} \\ \psi_{\alpha 2} \\ \psi_{\beta 2} \end{pmatrix} = \varepsilon_k \begin{pmatrix} \psi_{\alpha 1} \\ \psi_{\beta 1} \\ \psi_{\alpha 2} \\ \psi_{\beta 2} \end{pmatrix}, \quad (69)$$

where $\psi_{\alpha j}$ and $\psi_{\beta j}$ are the basis function for α - and β -electrons at the j -site of the unit

cell, respectively, and the Hamiltonian matrix \hat{h} is given by

$$\hat{h} = -t_0 \begin{pmatrix} 0 & 0 & \cos k & \cos(k - \phi) \\ 0 & 0 & \cos(k + \phi) & \cos k \\ \cos k & \cos(k + \phi) & 0 & 0 \\ \cos(k - \phi) & \cos k & 0 & 0 \end{pmatrix}. \quad (70)$$

To make the Hamiltonian in a block diagonalized form, we introduce two kinds of bonding and antibonding states as $\Phi_1^\pm = (\psi_{\alpha 1} \pm \psi_{\beta 1} \pm \psi_{\alpha 2} + \psi_{\beta 2})/2$ and $\Phi_2^\pm = (\psi_{\alpha 1} \mp \psi_{\beta 1} \pm \psi_{\alpha 2} - \psi_{\beta 2})/2$. For the states 1 and 2, we obtain two eigen equations as

$$-(t_0/2) \begin{pmatrix} 3 \cos k & \sqrt{3} \sin k \\ \sqrt{3} \sin k & -\cos k \end{pmatrix} \begin{pmatrix} \Phi_1^+ \\ \Phi_1^- \end{pmatrix} = E_k^{(1)} \begin{pmatrix} \Phi_1^+ \\ \Phi_1^- \end{pmatrix}, \quad (71)$$

and

$$-(t_0/2) \begin{pmatrix} \cos k & -\sqrt{3} \sin k \\ -\sqrt{3} \sin k & -3 \cos k \end{pmatrix} \begin{pmatrix} \Phi_2^+ \\ \Phi_2^- \end{pmatrix} = E_k^{(2)} \begin{pmatrix} \Phi_2^+ \\ \Phi_2^- \end{pmatrix}, \quad (72)$$

respectively. We can easily diagonalize each 2×2 matrix and obtain

$$E_k^{(1)} = (t_0/2)(-\cos k \pm \sqrt{\cos^2 k + 3}) \quad (73)$$

and

$$E_k^{(2)} = (t_0/2)(\cos k \pm \sqrt{\cos^2 k + 3}). \quad (74)$$

For the case of CE-type AF phase, it is necessary to solve eigen value problem in the 8×8 matrix. Readers interested in the detail of the calculations can refer the review article by Dagotto, Hotta, and Moreo [3]. Here we show only the results. Eight eigen energies have been obtained as

$$E_k = 0, \pm t_0 \sqrt{2 + \cos(2k)}, \pm t_0 \sqrt{2 - \cos(2k)}, \quad (75)$$

where the flat band $\varepsilon_{\mathbf{k}}=0$ has four-fold degeneracy.

The band structures for E-type and CE-type zigzag path are shown in Figs. 6(c) and 6(d). Note that the solid curves denote the occupied bands. The most remarkable feature is that the system is *band-insulating*, with a bandgap of value t_0 for $x=0.0$ [30, 31] and $x=0.5$ [141]. Remark that the band-insulator state at $x=0.5$ was independently obtained in Refs. [142, 143, 144]. This band insulating state, without any explicit potential among the electrons moving along the zigzag chains, is caused by the phase difference between $t_{\mu\nu}^x$ and $t_{\mu\nu}^y$. Since t_0 is at least of the order of 1000K, this band-insulating state is considered to be very robust.

Intuitively, the band-insulating state of the zigzag AF structure originates in the presence of a standing-wave state due to the interference between two traveling waves running along the x - and y -directions. In this interference picture, the nodes of the wavefunction can exist on the ‘‘corner’’ of the zigzag structure, and the probability amplitude becomes larger in the ‘‘straight’’ segment of the path. Thus, even a weak potential can produce the charge and orbital ordering based on this band-insulating

phase. In fact, if some potential is included into such an insulating phase, the system maintains its “insulating” properties, and a spatial modulation in the charge density appears. For $x=0.5$, since the charge density should be increased in the sites 2 and 4 in Fig. 6(b), it is easy to understand that checker-board type charge ordering occurs, when some potential is further included in the model.

Concerning the orbital shape, we should point out that the e_g -electron orbital is maximally polarized along the transfer direction in order to gain the kinetic energy. This effect may be called an “orbital double-exchange” in the sense that the orbitals align along the axis direction to make the transfer of the electron smooth, similarly as the FM alignment of t_{2g} spins in the usual DE mechanism. Namely, on the straight-line part in the x - and y -direction, the orbital is polarized as $3x^2 - r^2$ and $3y^2 - r^2$, respectively.

On the other hand, for the case of $x=0$, there is no straight-line part in the E-type zigzag structure. In this case, rather the cooperative Jahn-Teller effect is essential to determine the orbital shape, since each site is Jahn-Teller active. We cannot determine the orbital ordering pattern within the present simple discussion. It is necessary to consider a more realistic Hamiltonian. The actual orbital ordering will be discussed later.

3.2.3. Topological number In the previous subsection, we have emphasized that the shape of zigzag path plays an important role for the determination of the CE- and E-type AF phases. Now let us consider the quantity to specify the zigzag shape. For the purpose, we include the coupling between e_g electrons and JT phonons. Effect of Coulomb interaction will be discussed later. The model is given by

$$H = - \sum_{\mathbf{i}, \mathbf{a}, \gamma, \gamma'} D_{\mathbf{i}, \mathbf{i}+\mathbf{a}} t_{\gamma\gamma'}^{\mathbf{a}} c_{\mathbf{i}\gamma}^\dagger c_{\mathbf{i}+\mathbf{a}\gamma'} + J_{\text{AF}} \sum_{\langle \mathbf{i}, \mathbf{j} \rangle} \mathbf{S}_{\mathbf{i}} \cdot \mathbf{S}_{\mathbf{j}} + E_{\text{JT}} \sum_{\mathbf{i}} [2(q_{2\mathbf{i}} \tau_{x\mathbf{i}} + q_{3\mathbf{i}} \tau_{z\mathbf{i}}) + q_{2\mathbf{i}}^2 + q_{3\mathbf{i}}^2], \quad (76)$$

where E_{JT} is the static Jahn-Teller energy, $\tau_{x\mathbf{i}} = c_{\mathbf{i}\mathbf{a}}^\dagger c_{\mathbf{i}\mathbf{b}} + c_{\mathbf{i}\mathbf{b}}^\dagger c_{\mathbf{i}\mathbf{a}}$, and $\tau_{z\mathbf{i}} = c_{\mathbf{i}\mathbf{a}}^\dagger c_{\mathbf{i}\mathbf{a}} - c_{\mathbf{i}\mathbf{b}}^\dagger c_{\mathbf{i}\mathbf{b}}$. By using the phase $\xi_{\mathbf{i}}$ defined in Eq. (45), which is the angle to specify the Jahn-Teller distortion, it is convenient to transform $c_{\mathbf{i}\mathbf{a}}$ and $c_{\mathbf{i}\mathbf{b}}$ into the “phase-dressed” operators, $\tilde{c}_{\mathbf{i}\mathbf{a}}$ and $\tilde{c}_{\mathbf{i}\mathbf{b}}$, as

$$\begin{pmatrix} \tilde{c}_{\mathbf{i}\mathbf{a}} \\ \tilde{c}_{\mathbf{i}\mathbf{b}} \end{pmatrix} = \hat{R}(\xi_{\mathbf{i}}) \begin{pmatrix} c_{\mathbf{i}\mathbf{a}} \\ c_{\mathbf{i}\mathbf{b}} \end{pmatrix}. \quad (77)$$

where the unitary matrix $\hat{R}(\xi_{\mathbf{i}})$ is given by

$$\hat{R}(\xi_{\mathbf{i}}) = e^{i\xi_{\mathbf{i}}/2} \begin{pmatrix} \cos[\xi_{\mathbf{i}}/2] & \sin[\xi_{\mathbf{i}}/2] \\ -\sin[\xi_{\mathbf{i}}/2] & \cos[\xi_{\mathbf{i}}/2] \end{pmatrix}. \quad (78)$$

Note that if $\xi_{\mathbf{i}}$ is increased by 2π , the $\text{SU}(2)$ matrix itself changes its sign. This is the same phenomenon found in spin wavefunction, since in general, spinor is isomorphic to the wavefunction of a two-level system. In 1950’s, Longuet-Higgins et al. have pointed out that the electron wavefunction of Jahn-Teller molecule changes its sign for the

2π -rotation in the parameter space in the adiabatic approximation [145]. Note that the total wavefunction, given by the product of electron and phonon wavefunctions, is always single-valued, since the phonon part also changes its sign for the 2π -rotation. The spinor-like wavefunction for the electron part appears due to the adiabatic approximation for the JT system. It has been also mentioned that the change of sign is regarded as the effect of the Berry phase [146].

In order to keep the transformation unchanged upon a 2π -rotation in $\xi_{\mathbf{i}}$, a phase factor $e^{i\xi_{\mathbf{i}}/2}$ is needed. This is also regarded as the effect from the phonon wavefunction. In the expression for the ground state of the single JT molecule, namely, the single-site problem discussed before, this phase factor has not been considered explicitly, since the electron does not hop around from site to site and the phases do not correlate with each other. It was enough to pay attention to the fact that the electron wavefunction at a single site is double-valued. However, in the JT crystal in which e_g electrons move in the periodic array of the JT centers, the addition of this phase factor is useful to take into account the effect of the Berry phase arising from the circular motion of e_g -electrons around the JT center [147, 148]. It could be possible to carry out the calculation without including explicitly this phase factor, but in that case, it is necessary to pay due attention to the inclusion of the effect of the Berry phase. The qualitative importance of this effect will be explained later.

Note also that the phase $\xi_{\mathbf{i}}$ determines the electron orbital set at each site. In the previous section, the single-site problem was discussed and the ground-state at site \mathbf{i} was found to be

$$|\text{“b”}\rangle = [-\sin(\xi_{\mathbf{i}}/2)d_{\mathbf{ia}\sigma}^\dagger + \cos(\xi_{\mathbf{i}}/2)d_{\mathbf{ib}\sigma}^\dagger]|0\rangle, \quad (79)$$

which is referred to as the “b”-orbital, namely the combination with the lowest-energy at a given site. The excited-state or “a”-orbital is simply obtained by requesting it to be orthogonal to “b” as

$$|\text{“a”}\rangle = [\cos(\xi_{\mathbf{i}}/2)d_{\mathbf{ia}\sigma}^\dagger + \sin(\xi_{\mathbf{i}}/2)d_{\mathbf{ib}\sigma}^\dagger]|0\rangle. \quad (80)$$

For instance, at $\xi_{\mathbf{i}}=2\pi/3$, “a” and “b” denote the $d_{y^2-z^2}$ - and $d_{3x^2-r^2}$ -orbitals, respectively. It should be noted here that $d_{3x^2-r^2}$ and $d_{3y^2-r^2}$ never appear as the local orbital set. Sometimes those were treated as an orthogonal orbital set to reproduce the experimental results, but such a treatment is an approximation, since the orbital ordering is *not* due to the simple alternation of two arbitrary kinds of orbitals.

Using the above described transformations, the model Eq. (76) is rewritten after some algebra as

$$\begin{aligned} \tilde{H} = & - \sum_{\mathbf{ia}\gamma\gamma'} D_{\mathbf{i},\mathbf{i}+\mathbf{a}} \tilde{t}_{\gamma\gamma'}^{\mathbf{a}}(\mathbf{i}, \mathbf{i} + \mathbf{a}) \tilde{c}_{\mathbf{i}\gamma}^\dagger \tilde{c}_{\mathbf{i}+\mathbf{a}\gamma'} + J_{\text{AF}} \sum_{\langle \mathbf{i}, \mathbf{j} \rangle} \mathbf{S}_{\mathbf{i}} \cdot \mathbf{S}_{\mathbf{j}} \\ & + E_{\text{JT}} \sum_{\mathbf{i}} [2q_{\mathbf{i}}(\tilde{n}_{\mathbf{ia}} - \tilde{n}_{\mathbf{ib}}) + q_{\mathbf{i}}^2], \end{aligned} \quad (81)$$

where $\tilde{n}_{\mathbf{i}\gamma} = \tilde{c}_{\mathbf{i}\gamma}^\dagger \tilde{c}_{\mathbf{i}\gamma}$ and the hopping amplitude is changed as

$$\tilde{t}_{\gamma\gamma'}^{\mathbf{a}}(\mathbf{i}, \mathbf{j}) = \hat{R}(\xi_{\mathbf{i}})_{\gamma\eta} t_{\eta\eta'}^{\mathbf{a}} \hat{R}^{-1}(\xi_{\mathbf{j}})_{\eta'\gamma'}. \quad (82)$$

In order to characterize the shape of the zigzag path, it is useful to formulate the change of the phase. For the purpose, we use the concept of “the Berry-phase connection” and define “the winding number” by following Ref. [149]. The phase-dressed operator, $\tilde{c}_{i\gamma}$, naturally introduces a connection form, the Berry-phase connection, as [150]

$$\begin{aligned} A d\mathbf{r} &\equiv \begin{pmatrix} i\langle 0|\tilde{c}_{\mathbf{r}a}\nabla\tilde{c}_{\mathbf{r}a}^\dagger|0\rangle\cdot d\mathbf{r} & i\langle 0|\tilde{c}_{\mathbf{r}a}\nabla\tilde{c}_{\mathbf{r}b}^\dagger|0\rangle\cdot d\mathbf{r} \\ i\langle 0|\tilde{c}_{\mathbf{r}b}\nabla\tilde{c}_{\mathbf{r}a}^\dagger|0\rangle\cdot d\mathbf{r} & i\langle 0|\tilde{c}_{\mathbf{r}b}\nabla\tilde{c}_{\mathbf{r}b}^\dagger|0\rangle\cdot d\mathbf{r} \end{pmatrix} \\ &= \frac{1}{2} \begin{pmatrix} \nabla\xi\cdot d\mathbf{r} & -i\nabla\xi\cdot d\mathbf{r} \\ i\nabla\xi\cdot d\mathbf{r} & \nabla\xi\cdot d\mathbf{r} \end{pmatrix}, \end{aligned} \quad (83)$$

where $|0\rangle$ denotes the vacuum state.

Now we consider a 2D sheet of the JT crystal. In two space dimensions, there is a topologically conserved current for an arbitrary vector field \mathbf{v} as

$$j^\mu = \frac{1}{2\pi} \sum_{\nu,\lambda} \epsilon^{\mu\nu\lambda} \partial_\nu v_\lambda, \quad (84)$$

where \mathbf{j} is the current and $\epsilon^{\mu\nu\lambda}$ is the antisymmetric Levi-Civita tensor. This current obeys the continuity equation, expressed as

$$\sum_\mu \partial_\mu j^\mu = 0. \quad (85)$$

Therefore, if j^1 and j^2 are zero at the boundary of a closed surface S , the quantity Q (Chern number), defined by

$$Q \equiv \int_S d^2\mathbf{r} j^0 \quad (86)$$

is conserved, where indices 1 and 2 indicate the space-components and 0 indicates the time-component of a vector, respectively.

For time-independent solutions with which we are now concerned, we have $\partial_0 j^0 = 0$. Thus, Q is conserved for an arbitrary surface S . Substituting $\mathbf{a} = \text{Tr}(A) = \nabla\xi$ for \mathbf{v} into Eq. (84), we obtain the topologically conserved quantity, or “the winding number” as

$$\begin{aligned} w &= \int_S d^2\mathbf{r} j^0 = \frac{1}{2\pi} \int_S d^2\mathbf{r} (\partial_1 a_2 - \partial_2 a_1) \\ &= \frac{1}{2\pi} \oint_C d\mathbf{r} \cdot \mathbf{a} = \frac{1}{2\pi} \oint_C d\mathbf{r} \cdot \nabla\xi = m, \end{aligned} \quad (87)$$

where m is an integer representing the number for the twisting-around of the JT distortions along a path C enclosing S . Because of the conserved nature, we will use the winding number w to label a state hereafter.

In the system with zigzag AF structure, C is considered to be a closed loop for the 1D path in the periodic boundary condition. In this case, the winding number W may be decomposed into two terms as $w=w_g+w_t$. The former, w_g , is the geometric term, which becomes 0 (1) corresponding to the periodic (anti-periodic) boundary condition in the

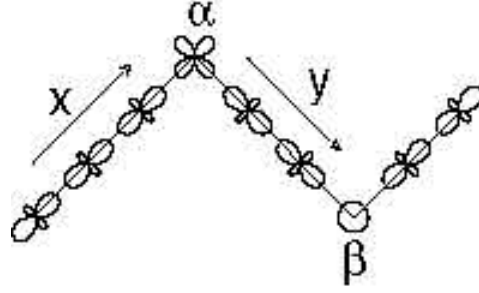


Figure 7. A typical building block for a zigzag 1D FM path for an e_g electron with orbital ordering.

e_g -electron wavefunction. The discussion on the kinetic energy leads us to conclude that the state with $w_g=0$ has lower energy than that with $w_g=1$ for $x \geq 1/2$, in agreement with the two-site analysis [151]. Thus, w_g is taken as zero hereafter.

In order to understand that only the number of corners in the zigzag path, N_v , determines the topological term w_t , let us consider the transfer of a single e_g electron along the path shown in Fig. 7. As mentioned above, on the straight-line part in the x -(y -)direction, the phase is fixed at $\theta_x=2\pi/3$ ($\theta_y=4\pi/3$), because the e_g -electron orbital is polarized along the transfer direction. Thus, w_t does not change on the straight-line part of the path. However, when the electron passes the vertex α (β), the phase changes from θ_x to θ_y (θ_y to θ_x), indicating that the electron picks up a phase change of $2\pi/3$ ($4\pi/3$). Since these two vertices appear in pairs, $w_t(=w)$ is evaluated as $w_t=(N_v/2)(2\pi/3+4\pi/3)/(2\pi)=N_v/2$. The phases at the vertices are assigned as an average of the phases sandwiching those vertices, $\theta_\alpha=\pi$ and $\theta_\beta=0$, to keep w_g invariant. Then, the phases are determined at all the sites, once θ_x , θ_y , θ_α , and θ_β are known.

Finally, we note that the problem in the zigzag one-dimensional chain provided us with a typical example to better understand the importance of the additional factor $e^{i\xi_i/2}$ in front of the 2×2 SU(2) unitary matrix to generate the phase dressed operator at each site. As clearly shown above, the “a” and “b” orbitals should be chosen as “a”= $y^2 - z^2$ and “b”= $3x^2 - r^2$ at site 2, and “a”= $z^2 - x^2$ and “b”= $3y^2 - r^2$ at site 4, respectively. Namely, $\xi_2=2\pi/3$ and $\xi_4=4\pi/3$. The reason for these choices of ξ_i is easily understood due to the fact that the orbital tends to polarize along the hopping direction to maximize the overlap. Thus, to make the Hamiltonian simple, it is useful to fix the orbitals at sites 2 and 4 as $\xi_2=2\pi/3$ and $\xi_4=4\pi/3$. Here, the phase factor $e^{i\xi_i/2}$ in the basis function is essential to reproduce exactly the same solution as obtained in the discussion above. As already mentioned, in a single-site problem, this phase factor can be neglected, since it provides only an additional phase to the whole wave function. However, if the e_g -electron starts moving from site to site, the accumulation of the phase difference between adjacent sites does not lead just to an additional phase factor to the whole wave function. In fact, if this additional phase is accidentally neglected, the band structure will shift in momentum space as $k \rightarrow k + \pi$, indicating that the minimum of

the lowest-energy band is not located at $k=0$, but at $k=\pi$, as already pointed out by Koizumi et al. [148]. Of course, this can be removed by the redefinition of k by including “the crystal momentum”, but it is not necessary to redefine k , if the local phase factors are correctly included in the problem.

3.2.4. Stability of zigzag structure Concerning the stability of the zigzag AF phase, from the results in Fig. 6, we can understand the following two points: (i) The zigzag structure of E- and CE-type shows the lowest energy compared with other zigzag paths with the same periodicity and compared with the straight 1D path. (ii) The energy of the zigzag AF phase becomes lower than that of the FM or other AF phases in the parameter region of J_{AF} around $J_{\text{AF}} \approx 0.1t_0$. However, in the calculation, we have just assumed the periodicity of four lattice spacing, but it is unclear whether such period actually produces the *global* ground state or not. As emphasized above, it is true that the zigzag 1D FM chain has a large band-gap, but this fact does not guarantee that this band-insulating phase is the lowest-energy state. In other words, we cannot exclude the possibility that the zigzag structure with another periodicity becomes the global ground state.

Unfortunately, it is quite difficult to carry out the direct comparison among the energies for all possible states, since there are infinite possibilities for the combinations of hopping directions. Instead, to mimic the periodic change of the phase $\phi_{\mathbf{a}}$ in the hopping process, let us imagine a virtual situation in which a JT distortion occurs in the 1D e_g -electron system, by following Koizumi et al. [147]. To focus on the effect of the local phase, it is assumed that the amplitude of the JT distortion q_i is independent of the site index, i.e., $q_i = q$, and only the phase ξ_i is changed periodically. For simplicity, the phase is uniformly twisted with the period of M lattice spacings, namely, $\xi_j = j \times (2\pi)/M$ for $1 \leq j \leq M$. Since the periodic change of the hopping direction is mimicked by the phase change of the JT distortion, $t_{\mu\nu}^{\mathbf{a}}$ is simply taken as the unit matrix $t_0 \delta_{\mu\nu}$ to avoid the double-counting of the effect of the phase change. If the potential amplitude is written as $v=2qE_{\text{JT}}$, the Hamiltonian for the present situation is given by

$$\begin{aligned}
 H = & -t_0 \sum_{\langle i,j \rangle} (c_{ia}^\dagger c_{ja} + c_{ib}^\dagger c_{jb} + \text{h.c.}) \\
 & + v \sum_i [\sin \xi_i (c_{ia}^\dagger c_{ib} + c_{ib}^\dagger c_{ia}) + \cos \xi_i (c_{ia}^\dagger c_{ia} - c_{ib}^\dagger c_{ib})], \quad (88)
 \end{aligned}$$

where the spinless e_g -electron operator is used, since the 1D FM chain is considered here. The potential term for the JT distortion is ignored, since it provides only a constant energy shift in this case. By using the transformation Eqs. (77) and (78), the Hamiltonian is rewritten as

$$\begin{aligned}
 H = & -t_0 \sum_{\langle i,j \rangle} [e^{i(\xi_i - \xi_j)/2} \{ \cos \frac{\xi_i - \xi_j}{2} (\tilde{c}_{ia}^\dagger \tilde{c}_{ja} + \tilde{c}_{ib}^\dagger \tilde{c}_{jb}) \\
 & + \sin \frac{\xi_i - \xi_j}{2} (\tilde{c}_{ia}^\dagger \tilde{c}_{jb} - \tilde{c}_{ib}^\dagger \tilde{c}_{ja}) \} + \text{h.c.}] + v \sum_i (\tilde{c}_{ia}^\dagger \tilde{c}_{ia} - \tilde{c}_{ib}^\dagger \tilde{c}_{ib}). \quad (89)
 \end{aligned}$$

The Hamiltonian in momentum space is obtained by the Fourier transform as

$$\begin{aligned}
H = & \sum_k [\varepsilon_k \cos(\pi/M) (\tilde{c}_{ka}^\dagger \tilde{c}_{ka} + \tilde{c}_{kb}^\dagger \tilde{c}_{kb}) + i s_k \sin(\pi/M) (\tilde{c}_{ka}^\dagger \tilde{c}_{kb} - \tilde{c}_{kb}^\dagger \tilde{c}_{ka})] \\
& + v \sum_k (\tilde{c}_{ka}^\dagger \tilde{c}_{ka} - \tilde{c}_{kb}^\dagger \tilde{c}_{kb}), \tag{90}
\end{aligned}$$

where $\varepsilon_k = -2t_0 \cos k$, $s_k = -2t_0 \sin k$, and the periodic boundary condition is imposed. Note that in this expression, k is the generalized quasimomentum, redefined as $k - \pi/M \rightarrow k$, to incorporate the additional phase π/M which appears to arise from a fictitious magnetic field (see Ref. [148]). The eigenenergies are easily obtained by diagonalization as

$$\begin{aligned}
E_k^\pm = & \varepsilon_k \cos(\pi/M) \pm \sqrt{v^2 + s_k^2 \sin^2(\pi/M)} \\
= & (1/2) [\varepsilon_{k+\pi/M} + \varepsilon_{k-\pi/M} \pm \sqrt{4v^2 + (\varepsilon_{k+\pi/M} - \varepsilon_{k-\pi/M})^2}]. \tag{91}
\end{aligned}$$

Since this is just the coupling of two bands, $\varepsilon_{k+\pi/M}$ and $\varepsilon_{k-\pi/M}$, it is easily understood that the energy gain due to the opening of the bandgap is the best for the filling of $n=2/M$, where $n=1-x$ with doping x . In other words, when the periodicity M is equal to $2/n$, the energy becomes the lowest among the states considered here with several possible periods. Although this is just a proof in an idealized special situation, it is believed that it captures the essence of the problem.

Here the effect of the local phase factor $e^{i\xi_i/2}$ should be again noted. If this factor is dropped, the phase π/M due to the fictitious magnetic field disappears and the eigenenergies are given by the coupling of $\varepsilon_{k+\pi+\pi/M}$ and $\varepsilon_{k+\pi-\pi/M}$, which has been also checked by the computational calculation. This “ π ” shift in momentum space appears at the boundary, modifying the periodic boundary condition to anti-periodic, even if there is no intention to use anti-periodic boundary condition. Of course, this is avoidable when the momentum k is redefined as $k + \pi \rightarrow k$, as pointed out in Ref. [148]. However, it is natural that the results for periodic boundary condition are obtained in the calculation using periodic boundary condition. Thus, also from this technical viewpoint, it is recommended that the phase factor $e^{i\xi_i/2}$ is added for the local rotation in the orbital space.

3.2.5. Summary In summary, at $x=0.5$, the CE-type AF phase can be stabilized even without the Coulomb and/or the JT phononic interactions, only with large Hund and finite J_{AF} couplings. We have also pointed out the appearance of E-type phase due to the same mechanism. Of course, as we will see in the next subsection, Coulombic and JT phononic interactions are needed to reproduce the charge and orbital ordering. However, as already mentioned in the above discussion, because of the special geometry of the one-dimensional zigzag FM chain, for instance, at $x=0.5$, it is easy to imagine that the checkerboard type charge-ordering and $(3x^2 - r^2/3y^2 - r^2)$ orbital-ordering pattern will be stabilized. Furthermore, the charge confinement in the straight segment, i.e., sites 2 and 4 in Fig. 6(b), will naturally lead to charge stacking along the z -axis, with

stability caused by the special geometry of the zigzag structure. Thus, the complex spin-charge-orbital structure for half-doped manganites can be understood intuitively simply from the viewpoint of its band-insulating nature.

3.3. Spin, charge, and orbital ordering

Now we review the theoretical results on spin, charge, and orbital ordering in undoped and doped manganites on the basis of realistic models. The Hamiltonian mainly used here is two-orbital double exchange model strongly coupled with Jahn-Teller phonons, explicitly given by

$$H = H_{\text{kin}}^{\text{eg}} + H_{\text{Hund}} + H_{\text{inter-site}}^{\text{AF}} + H_{\text{el-ph}}^{\text{eg}}. \quad (92)$$

In the infinite limit for J_{H} , we can further simplify the model into the following form.

$$\begin{aligned} H_{\text{JT}} = & - \sum_{\mathbf{i}\mathbf{a}\gamma\gamma'} D_{\mathbf{i},\mathbf{i}+\mathbf{a}} t_{\gamma\gamma'}^{\mathbf{a}} c_{\mathbf{i}\gamma}^{\dagger} c_{\mathbf{i}+\mathbf{a}\gamma'} + J_{\text{AF}} \sum_{\langle\mathbf{i},\mathbf{j}\rangle} \mathbf{S}_{\mathbf{i}} \cdot \mathbf{S}_{\mathbf{j}} \\ & + E_{\text{JT}} \sum_{\mathbf{i}} [2(q_{1\mathbf{i}} n_{\mathbf{i}} + q_{2\mathbf{i}} \tau_{x\mathbf{i}} + q_{3\mathbf{i}} \tau_{z\mathbf{i}}) + \beta q_{1\mathbf{i}}^2 + q_{2\mathbf{i}}^2 + q_{3\mathbf{i}}^2], \end{aligned} \quad (93)$$

where $n_{\mathbf{i}} = \sum_{\gamma} c_{\mathbf{i}\gamma}^{\dagger} c_{\mathbf{i}\gamma}$ and $\beta = k_{\text{br}}/k_{\text{JT}}$, the ratio of spring constants of breathing and Jahn-Teller phonons. Concerning the value of β , from experimental results and band-calculation data for the energy of breathing and Jahn-Teller modes [152], it is estimated as $\beta \approx 2$ for manganites. It is convenient to introduce non-dimensional electron-phonon coupling constant λ as

$$\lambda = \sqrt{2E_{\text{JT}}/t_0} = g/\sqrt{k_{\text{JT}}t_0}. \quad (94)$$

Here we simply drop the Coulomb interaction terms, but the reason will be discussed in the next subsection.

This model is analyzed by using both the numerical techniques (Monte Carlo simulation and relaxation method) and mean-field approximation. Note that in the numerical simulations, depending on the non-cooperative and cooperative treatments, the variables are angles $\theta_{\mathbf{i}}$ and $\phi_{\mathbf{i}}$ which specifies $t_{2\text{g}}$ spin directions and coordinates $\{q\}$ and oxygen positions $\{u\}$, respectively. In any case, all variables are classical and thus, there is no essential problems to perform almost exactly the simulation, within the limit of the power of computers. Recently, there has been an important progress in the simulation for the electron systems coupled with classical variables [153, 154, 155]. In particular, Motome and Furukawa have developed the efficient simulation technique for the acceleration of the calculation and the increase of the precision [154, 155].

3.3.1. Effect of Coulomb interaction Let us discuss briefly the effect of the Coulomb interaction. Since we consider the strong Hund's rule interaction between e_{g} electron and $t_{2\text{g}}$ localized spins, e_{g} electron spins tend to array in a site and thus, the effect of intra-orbital Coulomb interaction is automatically suppressed. However, inter-orbital Coulomb interaction still works between electrons with the same spin. Here we explain

the reason why we ignore the on-site Coulomb interaction. The effect of inter-site Coulomb interaction is discussed in the stabilization mechanism of charge stacking in the $x=0.5$ CE-type structure.

In the spinless model, the inter-orbital Coulomb interaction term is written by

$$H_{\text{el-el}} = U' \sum_{\mathbf{i}} n_{\mathbf{ia}} n_{\mathbf{ib}}, \quad (95)$$

where $n_{\mathbf{i}\gamma} = c_{\mathbf{i}\gamma}^\dagger c_{\mathbf{i}\gamma}$ and the present U' means $U' - J$ in the standard notation for the on-site Coulomb interaction. We also consider the inter-site Coulomb interaction term, given by

$$H_{\text{inter-site}} = V \sum_{\langle \mathbf{i}, \mathbf{j} \rangle} n_{\mathbf{i}} n_{\mathbf{j}}, \quad (96)$$

where $n_{\mathbf{i}} = \sum_{\gamma} c_{\mathbf{i}\gamma}^\dagger c_{\mathbf{i}\gamma}$. In order to understand the ignorance of on-site Coulomb interaction term, it is quite instructive to consider the mean-field approximation. As for the detail of the formulation, readers can refer the original paper [156] and the previous review [3]. Here we show the result of the mean-field Hamiltonian.

$$\begin{aligned} H_{\text{MF}} = & - \sum_{\mathbf{ia}\gamma\gamma'} D_{\mathbf{i}, \mathbf{i}+\mathbf{a}} t_{\gamma\gamma'}^{\mathbf{a}} c_{\mathbf{i}\gamma}^\dagger c_{\mathbf{i}+\mathbf{a}\gamma'} + J_{\text{AF}} \sum_{\langle \mathbf{i}, \mathbf{j} \rangle} \mathbf{S}_{\mathbf{i}} \cdot \mathbf{S}_{\mathbf{j}} \\ & + \tilde{E}_{\text{JT}} \sum_{\mathbf{i}} [-2(\langle \tau_{x\mathbf{i}} \rangle \tau_{x\mathbf{i}} + \langle \tau_{z\mathbf{i}} \rangle \tau_{z\mathbf{i}}) + \langle \tau_{x\mathbf{i}} \rangle^2 + \langle \tau_{z\mathbf{i}} \rangle^2] \\ & + \sum_{\mathbf{i}} [(\tilde{U}'/2) \langle n_{\mathbf{i}} \rangle + V \sum_{\mathbf{a}} \langle n_{\mathbf{i}+\mathbf{a}} \rangle] (n_{\mathbf{i}} - \langle n_{\mathbf{i}} \rangle / 2), \end{aligned} \quad (97)$$

where $\langle \dots \rangle$ denotes the average value. The renormalized JT energy is given by

$$\tilde{E}_{\text{JT}} = E_{\text{JT}} + U'/4, \quad (98)$$

and the renormalized inter-orbital Coulomb interaction is expressed as

$$\tilde{U}' = U' - 4E_{\text{br}}, \quad (99)$$

where $E_{\text{br}} = g^2 / (2k_{\text{br}})$. Physically, the former relation indicates that the JT energy is effectively enhanced by U' . Namely, the strong on-site Coulombic correlation plays the *same* role as that of the JT phonon, at least at the mean-field level, indicating that it is not necessary to include U' explicitly in the models, as emphasized in Ref. [156]. See also Ref. [24]. The latter equation for \tilde{U}' means that the one-site inter-orbital Coulomb interaction is effectively reduced by the breathing-mode phonon, since the optical-mode phonon provides an effective attraction between electrons. The expected positive value of \tilde{U}' indicates that e_g electrons dislike double occupancy at the site, since the energy loss is proportional to the average local electron number in the mean-field argument. Thus, to exploit the gain due to the static JT energy and avoid the loss due to the on-site repulsion, an e_g electron will singly occupy a given site.

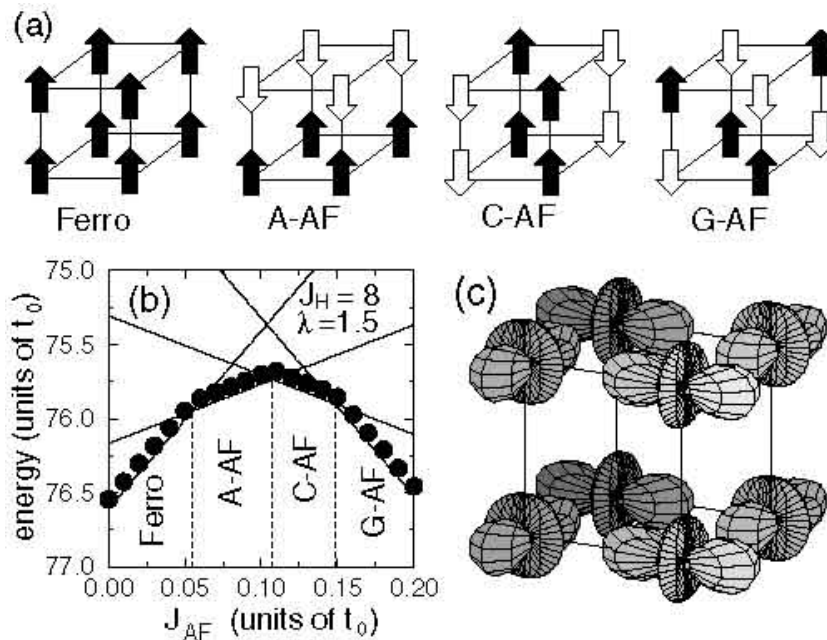


Figure 8. (a) The four spin arrangements for Ferro, A-AF, C-AF, and G-AF. (b) Total energy vs J_{AF} on a 2^3 cluster at low temperature with $J_H=8t_0$ and $\lambda=1.5$. The results were obtained using Monte Carlo and relaxational techniques, with excellent agreement among them. (c) Orbital order corresponding to the A-type AF state. For more details, the reader should consult Ref. [25].

3.3.2. $x=0$ First let us consider the mother material LaMnO_3 with one e_g electron per site. This material has the insulating AF phase with A-type AF spin order, in which t_{2g} spins are ferromagnetic in the a - b plane and AF along the c -axis. For the purpose to understand the appearance of A-AF phase, it is enough to consider a $2 \times 2 \times 2$ cube as a minimal cluster for undoped manganites. Results in a larger size cluster will be discussed later.

Recent investigations by Hotta et al. [25] have shown that, in the context of the model with Jahn-Teller phonons, the important ingredient to understand the A-type AF phase is J_{AF} , namely by increasing this coupling from 0.05 to larger values, a transition from a FM to an A-type AF exists. The relevance of Jahn-Teller couplings at $x=0.0$ has also been remarked in Ref. [27]. This can be visualized easily in Fig. 8, where the energy vs. J_{AF} at fixed intermediate λ and J_H is shown. Four regimes are identified: FM, A-AF, C-AF, and G-AF states that are sketched also in that figure. The reason is simple: As J_{AF} grows, the tendency toward spin AF must grow, since this coupling favors such an order. If J_{AF} is very large, then it is clear that a G-AF state must be the one that lowers the energy, in agreement with the Monte Carlo simulations. If J_{AF} is small or zero, there is no reason why spin AF will be favorable at intermediate λ and the density under consideration, and then the state is ferromagnetic to improve the electronic mobility. It should be no surprise that at intermediate J_{AF} , the dominant state is intermediate between the two extremes, with A-type and C-type antiferromagnetism

becoming stable in intermediate regions of parameter space.

It is interesting to note that similar results regarding the relevance of J_{AF} to stabilize the A-type order have been found by Koshibae et al. [15] in a model with Coulomb interactions. An analogous conclusion was found by Solovyev, Hamada, and Terakura [13, 14] and Ishihara et al. [17]. Betouras and Fujimoto [157], using bosonization techniques for the one-dimensional one-orbital model, also emphasized the importance of J_{AF} , similarly as did by Yi, Yu, and Lee based on Monte Carlo studies in two dimensions of the same model [158]. The overall conclusion is that there are clear analogies between the strong Coulomb and strong Jahn-Teller coupling approaches. Actually in the mean-field approximation, it was shown by Hotta, Malvezzi, and Dagotto [156] that the influence of the Coulombic terms can be hidden in simple redefinitions of the electron-phonon couplings (see also Ref. [24]). In our opinion, both approaches (Jahn-Teller and Coulomb) have strong similarities and it is not surprising that basically the same physics is obtained in both cases. Actually, Fig. 2 of Maezono, Ishihara, and Nagaosa [159] showing the energy vs. J_{AF} in mean-field calculations of the Coulombic Hamiltonian without phonons is very similar to our Fig. 8(b), aside from overall scales. On the other hand, Mizokawa and Fujimori [11, 12] states that the A-type AF is stabilized only when the Jahn-Teller distortion is included, namely, the FM phase is stabilized in the purely Coulomb model, based on the unrestricted Hartree-Fock calculation for the *d-p* model.

The issue of what kind of orbital order is concomitant with A-type AF order is an important matter. This has been discussed at length by Hotta et al. [25], and the final conclusion, after the introduction of perturbations caused by the experimentally known difference in lattice spacings between the three axes, is that the order shown in Fig. 8(c) minimizes the energy. This state has indeed been identified in resonant X-ray scattering experiments [10], and it is quite remarkable that such a complex pattern of spin and orbital degrees of freedom indeed emerges from mean-field and computational studies. Studies by van den Brink et al. [23] using purely Coulombic models arrived at similar conclusions. The orbital ordering has been also captured from the viewpoint of orbital density wave state by Koizumi et al. [147, 148]. The similar discussion has been done recently by Efremov and Khomskii [160].

Why does the orbital order occur here? In order to respond to this question, it is quite instructive to consider the situation perturbatively in the electron hopping. A hopping matrix only connecting the same orbitals, with hopping parameter t , is assumed for simplicity. The energy difference between e_g orbitals at a given site is E_{JT} , which is a monotonous function of λ . For simplicity, in the notation let us refer to orbital uniform (staggered) as orbital “FM” (“AF”). Case (a) corresponds to spin FM and orbital AF: In this case when an electron moves from orbital a on the left to the same orbital on the right, which is the only possible hopping by assumption, an energy of order E_{JT} is lost, but kinetic energy is gained. As in any second order perturbative calculation the energy gain is then proportional to t^2/E_{JT} . In case (b), both spin and orbital FM, the electrons do not move and the energy gain is zero (again, the nondiagonal hoppings are assumed negligible just for simplicity). In case (c), the spin are AF but the orbitals are FM. This

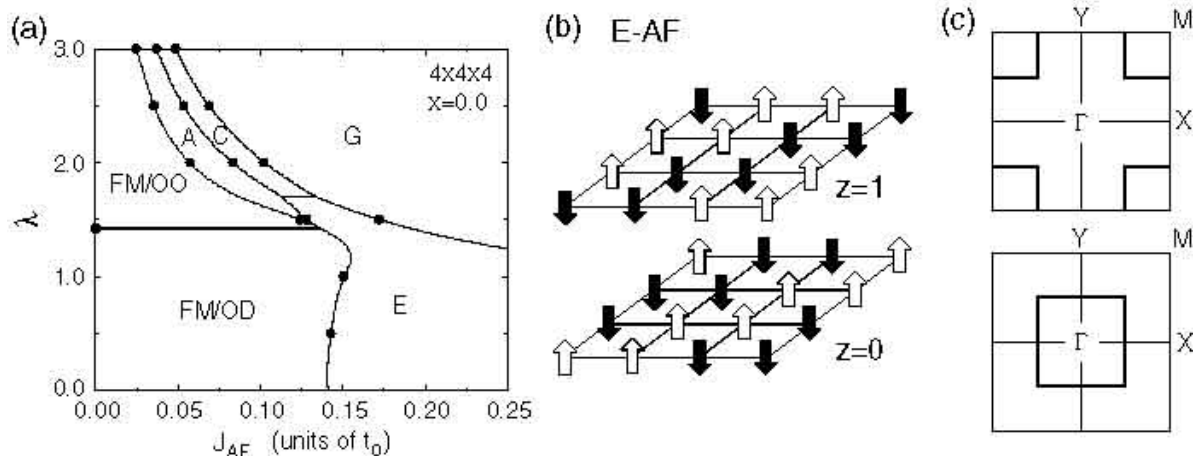


Figure 9. (a) Ground-state phase diagram for undoped manganites by using the $4 \times 4 \times 4$ lattice. Solid curves denote the mean-field results, while solid circles indicate the result for optimization. (b) Spin structure for E-AF phase in three-dimensional environment. (c) Fermi-surface lines of 2D e_g electron system at $x=0.0$.

is like a one orbital model and the gain in energy is proportional to $t^2/(2J_H)$. Finally, in case (d) with AF in spin and orbital, both Hund and orbital splitting energies are lost in the intermediate state, and the overall gain becomes proportional to $t^2/(2J_H + E_{JT})$. As a consequence, if the Hund coupling is larger than E_{JT} , then case (a) is the best, as it occurs at intermediate E_{JT} values. Then, the presence of orbital order can be easily understood from a perturbative estimation, quite similarly as done by Kugel and Khomskii in their pioneering work on orbital order [161].

Here readers may have a question in their mind. Where is the E-type phase emphasized in the previous subsection? In order to respond to this question, it is necessary to treat a larger-size cluster. In Fig. 9(a), we show the phase diagram of undoped manganites with the direct comparison between the mean-field and numerical results in the $4 \times 4 \times 4$ lattice [31]. Solid curves are depicted from the cooperative mean-field approximation, while solid circles denote the result for optimization both for t_{2g} spin directions and oxygen positions. The good agreements clearly indicate that the present mean-field procedure works quite well for undoped manganites.

Now the phase diagram includes six phases, but there is a clear separation around at $\lambda \approx 1.5$. For $\lambda > 1.5$, there occurs a chain of transitions in the order of FM, A-AF, C-AF, and G-AF phases with increasing J_{AF} , already obtained in $2 \times 2 \times 2$ calculations. Note that the boundary curve always indicates the first order transition. The present result shows that size effects are small in undoped strongly-coupled manganites, which is intuitively reasonable. The spin arrangement for each phase is shown in Fig. 8(a). Note that the FM phase is concomitant with orbital ordering (OO), which will be discussed later, and this FM/OO phase is considered to be insulating.

On the other hand, in the weak or intermediate coupling region for $\lambda < 1.5$, there is a transition between the FM orbital-disordered (OD) phase and E-type AF phase.

The spin arrangement for E-AF phase is shown in Fig. 9(b). Along the zigzag chains, t_{2g} spins order ferromagnetically, but they are antiparallel perpendicular to the zigzag direction. This is just the new AF phase, suggested by recent experiments on HoMnO_3 . As suggested in Fig. 9(b), the spin directions are reversed from plane to plane. Note that the orbital structure in the E-AF phase is the same as that of the A-AF phase, namely, the staggered pattern of $(3x^2-r^2)$ - and $(3y^2-r^2)$ -like orbitals. It is easily understood that the orbital ordering is closely related to the cooperative Jahn-Teller distortion in undoped manganites and such a cooperative effect should be very strong irrespective of the t_{2g} spin configuration.

Note that near $\lambda \sim 1.5$, which is a realistic value for manganites, the A-AF phase is adjacent to the E-type state. This region could correspond to the actual situation observed in experiments for RMnO_3 : When the ionic radius of the R-site decreases, a Néel temperature T_N of the A-AF phase decreases as well, and eventually the E-AF phase is stabilized for $\text{R}=\text{Ho}$. Another interesting point of the phase diagram is that the E-type spin arrangement is the ground-state for a wide range of J_{AF} , even at $\lambda=0$, indicating that the coupling with JT phonons is not a necessary condition for its stabilization. As pointed out in the previous subsection, the E-type phase is stable due to the zigzag geometry of the FM chains that induce a band-insulator. Namely, E-AF phase is always insulating irrespective of the value of λ .

Concerning the appearance of the E-AF phase, Kimura et al. have explained it on the basis of a frustrated spin system with FM nearest-neighbor and AF next-nearest-neighbor interactions within the MnO_2 plane [29]. They have found that the staggered orbital order associated with the GdFeO_3 -type distortion induced the anisotropic next-nearest-neighbor interaction, leading to unique sinusoidal and up-up-down-down AF order, i.e., E-type phase, in undoped manganites. In a conceptual level, the spin model is considered to be obtained in the strong coupling limit of the e_g -orbital degenerate double-exchange model. Thus, the band-insulating picture for the appearance of E-type phase in the present scenario is complementary to the result of Kimura et al., in the sense that the weak-coupling state is continuously connected to that in the strong-coupling limit.

In addition to the explanation of the A-AF of LaMnO_3 and E-AF of HoMnO_3 , Kimura et al. have also examined systematically the magnetic and orbital structures in a series of RMnO_3 as a function of r_R , the radius of rare-earth ion R. They have pointed out that the effect on the crystal structure by decreasing r_R appears as the enhancement of the GdFeO_3 -type distortion, indicating the shortening of oxygen-oxygen distance. Then, the superexchange interaction between next-nearest-neighbor sites is enhanced due to the shortened oxygen-oxygen path, leading to the frustrated spin model with the competition between FM nearest-neighbor and AF next-nearest-neighbor interactions. By analyzing the frustrated spin model on the staggered orbital-ordered background, Kimura et al. have explained the phase diagram of RMnO_3 . It is considered that the phase diagram can be also understood from the band-insulating picture, but for comparison with actual materials, it is necessary to include the effect of the GdFeO_3 -

type distortions, which has not been considered in the present model.

Near the transition region between A- and E-type AF phases, Salafranca and Brey have mentioned the importance of the competition between the nearest neighbor AF superexchange interaction and the double exchange induced long-range FM interaction [162]. They concluded that such competition results in the appearance of incommensurate phases. These phases consist of a periodic array of domain walls.

As discussed above, in the strong-coupling region, FM/OO insulating state appears, but when λ decreases, OO disappears and instead, an OD phase is observed. This is considered as a metallic phase, as deduced from the result of the density of states. Note that this metallic OD/FM phase is next to the insulating E-AF phase for $\lambda < 1.5$, which is a new and important result in the study of undoped manganites [163]. Namely, the competition between FM metallic and insulating phases is at the heart of the CMR phenomena, and then, by tuning experimentally the lattice parameters in RMnO_3 it may be possible to observe the magnetic-field induced metal-insulator transition even in undoped manganites.

Let us consider the reason why the metallic phase can exist even at half-filling. To clarify this point, it is quite useful to depict the Fermi-surface lines. As shown in Fig. 9(c), the nesting vector is $(\pi, 0)$ or $(0, \pi)$, *not* (π, π) . These nesting vectors are *not* compatible with the staggered orbital ordering pattern that is stabilized increasing λ . This is one of the remarkable features of the multiorbital e_g -electron system, which is not specific to two dimensionality. In fact, in the results for the three-dimensional (3D) case, we also observe the signal of the metal-insulator transition at a finite value of λ . In this case, the orbital ordering pattern becomes very complicated, but the pattern repeats periodically on lattice larger than $2 \times 2 \times 2$. In the 3D case, an intrinsic incompatibility between the Fermi surface and the orbital ordering pattern is also found. Even without invoking the numerical results discussed before, the qualitative arguments related with the nesting effects in H_{kin} incompatible with staggered orbital ordering strongly suggests the presence of a metallic phase in two and three dimensions at small λ .

3.3.3. $x=0.5$ Now let us move to another important doping $x=0.5$. For half-doped perovskite manganites, the so-called CE-type AF phase has been established as the ground state in the 1950's. This phase is composed of zigzag FM arrays of t_{2g} -spins, which are coupled antiferromagnetically perpendicular to the zigzag direction. Furthermore, the checkerboard-type charge ordering in the x - y plane, the charge stacking along the z -axis, and $(3x^2 - r^2/3y^2 - r^2)$ orbital ordering are associated with this phase. A schematic view of CE-type structure with charge and orbital ordering is shown in Fig. 10(a) for 2D case. In 3D, this pattern repeats along the z -axis by keeping charge and orbital structure, but changing spin directions.

Although there is little doubt that the famous CE-state of Goodenough is indeed the ground state of $x=0.5$ intermediate and low bandwidth manganites, only very recently such a state has received theoretical confirmation using unbiased techniques, at least within some models. In the early approach of Goodenough it was *assumed* that the

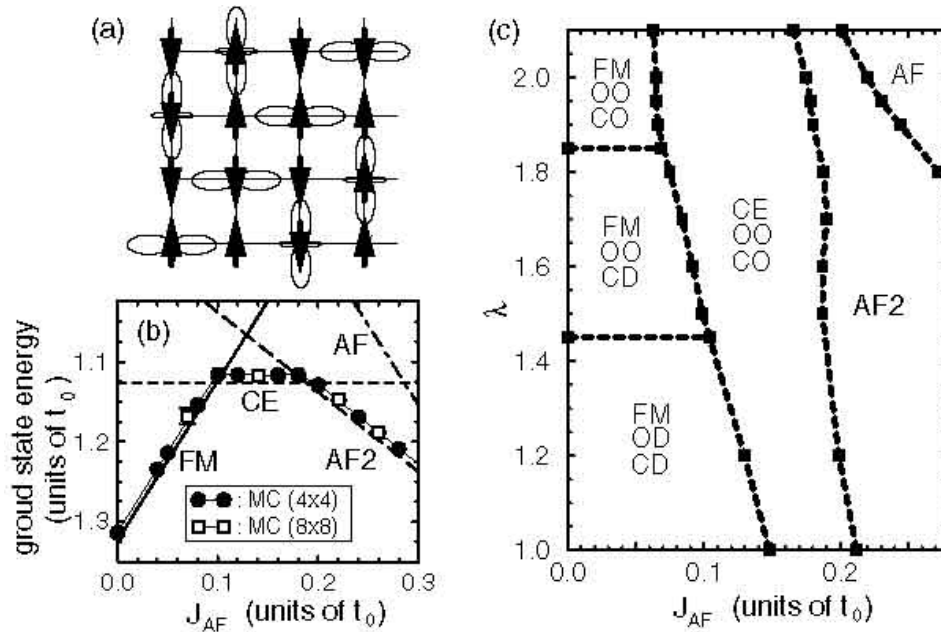


Figure 10. (a) Schematic view of CE-type structure at $x=0.5$ for 2D case. (b) Monte Carlo energy per site vs J_{AF} at density $x=0.5$, $\lambda=1.5$, low temperature $T=1/100$, and $J_H=\infty$, using the two-orbital model in two dimensions with non-cooperative Jahn-Teller phonons. As for AF2, see Fig. 6(c). (c) Phase diagram in the plane λ - J_{AF} at $x=0.5$, obtained numerically using up to 8×8 clusters. All transitions are of first-order. The notation is the standard one (CD = charge disorder, CO = charge order, OO = orbital order, OD = orbital disorder). Results are reproduced from Ref. [32] where more details can be found.

charge was distributed in a checkerboard pattern, upon which spin and orbital order was found. But it would be desirable to obtain the CE-state based entirely upon a more fundamental theoretical analysis, as the true state of minimum energy of a well-defined and realistic Hamiltonian. If such a calculation can be done, as a bonus one would find out which states compete with the CE-state in parameter space, an issue very important in view of the mixed-phase tendencies of Mn-oxides, which cannot be handled within the approach of Goodenough.

One may naively believe that it is as easy as introducing a huge nearest-neighbor Coulomb repulsion V to stabilize a charge-ordered state at $x=0.5$, upon which the reasoning of Goodenough can be applied. However, there are at least two problems with this approach [164]. First, such a large V quite likely will destabilize the FM charge-disordered state and others supposed to be competing with the CE-state. It may be possible to explain the CE-state with this approach, but not others also observed at $x=0.5$ in large bandwidth Mn-oxides. Second, a large V would produce a checkerboard pattern in the *three* directions. However, experimentally it has been known for a long time [8] that the charge *stacks* along the z -axis, namely the same checkerboard pattern is repeated along z -axis, rather than being shifted by one lattice spacing from plane to plane. A dominant Coulomb interaction V cannot be the whole story for $x=0.5$

low-bandwidth manganese oxides.

The nontrivial task of finding a CE-state without the use of a huge nearest-neighbors repulsion has been recently performed by Yunoki, Hotta, and Dagotto [32], using the two-orbital model with strong electron Jahn-Teller phonon coupling. The calculation proceeded using an unbiased Monte Carlo simulation, and as an output of the study, the CE-state indeed emerged as the ground-state in some region of coupling space. Typical results are shown in Figs. 10(b) and 10(c). In part (b) the energy at very low temperature is shown as a function of J_{AF} at fixed density $x=0.5$, $J_H=\infty$ for simplicity, and with a robust electron-phonon coupling $\lambda=1.5$ using the two orbital model H_{JT} . At small J_{AF} , a FM phase was found to be stabilized, according to the Monte Carlo simulation. Actually, at $J_{AF}=0.0$ it has not been possible to stabilize a partially AF-state at $x=0.5$, namely the states are always ferromagnetic at least within the wide range of λ 's investigated (but they can have charge and orbital order). On the other hand, as J_{AF} grows, a tendency to form AF links develops, as it happens at $x=0.0$. At large J_{AF} eventually the system transitions to states that are mostly antiferromagnetic, such as the so-called ‘‘AF(2)’’ state of Fig. 10(b) (with an up-up-down-down spin pattern repeated along one axis, and AF coupling along the other axis), or directly a fully AF-state in both directions.

However, the intermediate values of J_{AF} are the most interesting ones. In this case the energy of the two-dimensional clusters become flat as a function of J_{AF} suggesting that the state has the same number of FM and AF links, a property that the CE-state indeed has. By measuring charge-correlations it was found that a checkerboard pattern is formed particularly at intermediate and large λ 's, as in the CE-state. Finally, after measuring the spin and orbital correlations, it was confirmed that indeed the complex pattern of the CE-state was fully stabilized in the simulation. This occurs in a robust portion of the λ - J_{AF} plane, as shown in Fig. 10(c). The use of J_{AF} as the natural parameter to vary in order to understand the CE-state is justified based on Fig. 10(c), since the region of stability of the CE-phase is elongated along the λ -axis, meaning that its existence is not so much dependent on that coupling but much more on J_{AF} itself. It appears that some explicit tendency in the Hamiltonian toward the formation of AF links is necessary to form the CE-state. If this tendency is absent, a FM state is formed, while if it is too strong an AF-state appears. The $x=0.5$ CE-state, similar to the A-type AF at $x=0.0$, needs an intermediate value of J_{AF} for stabilization. The stability window is finite and in this respect there is no need to carry out a fine tuning of parameters to find the CE phase. However, it is clear that there is a balance of AF and FM tendencies in the CE-phase that makes the state somewhat fragile.

Note that the transitions among the many states obtained when varying J_{AF} are all of *first* order, namely they correspond to crossings of levels at zero temperature. The first-order character of these transitions is a crucial ingredient of the recent scenario proposed by Moreo et al. [165] involving mixed-phase tendencies with coexisting clusters with equal density. Recently, first-order transitions have also been reported in the one-orbital model at $x=0.5$ by Alonso et al. [166, 167], as well as tendencies toward phase

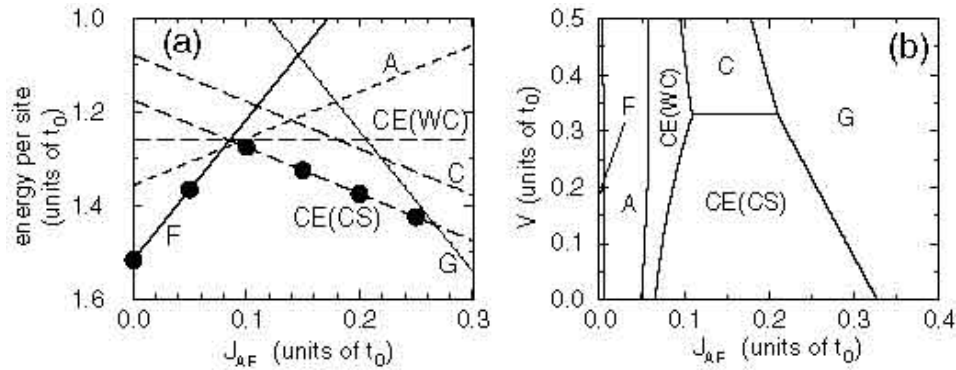


Figure 11. (a) Energy per site as a function of J_{AF} for $\lambda=1.6$ and $J_H=\infty$ for H_{JT} using a $4\times 4\times 4$ lattice. The curves denote the mean-field results and the solid symbols indicate the energy obtained by the relaxation method. Thick solid, thick broken, thin broken, thick dashed, thin dashed, thin broken, and thin solid lines denotes FM, A-type, CE-type with WC structure, charge-stacked CE-type, C-type, and G-type states, respectively. Note that the charge-stacked CE-state is observed in experiments. (b) Phase diagram in the (J_{AF}, V) plane for $4\times 4\times 4$ lattice. Note that the charge-stacked structure along the z -axis can be observed only in the CE-type AF phase. Results are reproduced from Ref. [156] where more details can be found.

separation.

Let us address now the issue of charge-stacking (CS) along the z -axis. For this purpose simulations using 3D clusters were carried out [156]. The result for the energy vs. J_{AF} is shown in Fig. 11(a), with $J_H=\infty$ and $\lambda=1.6$ fixed. The CE-state with charge-stacking has been found to be the ground state on a wide J_{AF} window. The reason that this state has lower energy than the so-called “Wigner-crystal” (WC) version of the CE-state, namely with the charge spread as much as possible, is once again the influence of J_{AF} . With a charge stacked arrangement, the links along the z -axis can all be simultaneously antiferromagnetic, thereby minimizing the energy. In the WC-state this is not possible.

It should be noted that this charge stacked CE-state is not immediately destroyed when the weak nearest-neighbor repulsion V is introduced to the model, as shown in Fig. 11(b), obtained in the mean-field calculations by Hotta, Malvezzi, and Dagotto [156]. If V is further increased for a realistic value of J_{AF} , the ground state eventually changes from the charge stacked CE-phase to the WC version of the CE-state or the C-type AF phase with WC charge ordering. As explained above, the stability of the charge stacked phase to the WC version of the CE-state is due to the magnetic energy difference. However, the competition between the charge-stacked CE-state and the C-type AF phase with the WC structure is not simply understood by the effect of J_{AF} , since those two kinds of AF phases have the same magnetic energy. In this case, the stabilization of the charge stacking originates from the difference in the geometry of the one-dimensional FM path, namely a zigzag-path for the CE-phase and a straight-line path for the C-type AF state. As discussed above, the energy for e_g electrons in the zigzag path is lower than

that in the straight-line path, and this energy difference causes the stabilization of the charge stacking. In short, the stability of the charge-stacked structure at the expense of V is supported by “the geometric energy” as well as the magnetic energy. Note that each energy gain is just a fraction of t_0 . Thus, in the absence of other mechanisms to understand the charge-stacking, another consequence of this analysis is that V actually must be substantially *smaller* than naively expected, otherwise such a charge pattern would not be stable. In fact, estimations given by Yunoki, Hotta, and Dagotto [32] suggest that the manganites must have a large dielectric function at short distances (see Ref. [168]) to prevent the melting of the charge-stacked state.

Note also that the mean-field approximations by Hotta, Malvezzi, and Dagotto [156] have shown that on-site Coulomb interactions U and U' can also generate a two-dimensional CE-state, in agreement with the calculations by van den Brink et al. [142]. Then, we believe that strong Jahn-Teller and Coulomb couplings tend to give similar results. This belief finds partial confirmation in the mean-field approximations of Hotta, Malvezzi, and Dagotto [156], where the similarities between a strong λ and (U, U') were investigated. Even doing the calculation with Coulombic interactions, the influence of J_{AF} is still crucial to inducing charge-stacking. The importance of this parameter has also been remarked by Mathieu, Svedlindh and Nordblad [169] based on experimental results.

Many other authors carried out important work in the context of the CE-state at $x=0.5$. For example, with the help of Hartree-Fock calculations, Mizokawa and Fujimori [170] reported the stabilization of the CE-state at $x=0.5$ only if Jahn-Teller distortions were incorporated into a model with Coulomb interactions. This state was found to be in competition with a uniform FM state, as well as with an A-type AF-state with uniform orbital order. In this respect the results are very similar to those found by Yunoki, Hotta and Dagotto [32] using Monte Carlo simulations. In addition, using a large nearest-neighbor repulsion and the one-orbital model, charge ordering and a spin structure compatible with the zigzag chains of the CE state was found by Lee and Min at $x=0.5$ [171]. Jackeli, Perkins, and Plakida also obtained charge-ordering at $x=0.5$ using mean-field approximations and a large V [172]. Charge-stacking was not investigated by those authors. The CE-state in $\text{Pr}_{0.5}\text{Ca}_{0.5}\text{MnO}_3$ was also obtained by Anisimov et al. using LSDA+U techniques [173].

3.3.4. $x > 0.5$ In the previous subsection, the discussion focused on the CE-type AF phase at $x=0.5$. Naively, it may be expected that similar arguments can be extended to the regime $x > 1/2$, since in the phase diagram for $\text{La}_x\text{Ca}_{1-x}\text{MnO}_3$, the AF phase has been found at low temperatures in the region $0.50 < x < 0.88$. Then, let us try to consider the band-insulating phase for density $x=2/3$ based on the minimal model Eq. (65) without both the Jahn-Teller phononic and Coulombic interactions, since this doping is quite important for the appearance of the bi-stripe structure (see Refs. [174, 175]).

After several calculations for $x=2/3$, as reported by Hotta et al. [141], the lowest-energy state was found to be characterized by the straight path, not the zigzag one,

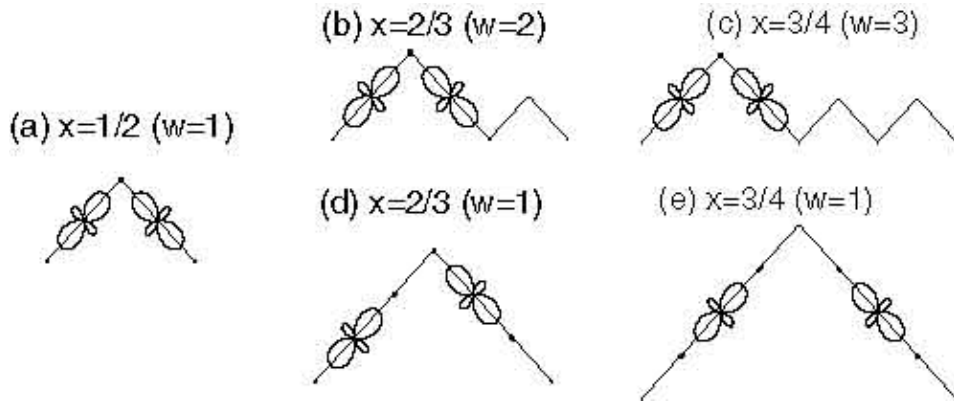


Figure 12. (a) Path with $w=1$ at $x=1/2$. Charge and orbital densities are calculated in the MFA for $E_{JT}=2t$. At each site, the orbital shape is shown with its size in proportion to the orbital density. (b) The BS-structure path with $w=2$ at $x=2/3$. (c) The BS-structure path with $w=3$ at $x=3/4$. (d) The WC-structure path with $w=1$ at $x=2/3$. (e) The WC-structure path with $w=1$ at $x=3/4$.

leading to the C-type AF phase which was also discussed in previous subsection. For a visual representation of the C-type state, see Fig. 4 of Ref. [176]. At first glance, the zigzag structure similar to that for $x=0.5$ could be the ground-state for the same reason as it occurs in the case of $x=0.5$. However, while it is true that the state with such a zigzag structure is a band-insulator, the energy gain due to the opening of the bandgap is not always the dominant effect. In fact, even in the case of $x=0.5$, the energy of the bottom of the band for the straight path is $-2t_0$, while for the zigzag path, it is $-\sqrt{3}t_0$. For $x=1/2$, the energy gain due to the gap opening overcomes the energy difference at the bottom of the band, leading to the band-insulating ground-state. However, for $x=2/3$ even if a band-gap opens the energy of the zigzag structure cannot be lower than that of the metallic straight-line phase. Intuitively, this point can be understood as follows: An electron can move smoothly along the one-dimensional path if it is straight. However, if the path is zigzag, “reflection” of the wavefunction occurs at the corner, and then a smooth movement of one electron is no longer possible. Thus, for small numbers of carriers, it is natural that the ground-state is characterized by the straight path to optimize the kinetic energy of the e_g electrons.

However, in neutron scattering experiments a spin pattern similar to the CE-type AF phase has been suggested by Radaelli et al. [177]. In order to stabilize the zigzag AF phase to reproduce those experiments it is necessary to include the Jahn-Teller distortion effectively. As discussed by Hotta et al. [141], a variety of zigzag paths could be stabilized when the Jahn-Teller phonons are included. In such a case, the classification of zigzag paths is an important issue to understand the competing “bi-stripe” vs. “Wigner-crystal” structures. The former has been proposed by Mori et al. [174, 175], while the latter was claimed to be stable by Radaelli et al. [177]. As shown in the previous subsection, the shape of the zigzag structure is characterized by

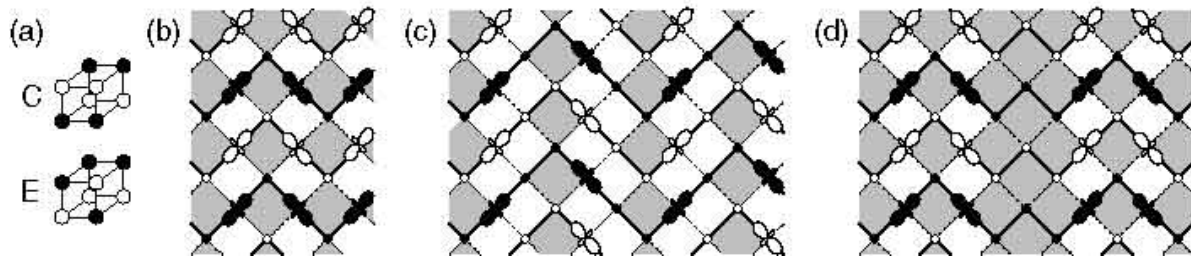


Figure 13. (a) C- and E-type unit cells [8]. (b) The spin structure in the *a-b* plane at $x=1/2$. Open and solid symbols denote the spin up and down, respectively. The thick line indicates the zigzag FM path. The open and shaded squares denote the C- and E-type unit cells. At $x=1/2$, C-type unit cell occupies half of the two-dimensional plane, clearly indicating the “CE” type phase. (c) The spin structure at $x=2/3$ for Wigner-crystal type phase. Note that 66% of the two-dimensional lattice is occupied by C-type unit cell. Thus, it is called “ $C_{2/3}E_{1/3}$ ”-type AF phase. (d) The spin structure at $x=2/3$ for bi-stripe type phase. Note that 33% of the two-dimensional lattice is occupied by C-type unit cell. Thus, it is called “ $C_{1/3}E_{2/3}$ ”-type AF phase.

the winding number w associated with the Berry-phase connection of an e_g -electron parallel-transported through Jahn-Teller centers, along zigzag one-dimensional paths. As shown above, the total winding number is equal to half of the number of corners included in the zigzag unit path. Namely, the winding number w is a good label to specify the shape of the zigzag one-dimensional FM path.

After several attempts to include effectively the Jahn-Teller phonons, it was found that the bi-stripe phase and the Wigner crystal phase universally appear for $w=x/(1-x)$ and $w=1$, respectively. Note here that the winding number for the bi-stripe structure has a remarkable dependence on x , reflecting the fact that the distance between adjacent bi-stripes changes with x . This x -dependence of the modulation vector of the lattice distortion has been observed in electron microscopy experiments [174, 175]. The corresponding zigzag paths with the charge and orbital ordering are shown in Fig. 12. In the bi-stripe structure, the charge is confined in the short straight segment as in the case of the CE-type structure at $x=0.5$. On the other hand, in the Wigner-crystal structure, the straight segment includes two sites, indicating that the charge prefers to occupy either of these sites. Then, to minimize the Jahn-Teller energy and/or the Coulomb repulsion, the e_g electrons are distributed with equal spacing. The corresponding spin structure is shown in Fig. 13. A difference in the zigzag geometry can produce a significant different in the spin structure. The definitions for the C- and E-type AF structures [8] are shown in Fig. 13(a) for convenience. At $x=1/2$, as clearly shown in Fig. 13(b), half of the plane is filled by the C-type, while another half is covered by the E-type, clearly illustrating the meaning of “CE” in the spin structure of half-doped manganites. On the other hand, as shown in Figs. 13(c) and 13(d), the bi-stripe and Wigner crystal structure have $C_{1-x}E_x$ -type and C_xE_{1-x} -type AF spin arrangements, respectively. Such zigzag-based AF structure has been discussed experimentally in single

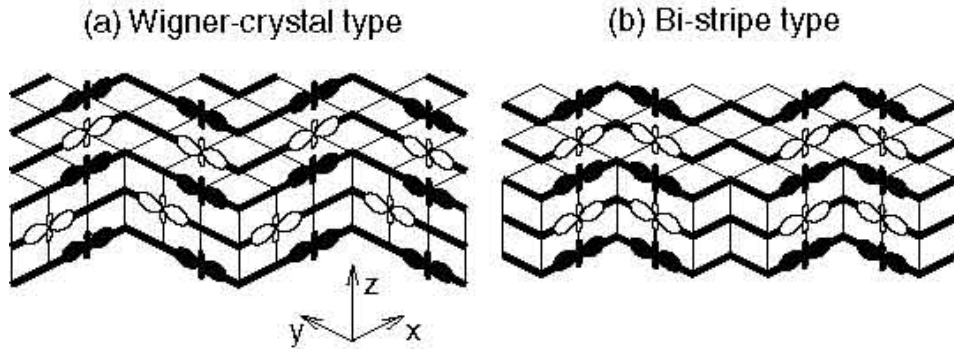


Figure 14. Schematic views for spin, charge, and orbital ordering for (a) Wigner-crystal structure and (b) bi-stripe type structures at $x=2/3$ in 3D environment. The open and solid symbols indicate the spin up and down, respectively. The FM one-dimensional path is denoted by the thick line. The empty sites denote Mn^{4+} ions, while the robes indicate the Mn^{3+} ions in which $3x^2 - r^2$ or $3y^2 - r^2$ orbitals are occupied.

layered manganites $\text{Nd}_{1-x}\text{Sr}_{1+x}\text{MnO}_4$ by Kimura et al. [178].

The charge structure along the z -axis for $x=2/3$ has been discussed by Hotta et al. [179]. As schematically shown in Figs. 14(a) and (b), a remarkable feature can be observed. Due to the confinement of charge in the short straight segment for the bi-stripe phase, the charge stacking is suggested from our topological argument. On the other hand, in the Wigner-crystal type structure, charge is not stacked, but it is shifted by one lattice constant to avoid the Coulomb repulsion. Thus, if the charge stacking is also observed in the experiment for $x=2/3$, our topological scenario suggests the bi-stripe phase as the ground-state in the low temperature region. To establish the final “winner” in the competition between the bi-stripe and Wigner-crystal structure at $x=2/3$, more precise experiments, as well as quantitative calculations, will be further needed.

3.3.5. $x < 0.5$ Regarding densities smaller than 0.5, the states at $x=1/8$, $1/4$ and $3/8$ have received considerable attention. See Refs. [180, 181, 182]. These investigations are still in a “fluid” state, and the experiments are not quite decisive yet, and for this reason, this issue will not be discussed in much detail here. However, without a doubt, it is very important to clarify the structure of charge-ordered states that may be in competition with the FM states in the range in which the latter is stable in some compounds. “Stripes” may emerge from this picture, as recently remarked in experiments [183, 184, 185, 186] and calculations [33], and surely the identification of charge/orbital arrangements at $x < 0.5$ will be an important area of investigations in the very near future.

Here a typical result for this stripe-like charge ordering is shown in Fig. 15, in which the lower-energy orbital at each site is depicted, and its size is in proportion to the electron density occupying that orbital. This pattern is theoretically obtained by

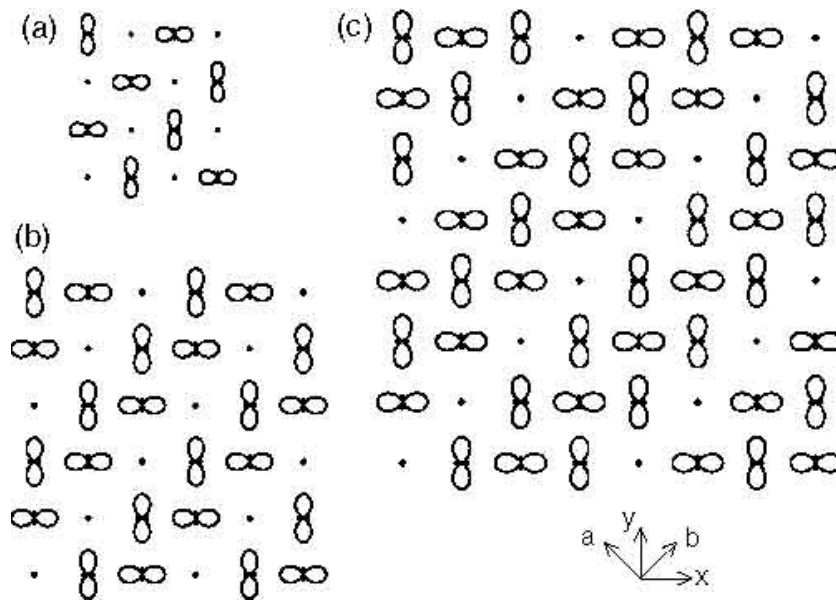


Figure 15. Numerical results for orbital densities in the FM phase for (a) $x=1/2$, (b) $1/3$, and (c) $1/4$ [33]. The charge density in the lower-energy orbital is shown, and the size of the orbital is exactly in proportion to this density.

the relaxation technique for the optimization of oxygen positions, namely including the cooperative Jahn-Teller effect. At least in the strong electron-phonon coupling region, the stripe charge ordering along the *diagonal* direction in the *xy* plane becomes the global ground-state. Note, however, that many meta-stable states can appear very close to this ground state. Thus, the shape of the stripe is considered to fluctuate both in space and time, and in experiments it may occur that only some fragments of this stripe can be detected. It should also be emphasized that the orbital ordering occurs concomitant with this stripe charge ordering. In the electron-rich region, the same antiferro orbital-order exists as that corresponding to $x=0.0$. On the other hand, the pattern around the diagonal array of electron-poor sites is quite similar to the building block of the charge/orbital structure at $x=0.5$.

In Fig. 15, it is found that the same charge and orbital structure stacks along the *b*-axis. Namely, it is possible to cover the whole two-dimensional plane by some periodic charge-orbital array along the *a*-axis. If this periodic array is taken as the closed loop C , the winding numbers are $w=1, 2$, and 3 , for $x=1/2, 1/3$, and $1/4$, respectively. Note that in this case w is independent of the path along the *a*-axis. The results imply a general relation $w=(1-x)/x$ for the charge-orbital stripe in the FM phase, reflecting the fact that the distance between the diagonal arrays of holes changes with x . Our topological argument predicts stable charge-orbital stripes at special doping such as $x=1/(1+w)$, with w an integer.

This orbital ordering can be also interpreted as providing a “ π ”-shift in the orbital sector, by analogy with the dynamical stripes found in cuprates [187], although in copper oxides the charge/spin stripes mainly appear along the *x*- or *y*-directions. The study of

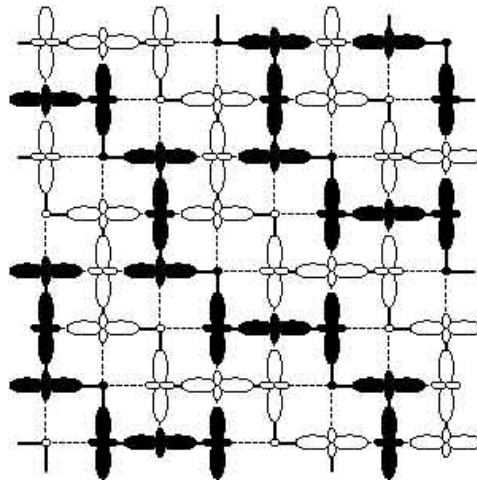


Figure 16. Schematic figure of the possible spin-charge-orbital structure at $x=1/4$ in the zigzag AF phase at low temperature and large electron-phonon coupling [33]. This figure was obtained using numerical techniques, and cooperative phonons, for $J_H=\infty$ and $J_{AF}=0.1t_0$. For the non-cooperative phonons, basically the same pattern can be obtained.

the similarities and differences between stripes in manganites and cuprates is one of the most interesting open problems in the study of transition metal oxides, and considerable work is expected in the near future.

Finally, a new zigzag AF spin configuration for $x<0.5$ is here briefly discussed [33]. In Fig. 16, a schematic view of this novel spin-charge-orbital structure on the 8×8 lattice at $x=1/4$ is shown, deduced using the numerical relaxation technique applied to cooperative Jahn-Teller phonons in the strong-coupling region. This structure appears to be the global ground state, but many excited states with different spin and charge structures are also found with small excitation energy, suggesting that the AF spin structure for $x<0.5$ in the layered manganites is easily disordered due to this “quasi-degeneracy” in the ground state. This result may be related to the “spin-glass” nature of the single layer manganites reported in experiments [188].

It should be noted that the charge-orbital structure is essentially the same as that in the two-dimensional FM phase, as shown in Fig. 15. This suggests the following scenario for the layered manganites: When the temperature is decreased from the higher temperature region, first charge ordering occurs due to the cooperative Jahn-Teller distortions in the FM (or paramagnetic) region. If the temperature is further decreased, the zigzag AF spin arrangement is stabilized, adjusting itself to the orbital structure. Thus, the separation between the charge ordering temperature T_{CO} and the Néel temperature T_N occurs naturally in this context. This is not surprising, since T_{CO} is due to the electron-lattice coupling, while T_N originates in the coupling J_{AF} . However, if the electron-phonon coupling is weak, then T_{CO} becomes very low. In this case, the transition to the zigzag AF phase may occur prior to the charge ordering. As discussed above, the e_g electron hopping is confined to one dimensional structures in the

zigzag AF environment. Thus, in this situation, even a weak coupling electron-phonon coupling can produce the charge-orbital ordering, as easily understood from the Peierls instability argument. Namely, just at the transition to the zigzag AF phase, the charge-orbital ordering occurs simultaneously, indicating that $T_{CO}=T_N$. Note also that in the zigzag AF phase, there is no essential difference in the charge-orbital structures for the non-cooperative and cooperative phonons, due to the one-dimensionality of those zigzag chains.

3.4. Summary

In this section, we have reviewed the theoretical results on spin, charge, and orbital ordering in manganites. We believe that the complicated ordering in manganites is caused by (i) competition between FM metallic and AF insulating phases and (ii) active e_g orbital degree of freedom. The existence of the FM metallic phase in the issue (i) has been understood by the double-exchange concept, while the variety of AF insulating originating from the point (ii) has not been considered satisfactorily in the standard double-exchange mechanism. Here we stress that the existence of active orbital does not simply indicate the increase of internal degrees of freedom in addition to spin and charge. We should remark an important effect of the orbital shape, leading to the geometrical pattern in the spin configuration. This point has been emphasized in this section in the context of topological aspect of orbital ordering.

We have not mentioned another important characteristic issue of manganites, i.e., phase separation tendency, which is a driving force of colossal magneto-resistance phenomenon in manganites. The strong tendency of the phase separation is easily understood in the complex phase diagram including several kinds of first order transition. Readers should refer the previous review and textbook [3, 6], in which the phase-separation tendency and related physics have been explained in detail.

4. Orbital physics in other *d*-electron materials

In the previous section, we have concentrated on the orbital physics of manganites. However, we can also observe orbital ordering phenomena in other transition metal oxides. Here we introduce possible orbital ordering in nickelates and ruthenates as typical materials of e_g and t_{2g} electron systems, respectively, in the sense that H_{e_g} and $H_{t_{2g}}$ can be applied. Finally, we also discuss a potential role of orbital ordering in geometrically frustrated electron systems with orbital degeneracy.

4.1. e_g electron systems

The existence and origin of “striped” structures continues attracting considerable attention in the research field of transition metal oxides [189, 190]. In a system with dominant electron-electron repulsion, the Wigner-crystal state should be stabilized, but in real materials, more complicated non-uniform charge structures have been

found. In Nd-based lightly-doped cuprates, neutron scattering experiments revealed incommensurate spin structures [191, 192, 193], where AF spin stripes are periodically separated by domain walls of holes. In $\text{La}_{2-x}\text{Sr}_x\text{CuO}_4$, dynamical stripes are believed to exist along vertical or horizontal directions (Cu-O bond direction). Note that for $x < 0.055$, the spin-glass phase exhibits a diagonal spin modulation [194, 195]. In nickelates, the charge-ordered stripes are along the diagonal direction [196, 197, 198, 199]. In manganites, as mentioned in the previous section, evidence for striped charge-ordering also along the diagonal direction has been reported in the AF phase for $x > 1/2$ [174, 175], while short-range diagonal stripe correlations have been found in the FM phase at $x < 1/2$ [183, 184].

In general, stripes can be classified into metallic or insulating. In $\text{La}_{2-x}\text{Sr}_x\text{CuO}_4$, the dynamical stripes exhibit metallic properties, but they are easily pinned by lattice effects and impurities. In $\text{La}_{1.6-x}\text{Nd}_{0.4}\text{Sr}_x\text{CuO}_4$, stripes along the bond-direction are pinned by lattice distortions [189], but they are still metallic. Intuitively, vertical or horizontal stripes could be associated with the formation of “rivers of holes”, to prevent individual charges from fighting against the AF background [200, 187, 201]. Such stripes should be metallic, even if they are pinned, since they are induced by the optimization of hole motion between nearest-neighbor Cu-sites via oxygens.

However, in the diagonal stripes observed in manganites and nickelates, charges are basically localized, indicating that such insulating stripes are *not* determined just by the optimization of the hole motion. In the FM state of manganites, the hole movement is already optimal and, naively, charges should not form stripes. Obviously, an additional effective local potential must be acting to confine electrons into stripes. If such a potential originates in lattice distortions, it is expected to occur along the bond direction to avoid energy loss due to the conflict between neighboring lattice distortions sharing the same oxygens. Then, static stripes stabilized by lattice distortions tends to occur along the *diagonal* direction, as shown Fig. 16, which are stabilized by Jahn-Teller distortions [33].

In simple terms, vertical or horizontal stripes in cuprates can be understood by the competition between Coulomb interaction and hole motion, while diagonal stripes are better explained as a consequence of a robust electron-lattice coupling. However, a difficulty has been found for theoretical studies of stripe formation in doped nickelates, since both Coulomb interaction and electron-lattice coupling appear to be important. Since the Ni^{2+} ion has two electrons in the e_g orbitals, on-site Coulomb interactions certainly play a crucial role to form spins $S=1$. When holes are doped, one electron is removed and another remains in the e_g orbitals, indicating that the hole-doped site should become JT active. Then, in hole-doped nickelates *both* Coulombic and phononic interactions could be of relevance, a fact not considered in previous theoretical investigations.

In the following, we will review the recent results by Hotta and Dagotto [202]. The model for nickelates is the e_g orbital Hubbard Hamiltonian Eq. (63), but another important ingredient is added here. Namely, the electron-lattice term is divided into

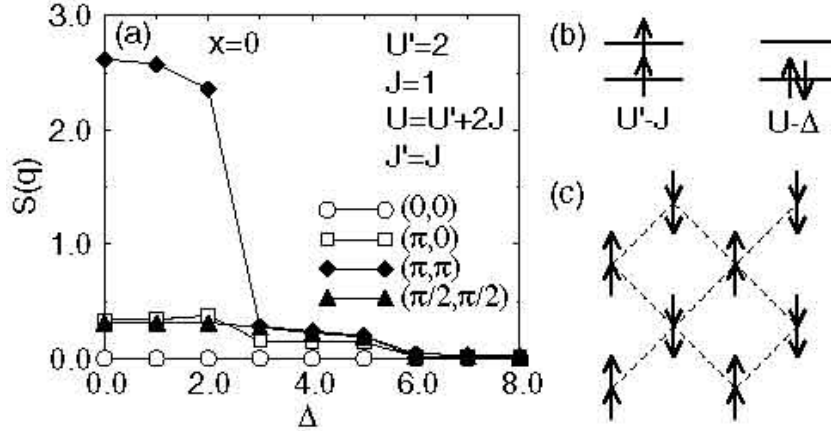


Figure 17. (a) Spin correlation $S(\mathbf{q})$ vs. Δ for $x=0$. (b) Two kinds of local e_g -electron arrangements for $x=0$. (c) AF spin pattern theoretically determined for $\Delta < 3$.

couplings for the apical and in-plane oxygen motions. In layered nickelates, all NiO_6 octahedra are significantly elongated along the c -axis, splitting the e_g orbitals. This splitting from apical oxygens should be included explicitly from the start as the level splitting between a- and b-orbitals. Then, the model is defined as

$$H = H_{\text{kin}}^{e_g} + H_{\text{el-el}}^{e_g} + \Delta \sum_{\mathbf{i}} (n_{\text{ia}} - n_{\text{ib}})/2, \quad (100)$$

where Δ is the level splitting. Later, the in-plane motion of oxygens should be studied by adding $H_{\text{ep-ph}}^{e_g}$. Note that the energy unit is also t_0 in this subsection.

First, consider the undoped case. The calculation is done for an 8-site tilted cluster, equivalent in complexity to a 16-site lattice for the single-band Hubbard model. Since at all sites the two orbitals are occupied due to the Hund's rule coupling, the JT distortions are not active and it is possible to grasp the essential ground-state properties using H . In Fig. 17(a), the Fourier transform of spin correlations is shown vs. Δ , where $S(\mathbf{q}) = (1/N) \sum_{\mathbf{i}, \mathbf{j}} e^{i\mathbf{q} \cdot (\mathbf{i} - \mathbf{j})} \langle S_{\mathbf{i}}^z S_{\mathbf{j}}^z \rangle$, with $S_{\mathbf{i}}^z = \sum_{\gamma} (d_{\mathbf{i}\gamma\uparrow}^\dagger d_{\mathbf{i}\gamma\uparrow} - d_{\mathbf{i}\gamma\downarrow}^\dagger d_{\mathbf{i}\gamma\downarrow})/2$. As expected, a robust (π, π) peak can be observed for $\Delta < 3$, suggesting that the AF phase is stabilized by super-exchange interactions. The rapid decrease of $S(\pi, \pi)$ for $\Delta > 3$ is understood by comparing the energies for local triplet and singlet states, as shown in Fig. 17(b). The ground-state properties change at $U' - J = U - \Delta$, leading to $\Delta = 3J$ for the transition. The spin structure at $x=0$ is schematically shown in Fig. 17(c).

Let us turn our attention to the case $x=1/2$. The 8-site tilted lattice is again used for the analysis, and the phase diagram Fig. 18(a) is obtained for $\Delta=0.5$. Since Δ of nickelates is half of that of cuprates from the lattice constants for CuO_6 and NiO_6 octahedra, it is reasonable to select $\Delta=0.5$ in the unit of t_0 . Increasing J , an interesting transformation from AF to FM phases is found. This is natural, since at large J the system has a formal similarity with manganite models, where kinetic-energy gains lead to ferromagnetism, while at small J the magnetic energy dominates. However, between the G-type AF for $J \approx 0$ and FM phase for $J \approx U'$, unexpected states appear which are

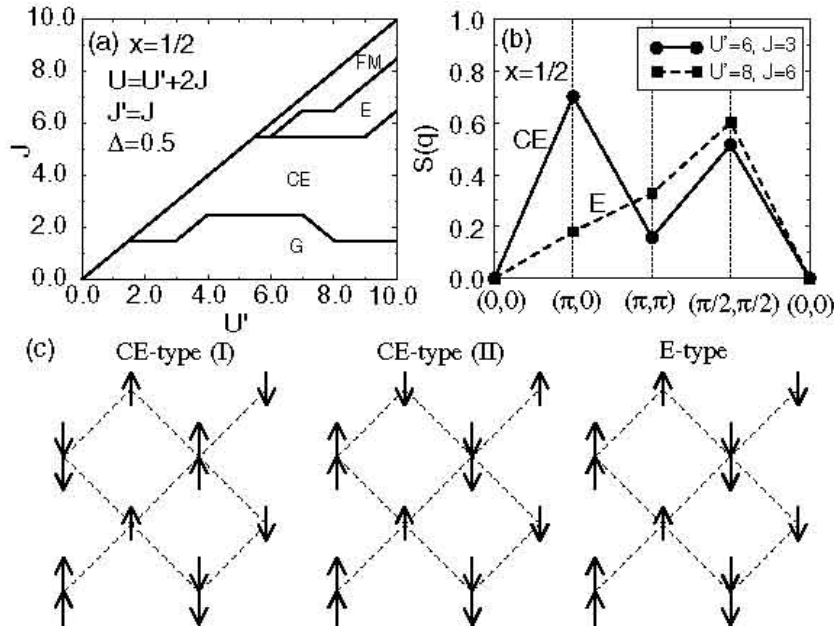


Figure 18. (a) Ground-state phase diagram at $x=1/2$ without electron-phonon coupling. (b) $S(\mathbf{q})$ for the CE- and E-type phases, at the couplings indicated. (c) Spin and charge patterns for the CE- and E-type phases. These are schematic views, since local charge-densities in practice are not exactly 1 and 2.

mixtures of FM and AF phases, due to the competition between kinetic and magnetic energies. Typical spin correlations $S(\mathbf{q})$ are shown in Fig. 18(b). Note that peaks at $\mathbf{q}=(\pi, 0)$ and $(\pi/2, \pi/2)$ indicate “C” and “E” type spin-structures, respectively. Double peaks at $\mathbf{q}=(\pi, 0)$ and $(\pi/2, \pi/2)$ denote the CE-type structure, frequently observed in half-doped manganites [203]. In half-doped nickelates, the CE-phase is expressed as a mixture of type (I) and (II) in Fig. 18(c), depending on the positions of the $S=1$ and $S=1/2$ sites, although the “zigzag” FM chain structure is common for both types. The E-type phase is also depicted in Fig. 18(c). Note that the charge correlation always exhibits a peak at $\mathbf{q}=(\pi, \pi)$ (not shown here), indicating the checkerboard-type charge ordering.

In experimental results, a peak at $(\pi/2, \pi/2)$ in $S(\mathbf{q})$ has been reported, suggesting an AF pair of $S=1$ spins *across* the singly-occupied sites with holes. Moreover, the checkerboard-type charge ordering has been experimentally observed [196, 197, 198, 199]. Thus, the spin-charge patterns of CE(II)- and E-type are consistent with the experimental results. Our phase diagram has a robust region with a peak at $(\pi/2, \pi/2)$, both for CE- and E-type phases, although the CE-phase exhibits an extra peak at $(\pi, 0)$. Whether the E- or CE-phases are present in nickelates can be studied experimentally in the future by searching for this $(\pi, 0)$ peak. Note that if diffuse scattering experiments detect the AF correlation *along* the hole stripe, as has been found at $x=1/3$ [204], the CE(II)-type may be the only possibility. Summarizing, the spin-charge structure in $x=1/2$ experiments can be understood within the Hamiltonian H by assuming a

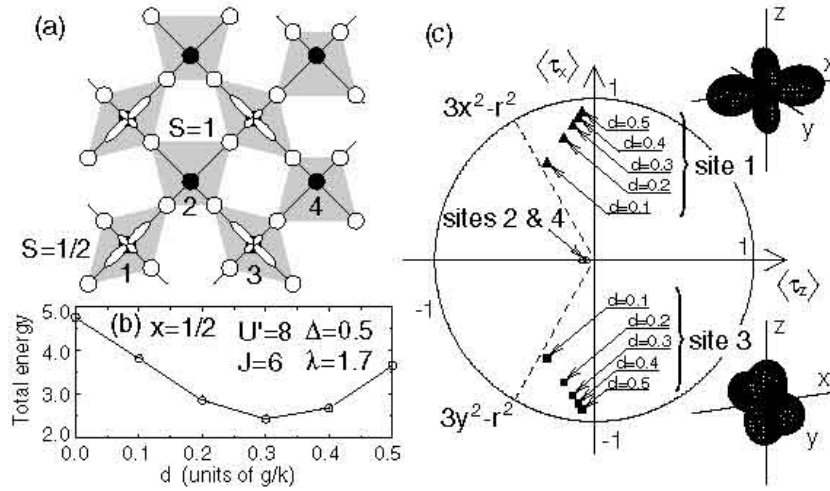


Figure 19. (a) Numerically obtained cooperative distortion pattern for an 8-site lattice at $x=1/2$ including $H_{\text{el-ph}}^{\text{eg}}$. Black and open circles indicate Ni and O ions, respectively. Open symbols indicate e_g orbitals in the optimized state. (b) Total ground-state energy vs. d for $x=1/2$. (c) Orbital densities $\langle \tau_{zi} \rangle$ and $\langle \tau_{xi} \rangle$ for sites 1–4. See (d) for the site labels. Optimized orbitals at $d=0.3$ for sites 1 and 3 are also shown.

relatively large J .

Consider now the effect of in-plane oxygen motion. Note that apical oxygen motions have already been included as an e_g -level splitting. The extra electron-phonon coupling term is $H_{\text{el-ph}}^{\text{eg}}$, Eq. (49). Since all oxygens are shared by adjacent NiO_6 octahedra, the distortions are *not independent*. To consider such cooperative effect, in principle, the O-ion displacements should be optimized. However, in practice it is not feasible to perform both the Lanczos diagonalization and the optimization of all oxygen positions for 6- and 8-site clusters. In the actual calculations, Q_{1i} , Q_{2i} , and Q_{3i} are expressed by a single parameter d , for the shift of the O-ion coordinate. Note that the unit of d is g/k , typically $0.1 \sim 0.3 \text{ \AA}$. Then, the total energy is evaluated as a function of d to find the minimum energy state. Repeating these calculations for several distortion patterns, it is possible to deduce the optimal state.

After several trials, the optimal distortion at $x=1/2$ is shown in Fig. 19(a). The diagonalization has been performed at several values of d on the 8-site distorted lattice and the minimum in the total energy is found at $d=0.3$, as shown in Fig. 19(b). As mentioned above, even without $H_{\text{el-ph}}^{\text{eg}}$, the checkerboard-type charge ordering has been obtained, but the peak at $\mathbf{q}=(\pi, \pi)$ significantly grows due to the effect of lattice distortions. Note that the distortion pattern in Fig. 19(a) is essentially the same as that for half-doped manganites. This is quite natural, since JT active and inactive ions exist bipartitely also for half-doped nickelates. Then, due to this JT-type distortion, orbital ordering for half-doped nickelates is predicted, as schematically shown in Fig. 19(a). The shapes of orbitals are determined from the orbital densities, $\langle \tau_{zi} \rangle$ and $\langle \tau_{xi} \rangle$, as shown in Fig. 19(c). The well-known alternate pattern of $3x^2-r^2$ and $3y^2-r^2$ orbitals

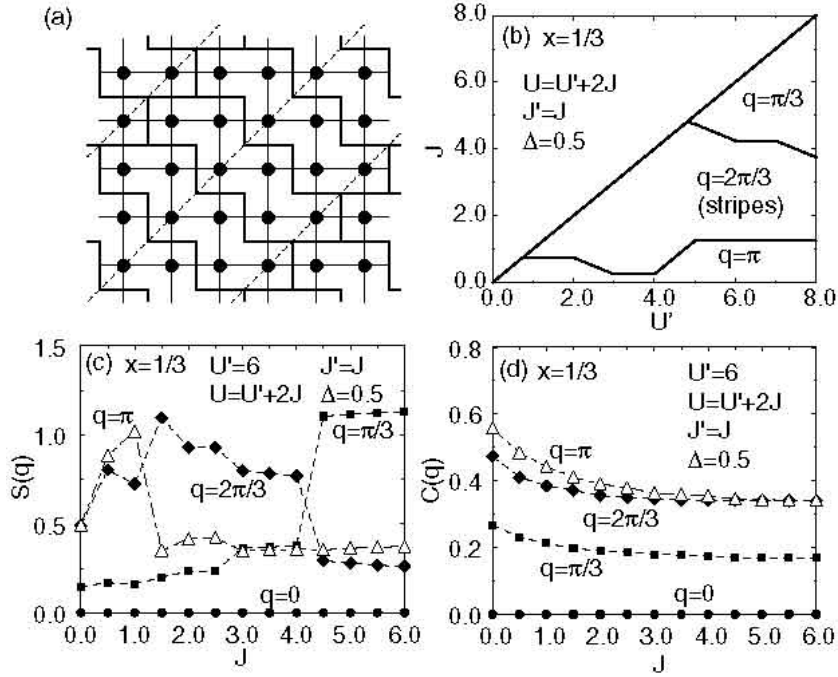


Figure 20. (a) Zigzag 6-sites cluster covering the 2D lattice. Black circles denote Ni ions, and dashed lines indicate hole positions. (b) Phase diagram at $x=1/3$ without $H_{\text{el-ph}}^{\text{eg}}$. Each phase is characterized by the momentum that shows a peak in $S(q)$. (c) $S(q)$ and (d) $C(q)$ vs. J for $U'=6$ and $\Delta=0.5$.

in half-doped manganites is denoted by dashed lines. Increasing d , the shape of orbitals deviates from $3x^2-r^2$ and $3y^2-r^2$, but it is still characterized by the orbitals elongating along the x - and y -directions. See insets of Fig. 19(c). It would be very interesting to search for orbital ordering in half-doped nickelates, using the resonant X-ray scattering technique.

Now let us move to the case $x=1/3$. If the actual expected stripe structure at $x=1/3$ is faithfully considered [196, 197, 198, 199], it is necessary to analyze, at least, a 6×6 cluster. However, such a large-size cluster with orbital degeneracy cannot be treated exactly due to the exponential growth of the Hilbert space with cluster size. Then, a covering of the two-dimensional (2D) lattice using zigzag 6-sites clusters as shown in Fig. 20(a) is considered by assuming a periodic structure along the diagonal direction.

First we consider the case without $H_{\text{el-ph}}^{\text{eg}}$. The phase diagram obtained by analyzing the zigzag 6-site cluster for H is in Fig. 20(b). Typical spin and charge correlations are shown in Figs. 20(c) and 20(d), where $C(\mathbf{q}) = (1/N) \sum_{i,j} e^{i\mathbf{q} \cdot (\mathbf{i}-\mathbf{j})} \langle (n_i - \langle n \rangle) \cdot (n_j - \langle n \rangle) \rangle$, with $n_i = \sum_{\gamma} n_{i\gamma}$.

Since the momentum q is defined along the zigzag direction in the unit of $\sqrt{2}/a$, where a is the lattice constant, the phase labeled by $q=2\pi/3$ in Fig. 20(b) denotes an *incommensurate AF phase* with the proper spin stripe structure. The phase labeled by $q=\pi/3$ indicates a spin spiral state, which will eventually turn to the FM phase in the thermodynamic limit. Thus, the spin stripe phase appears between the commensurate

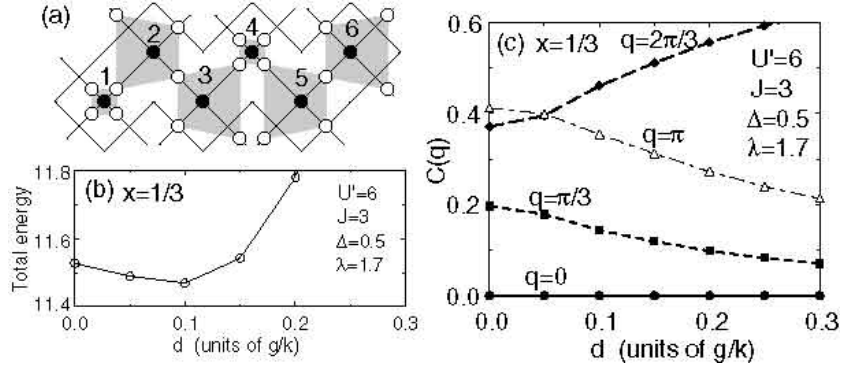


Figure 21. (a) Cooperative distortion pattern for the zigzag 6-sites cluster at $x=1/3$. (b) Total ground-state energy and (c) $C(q)$ vs. d for $x=1/3$.

AF and FM-like phases, similar to the case of $x=1/2$. However, as seen in Fig. 20(d), $C(q)$ in the spin stripe phase does *not* show the striped charge structure ($q=2\pi/3$). Rather, bipartite charge ordering characterized by a peak at $q=\pi$ still remains. Namely, the Hamiltonian without $H_{\text{el-ph}}^{\text{eg}}$ can explain the spin stripe, but does not reproduce the striped charge ordering at $x=1/3$, indicating the importance of H_{eph} .

Consider now the effect of $H_{\text{el-ph}}^{\text{eg}}$ for $x=1/3$. After evaluating total ground-state energies for several kinds of distortions, the pattern in Fig. 21(a) has been found to provide the optimal state at $x=1/3$. This type of distortion induces a spatial modulation of the level splitting as $-\delta_1/2=\delta_2=\delta_3=-\delta_4/2=\delta_5=\delta_6$, where δ_i is the level splitting caused by the in-plane oxygen motions. Note that this breathing-mode modulation is consistent with experimental results [205]. The site numbers are found in Fig. 21(a). The minimum energy is found at $d=0.1$, as shown in Fig. 21(b). The modulation of level splitting stabilizes the striped charge ordering characterized by a $q=2\pi/3$ peak in $C(q)$, as clearly shown in Fig. 21(c).

Note that $(3x^2-r^2/3y^2-r^2)$ -type orbital ordering does *not* occur in Fig. 21(a). Phenomenologically, such orbital ordering tends to appear in a hole pair separated by one site, the unit of the “bi-stripe” of manganites [174, 175]. However, such a bi-stripe-type ordering contradicts the $x=1/3$ striped charge-ordering, and the bi-stripe-type solution was found to be unstable in these calculations. One may consider other distortion patterns which satisfy both $(3x^2-r^2/3y^2-r^2)$ -type orbital and striped charge-ordering, but in such distortions no energy minimum was obtained for $d>0$. After several trials, Fig. 21(a) has provided the most optimal state.

In summary, possible spin, charge, *and* orbital structures of layered nickelates have been discussed based on the e_g -orbital degenerate Hubbard model coupled with lattice distortions. To understand the nickelate stripes, both Hund’s rule interaction and electron-lattice coupling appear essentially important. At $x=1/2$, $(3x^2-r^2/3y^2-r^2)$ -type orbital ordering similar to that in half-doped manganites is predicted. Even FM phases could be stabilized by chemically altering the carrier’s bandwidth. For $x=1/3$, a spatial modulation in level splitting plays an important role for stripe formation.

4.2. t_{2g} electron systems

Let us now consider orbital ordering in a system with active t_{2g} -orbital degree of freedom. As is well known, t_{2g} -electron systems such as titanates and vanadates have been studied for a long time. After the discovery of superconductivity in layered cobalt oxyhydrate $\text{Na}_{0.35}\text{CoO}_2 \cdot 1.3\text{H}_2\text{O}$ [206], magnetic properties of cobaltites have been discussed intensively both from experimental and theoretical sides. In relation with cobaltites, one-dimensional t_{2g} electron model has been studied theoretically for the understanding of spin and orbital state of t_{2g} electrons [207, 208]. When we turn our attention to $4d$ electron systems, Ru-oxides have been also focused, after the discovery of triplet superconductivity in the layered ruthenate Sr_2RuO_4 [209]. In addition, the isostructural material Ca_2RuO_4 has been studied as a typical stage of spin and orbital ordering of t_{2g} electrons. In this subsection, we review the orbital ordering phenomenon in Ca_2RuO_4 .

As mentioned in Sec. 2, Ru^{4+} ion include four electrons in the low-spin state, since the crystalline electric field is effectively larger than the Hund's rule interaction. Thus, four electrons occupy t_{2g} orbitals, leading to $S=1$ spin. The G-type AF phase in Ca_2RuO_4 is characterized as a standard Néel state with spin $S=1$ [210, 211, 212]. The Néel temperature T_N is 125K. To understand the Néel state observed in experiments, one may consider the effect of the tetragonal crystal field, leading to the splitting between xy and $\{yz, zx\}$ orbitals, where the xy -orbital state is lower in energy than the other levels. When the xy -orbital is fully occupied, a simple superexchange interaction at strong Hund's rule coupling can stabilize the AF state. However, X-ray absorption spectroscopy studies have shown that 0.5 holes per site exist in the xy -orbital, while 1.5 holes are contained in the zx - and yz -orbitals [213], suggesting that the above naive picture based on crystal field effects seems to be incomplete. This fact suggests that the orbital degree of freedom may play a more crucial role in the magnetic ordering in ruthenates than previously anticipated.

First let us briefly review the result by Hotta and Dagotto [214]. The Hamiltonian is the t_{2g} Hubbard model coupled with Jahn-Teller distortions, already given by $H_{t_{2g}}$, Eq. (63) in Sec. 2. This model is believed to provide a starting point to study the electronic properties of ruthenates, but it is difficult to solve even approximately. To gain insight into this complex system, an unbiased technique should be employed first. Thus, Hotta and Dagotto have analyzed a small 2×2 plaquette cluster in detail by using the Lanczos algorithm for the exact diagonalization, and the relaxation technique to determine the oxygen positions. In actual calculations, at each step for the relaxation, the electronic portion of the Hamiltonian is exactly diagonalized for a fixed distortion. Iterations are repeated until the system converges to the global ground state.

The ground state phase diagram obtained by Hotta and Dagotto is shown in Fig. 22. There are six phases in total, which are categorized into two groups. One group is composed of phases stemming from the $U'=0$ or $E_{JT}=0$ limits. The origin of these phases will be addressed later, but first their main characteristics are briefly discussed.

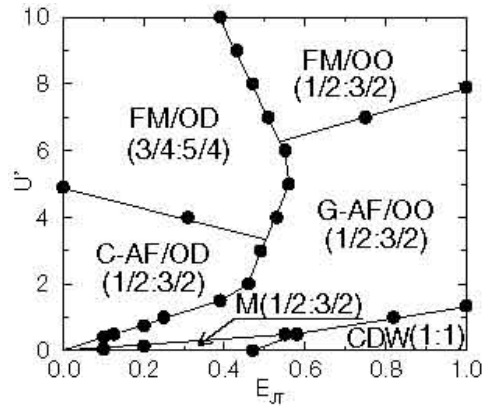


Figure 22. Ground state phase diagram for the t_{2g} Hubbard model coupled with Jahn-Teller phonons for $J=3U'/4$. The notation is explained in the maintext.

For $E_{JT}=0$, a C-type AF orbital disordered (OD) phase appears in the region of small and intermediate U' . This state is characterized by $n_{xy}:n_{yz}+n_{zx}=1/2:3/2$, where n_γ is the hole number per site at the γ -orbital. Hereafter, a shorthand notation such as “1/2:3/2” is used to denote the hole configuration. For large U' , and still $E_{JT}=0$, a FM/OD phase characterized by 3/4:5/4 is stable, which may correspond to Sr_2RuO_4 . On the other hand, for $U'=0$ and small E_{JT} , a “metallic” (M) phase with small lattice distortion is observed, while for large E_{JT} , a charge-density-wave (CDW) state characterized by 1:1 was found. In short, the G-type AF phase observed experimentally [212] does *not* appear, neither for $E_{JT}=0$ nor for $U'=0$.

Another group includes two phases which are not connected to either $E_{JT}=0$ or $U'=0$. It is only in this group, with *both* lattice and Coulomb effects being relevant, that for intermediate U' the G-type AF and orbital ordered (OO) phase with 1/2:3/2 found in experiments [213] is stabilized. At larger U' , a FM/OO phase occurs with the same hole arrangement. In the FM phase, since an $S=1$ spin with $S_z=+1$ is formed at each site, the up-spin number is unity at each orbital, while the down-spin distribution depends on the orbital. In the AF state, the configuration of double-occupied orbitals is the same as in the FM phase, but the single-occupied orbital contains 0.5 up- and 0.5-down spins on average, since the $S=1$ spin direction fluctuates due to the AF coupling between neighboring $S=1$ spins. However, the spin correlations peak at (π,π) , indicating the G-AF structure. Except for the spin direction, the charge and orbital configuration in the FM/OO phase is the same as in the G-AF/OO state. An antiferro-orbital ordering pattern including xy, yz, and zx orbitals has been suggested for these FM and AF phases.

On the other hand, a ferro “0:2” xy-orbital ordered state has been suggested by Anisimov *et al.* [215]. Fang *et al.* also predicted the ferro-type orbital ordering [216]. It seems to be different from experiments on the hole distribution in Ref. [213], but due to the combination of optical conductivity measurement and LDA+U calculations [217], it has been found that xy-orbital ferro ordering occurs and the change of hole population can be explained due to the temperature dependence of electronic structure.

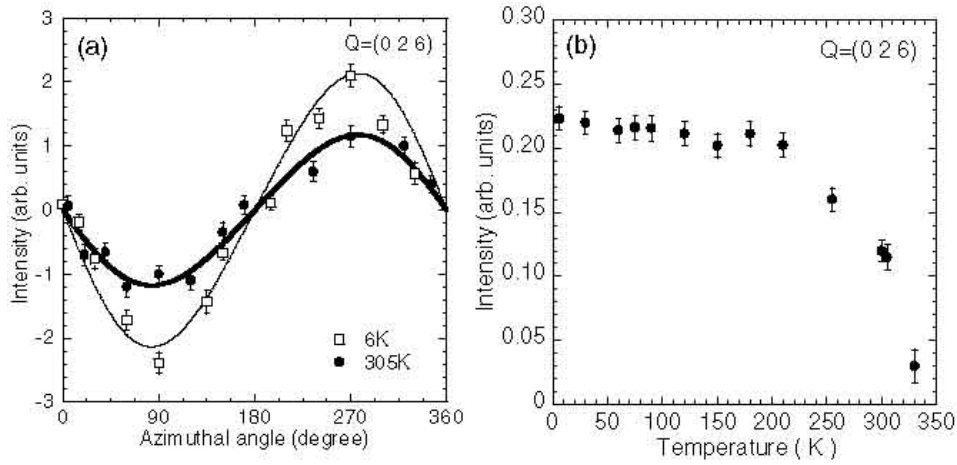


Figure 23. (a) Azimuthal angle dependence of the interference term for a main edge peak at 305 and 6 K at $Q=(0, 2, 6)$. The thick and thin curves denote the analysis results at 305 and 6 K, respectively. (b) Temperature dependence of the interference term at $Q=(0, 2, 6)$. As for details, readers refer Ref. [218]

Recently, Kubota et al. have performed the experiment to determine the orbital ordering in Ca_2RuO_4 by using the resonant X-ray scattering interference technique at the K edge of Ru [218]. In this new and skillful technique, it is remarkable that the d_{xy} orbital ordering is observed even at room temperature, in which the Jahn-Teller distortion is negligible. Note here that the Jahn-Teller distortion is defined as the ratio of the apical Ru-O bond length to the equatorial Ru-O bond length in the RuO_6 octahedron.

The resonant x-ray scattering (RXS) measurement has been very powerful method to detect the orbital ordering, but the conventional RXS measurement is not useful for the observation of a ferro-type orbital state, since it is difficult to extract the signal for the ferro-orbital ordered state at Γ point in a momentum space, which is accompanied with a large amplitude of a fundamental reflection by Thomson scattering. However, the RXS interference technique can observe the ferro-type orbital ordered state, in which the signal is magnified by the interference with a fundamental signal.

In Figs. 23, we show typical results at the K edge of Ru, obtained by Kubota et al. Figure 23(a) denotes the azimuthal angle dependence of the interference term for a main edge peak. We note that the signal exhibits the characteristic oscillation with the period of 360 degrees. Moreover, the significant signal can be found even at 305 K, in which the Jahn-Teller distortion is negligible. This fact suggests that the interference term is directly related to the orbital ordering. In Fig. 23(b), the temperature dependence of the RXS signal is shown. Below 200K, we can observe that the RXS signal for the ferro-type xy -orbital ordering is almost saturated due to the occurrence of the G-AF Néel state. Above 200 K, the magnitude of the signal is gradually decreased and becomes zero at the metal-insulator transition temperature (~ 357 K). Since the apical bond length of RuO_6 becomes almost equal to the averaged equatorial bond length around at 300K [212], it is

difficult to consider that the Jahn-Teller distortion is the origin of the orbital ordering. Thus, the coupling of t_{2g} electron with Jahn-Teller distortion is not the primary term of the electron-phonon coupling part. Rather, the tilting and/or buckling modes should be included seriously in the model Hamiltonian.

Finally, let us briefly mention another result of a resonant X-ray diffraction study on Ca_2RuO_4 at the Ru L_{II} and L_{III} edges [219]. Zegkinoglou et al. have observed a significant enhancement of the magnetic scattering intensity at the wave vector which characterizes the AF ordering. Then, they have found a phase transition between two paramagnetic phases around 260 K, in addition to the well-known AF transition at $T_{\text{N}}=110\text{K}$. Due to the analysis of polarization and azimuthal angle dependence of the diffraction signal, Zegkinoglou et al. have concluded that the transition at 260K is attributed to the orbital ordering of Ru t_{2g} electrons. This orbital order is characterized by the same propagation vector as the low-temperature AF phase. Note, however, that the ferro-orbital component of the ordering pattern cannot be ruled out, as mentioned by Zegkinoglou et al.

4.3. Geometrically frustrated systems

As an important ingredient to understand novel magnetism of actual strongly correlated electron materials, thus far we have emphasized a potential role of orbital degree of freedom, when electrons partially fill degenerate orbitals. However, on the lattice with *geometrical frustration*, a subtle balance among competing interactions easily leads to a variety of interesting phenomena such as unconventional superconductivity and exotic magnetism. The recent discovery of superconductivity in layered cobalt oxyhydrate $\text{Na}_{0.35}\text{CoO}_2 \cdot 1.3\text{H}_2\text{O}$ [206] has certainly triggered intensive investigations of superconductivity on the triangular lattice. Concerning the magnetism, antiferromagnetism on the triangle-based structure has a long history of investigation [220]. In the low-dimensional system, the combined effect of geometrical frustration and strong quantum fluctuation is a source of peculiar behavior in low-energy physics, as typically found in the Heisenberg zigzag chain with spin $S=1/2$. As the strength of frustration is increased, the ground state is known to be changed from a critical spin-liquid to a gapped dimer phase [221, 222, 223, 224]. In the dimer phase, neighboring spins form a valence bond to gain the local magnetic energy, while the correlation among the valence bonds is weakened to suppress the effect of spin frustration.

Here we have a naive question: What happens in a system with *both* active orbital degree of freedom and geometrical frustration? It is considered to be an intriguing issue to clarify the influence of orbital ordering on magnetic properties in geometrically frustrated systems. For instance, significant role of t_{2g} -orbital degree of freedom has been remarked to understand the mechanism of two phase transitions in spinel vanadium oxides AV_2O_4 ($A=\text{Zn}$, Mg , and Cd) [225, 226, 227]. It has been proposed that orbital ordering brings a spatial modulation in the spin exchange and spin frustration is consequently relaxed. Similarly, for MgTi_2O_4 , the formation of a valence-bond crystal

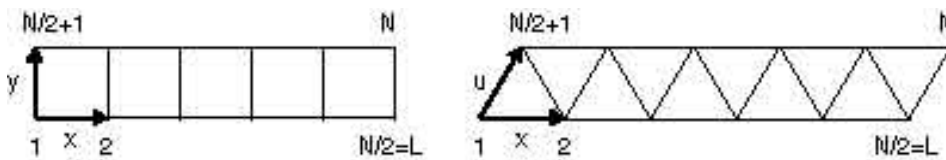


Figure 24. Lattice location and site numbering of N -site ladder and zigzag chain. The length is defined as $L=N/2$.

due to orbital ordering has been also suggested [228, 229].

Since d - and f -electron orbitals are spatially anisotropic, there always exist easy and hard directions for electron motion. Thus, it is reasonable to expect that the effect of geometrical frustration would be reduced due to orbital ordering, depending on the lattice structure and the type of orbital, in order to arrive at the spin structure which minimizes the influence of frustration. However, the spin structure on such an orbital-ordered background may be fragile, since the effect of geometrical frustration never vanishes, unless the lattice distortion is explicitly taken into account. It is a highly non-trivial problem, whether such an orbital arrangement actually describes the low-energy physics of geometrically frustrated systems. In particular, it is important to clarify how the orbital-arranged background is intrinsically stabilized through the spin-orbital correlation even without the electron-lattice coupling. In this subsection, we review the recent result by Onishi and Hotta concerning the role of orbital ordering in the geometrically frustrated lattice [230, 231, 232, 233].

Onishi and Hotta have considered an e_g -orbital model on the N -site ladder or zigzag chain, including one electron per site with two orbitals, i.e., quarter filling. The lattice they have used is shown in Fig. 24. Note that the zigzag chain is composed of equilateral triangles. The e_g -orbital degenerate Hubbard model is already given by Eq. (63), but the electron-phonon term is not considered. Namely, the model is written as

$$H_{e_g} = H_{\text{kin}}^{e_g} + H_{\text{el-el}}^{e_g}. \quad (101)$$

Here the d -electron hopping amplitude $t_{\gamma,\gamma'}^{\mathbf{a}}$ for the oblique u direction is defined by $t_{aa}^{\mathbf{u}}=t_1/4$, $t_{ab}^{\mathbf{u}}=t_{ba}^{\mathbf{u}}=\sqrt{3}t_1/8$, $t_{bb}^{\mathbf{u}}=3t_1/16$. Note the relation of $t_{\gamma\gamma'}^{\mathbf{u-x}}=t_{\gamma\gamma'}^{\mathbf{u}}$. Concerning hopping amplitudes along x - and y -directions, see Eqs. (55) and (56). In this subsection, t_1 is taken as the energy unit.

In order to analyze the complex model including both orbital degree of freedom and geometrical frustration, Onishi and Hotta have employed the finite-system density matrix renormalization group (DMRG) method, which is appropriate for the analysis of quasi-one-dimensional systems with the open boundary condition [234, 235, 236]. Since one site includes two e_g orbitals and the number of bases is 16 per site, the size of the superblock Hilbert space becomes very large as $m^2 \times 16^2$, where m is the number of states kept for each block. To accelerate the calculation and to save memory resources, Onishi has skillfully reduced the size of the superblock Hilbert space to $m^2 \times 4^2$, by treating each orbital as an effective site. In the actual calculations, m states up to $m=200$ were

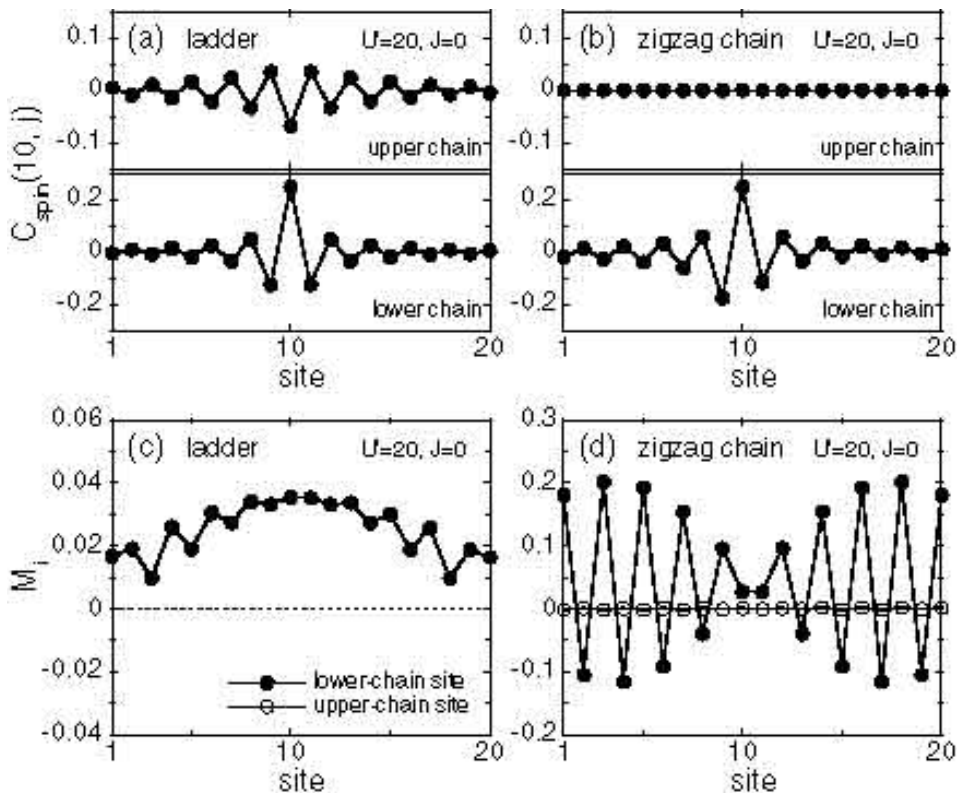


Figure 25. The spin-correlation function measured from the center of the lower chain for the PM ground state in (a) the ladder and (b) the zigzag chain. The local magnetization for the first spin-excited state in (c) the ladder and (d) the zigzag chain.

kept in the renormalization process and the truncation error was estimated to be 10^{-5} at most.

Now we introduce the results on the spin structure of the paramagnetic (PM) ground state at $J=0$, since the zigzag chain is relevant to a geometrically frustrated antiferromagnet in the spin-singlet PM phase. Here we refer only the result for $J=0$, but readers should consult with Ref. [230] about the results for $J \neq 0$. In Figs. 25(a) and 25(b), we show the DMRG results for $N=40$ of the spin-correlation function $C_{\text{spin}}(\mathbf{i}, \mathbf{j}) = \langle S_i^z S_j^z \rangle$ with $S_i^z = \sum_{\gamma} (\rho_{i\gamma\uparrow} - \rho_{i\gamma\downarrow})/2$. Note that a large value of $U'=20$ was used to consider the strong-coupling region, but the results did not change qualitatively for smaller values of U' . As shown in Fig. 25(a), we observe a simple Néel structure in the ladder. On the other hand, in the zigzag chain, there exists AF correlation between intra-chain sites in each of lower and upper chains, while the spin correlation between inter-chain sites is much weak. Namely, the zigzag chain is considered to be decoupled to a double chain in terms of the spin structure.

In order to clarify the characteristics of the spin structure in the excited state, Onishi and Hotta have investigated the local magnetization $M_i = \langle S_i^z \rangle$ for the lowest-energy state with $S_{\text{tot}}^z = 1$, i.e., the first spin-excited state, where S_{tot}^z is the z component of the total spin. In the ladder, the total moment of $S_{\text{tot}}^z = 1$ is distributed to the whole

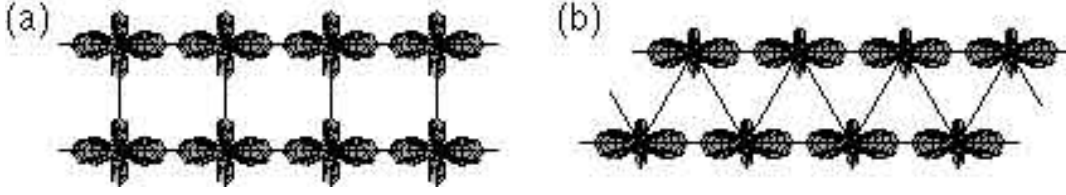


Figure 26. Optimal orbital arrangement in (a) the ladder and (b) the zigzag chain.

system and there is no significant structure, as shown in Fig. 25(c). On the other hand, the situation is drastically changed in the zigzag chain. As shown in Fig. 25(d), the total moment of $S_{\text{tot}}^z=1$ is confined in the lower chain and it forms a sinusoidal shape with a node, while nothing is found in the upper chain. Note that the sinusoidal shape of the local magnetization is characteristic of the $S=1/2$ AF Heisenberg chain with edges at low temperatures [237, 238]. Thus, the double-chain nature in the spin structure remains robust even for the spin-excited state.

Onishi and Hotta have also discussed the orbital arrangement to understand the mechanism of the appearance of the spin structures. For the determination of the orbital arrangement, orbital correlations are usually measured, but due care should be paid to the definition. By analogy with Eqs. (77) and (78) which have treated the phase of the JT distortions, phase-dressed operators are introduced as

$$\begin{cases} \tilde{d}_{ia\sigma} = e^{i\theta_i/2}[\cos(\theta_i/2)d_{ia\sigma} + \sin(\theta_i/2)d_{ib\sigma}], \\ \tilde{d}_{ib\sigma} = e^{i\theta_i/2}[-\sin(\theta_i/2)d_{ia\sigma} + \cos(\theta_i/2)d_{ib\sigma}]. \end{cases} \quad (102)$$

Then, the optimal set of $\{\theta_i\}$ is determined so as to maximize the orbital-correlation function, which is defined as

$$T(\mathbf{q}) = (1/N^2) \sum_{\mathbf{i}, \mathbf{j}} \langle \tilde{T}_{\mathbf{i}}^z \tilde{T}_{\mathbf{j}}^z \rangle e^{i\mathbf{q} \cdot (\mathbf{i} - \mathbf{j})}, \quad (103)$$

with $\tilde{T}_{\mathbf{i}}^z = \sum_{\sigma} (\tilde{d}_{ia\sigma}^\dagger \tilde{d}_{ia\sigma} - \tilde{d}_{ib\sigma}^\dagger \tilde{d}_{ib\sigma})/2$.

As shown in Fig. 26(a), in the case of the ladder, Onishi and Hotta have found that a ferro-orbital (FO) ordering, characterized by $\theta_i/\pi \sim 1.18$, appears in the ground state. In the first spin-excited state, the FO structure also appears, but the angle characterizing the orbital shape is slightly changed as $\theta_i/\pi \sim 1.20$ to further extend to the leg direction. On the other hand, in the zigzag chain, it is observed that *both* in the ground and first spin-excited states, $T(\mathbf{q})$ becomes maximum at $\mathbf{q}=0$ with $\theta_i/\pi \sim 1.32$, indicating a $3x^2-r^2$ orbital at each site, as shown in Fig. 26(b). Note that the orbital arrangement is unchanged even in the spin-excited state. Namely, the orbital degree of freedom spontaneously becomes “dead” in low-energy states to suppress the effect of spin frustration.

It is interesting to remark that the spin-exchange interactions become anisotropic due to the orbital-arranged background. First let us consider the zigzag chain, which is effectively described by the Hubbard model composed of $3x^2-r^2$ orbital. It is intuitively understood that the AF exchange interaction along the u direction J_1 should be much

weaker than that along the x direction J_2 , since the orbital shape extends along the double chain, not along the zigzag path, as shown in Fig. 26(b). In order to estimate the ratio of J_1/J_2 , it is enough to consider the hopping amplitudes between adjacent optimal “a”-orbitals, $3x^2-r^2$ in this case, which are given by $\tilde{t}_{aa}^x=1$ and $\tilde{t}_{aa}^u=1/64$. Then, taking account of the second-order process in terms of electron hopping between only $3x^2-r^2$ orbitals, we obtain $J_1/J_2 = [2(\tilde{t}_{aa}^u)^2/U]/[2(\tilde{t}_{aa}^x)^2/U] = 1/64^2$. This small value of J_1/J_2 clearly indicates that the spin correlation on the zigzag path is reduced due to the spatial anisotropy of $3x^2-r^2$ orbital. Thus, the zigzag chain is effectively reduced to a double-chain system of the $S=1/2$ AF Heisenberg chain, suggesting that the spin gap should be extremely suppressed, since the spin gap decreases exponentially with the increase of J_2/J_1 in the gapped dimer phase in the zigzag spin chain [224].

On the other hand, in the ladder with the ferro-orbital structure as shown in Fig. 26(a), the orbital shape extends to the rung direction as well as to the leg direction. When we define J_{leg} and J_{rung} as the AF exchange interactions along the leg and rung directions, respectively, we obtain $J_{\text{rung}}/J_{\text{leg}}=0.26$, which is much larger than $J_1/J_2=1/64^2$ in the case of the zigzag chain. The spin correlation on the rung is considered to remain finite, leading to the simple Néel structure. Thus, the spin excitation in the ladder is expected to be gapful similar to the spin ladder [239, 240].

We have reviewed both ground- and excited-state properties of the e_g -orbital degenerate Hubbard model on the ladder and the zigzag chain. It has been found that the zigzag chain is reduced to a decoupled double-chain spin system due to the selection of a specific orbital. It is considered as a general feature of geometrically frustrated multi-orbital systems that the orbital selection spontaneously occurs so as to suppress the effect of spin frustration.

Finally, let us briefly comment on the effect of level splitting between x^2-y^2 and $3z^2-r^2$ orbitals, which has not been considered in the present Hamiltonian. In particular, when $3z^2-r^2$ orbital is the lower level which is well separated from x^2-y^2 orbital, the hopping amplitude does not depend on the direction and the effect of spin frustration revives for the system with isotropic AF interactions. In such a region with strong spin frustration, a finite energy gap between ground and first-excited states can be clearly observed. Naively thinking, it may be called a spin gap, but we should note that the orbital arrangement is significantly influenced by the spin excitation. In general, the energy gap between ground and first-excited states in multi-orbital systems should be called a *spin-orbital* gap. As for details, readers consult with Ref. [241]

5. Model Hamiltonian for f -electron systems

Thus far, we have reviewed the theoretical results on orbital ordering phenomena of d -electron systems. As typical examples, we have picked up manganites, nickelates, and ruthenates. However, there exists another spin-charge-orbital complex system such as f -electron compounds. In the latter half of this article, we review orbital ordering phenomena of f -electron systems. Before proceeding to the description of the theoretical

results, again it is necessary to set the model Hamiltonian for *f*-electron systems. In order to construct such a microscopic Hamiltonian, we must include simultaneously the itinerant nature of *f* electrons as well as the effects of strong electron correlation, CEF, and spin-orbit interaction. Among them, the existence of strong spin-orbit interaction is essential difference from *d*-electron systems. The inclusion of the spin-orbit interaction is a key issue, when we construct the model Hamiltonian for *f* electron materials. Since this is a complicated problem, it is instructive to start the discussion with a more basic level. Namely, we first review in detail the single ion problem focusing on the properties of local *f*-electron states in comparison with those obtained in the *LS* and *j-j* coupling schemes. Then, we move on to the explanation of the microscopic *f*-electron model on the basis of the *j-j* coupling scheme.

5.1. *LS* vs. *j-j* coupling schemes

In the standard textbook, it is frequently stated that for rare-earth ion systems, the *LS* coupling scheme works well, while for actinides, in particular, heavy actinides, the *j-j* coupling scheme becomes better. However, do we simply accept such a statement? Depending on the level of the problem in the condensed matter physics, the validity of the approximation should be changed, but such a point has not been explained in the textbook. It is important to clarify which picture is appropriate for the purpose to consider the many-body phenomena in *f*-electron systems.

Let us generally consider the f^n configuration, where n is the number of *f* electrons included on a localized ion. In the *LS* coupling scheme, first the spin \mathbf{S} and angular momentum \mathbf{L} are formed due to Hund's rules as $\mathbf{S}=\sum_{i=1}^n \mathbf{s}_i$ and $\mathbf{L}=\sum_{i=1}^n \mathbf{l}_i$, where \mathbf{s}_i and \mathbf{l}_i are spin and angular momentum for *i*-th *f* electron. Note that the Hund's rules are based on the Pauli principle and Coulomb interactions among *f* electrons. After forming \mathbf{S} and \mathbf{L} , we include the effect of spin-orbit interaction, given by $\lambda\mathbf{L}\cdot\mathbf{S}$, where λ is the spin-orbit coupling. We note that $\lambda>0$ for $n<7$, while $\lambda<0$ for $n>7$. Note also that a good quantum number to label such a state is the total angular momentum \mathbf{J} , given by $\mathbf{J}=\mathbf{L}+\mathbf{S}$. Following from simple algebra, the ground-state level is characterized by $J=|L-S|$ for $n<7$, while $J=L+S$ for $n>7$.

On the other hand, when the spin-orbit interaction becomes larger than the Coulomb interactions, it is useful to consider the problem in the *j-j* coupling scheme. First, we include the spin-orbit coupling so as to define the state labeled by the total angular momentum \mathbf{j}_i for the *i*-th electron, given by $\mathbf{j}_i=\mathbf{s}_i+\mathbf{l}_i$. For *f*-orbitals with $\ell=3$, we immediately obtain an octet with $j=7/2(=3+1/2)$ and a sextet with $j=5/2(=3-1/2)$, which are well separated by the spin-orbit interaction. Note here that the level for the octet is higher than that of the sextet. Then, we take into account the effect of Coulomb interactions to accommodate n electrons among the sextet and/or octet, leading to the ground-state level in the *j-j* coupling scheme.

As is easily understood from the above discussion, the *LS* coupling scheme works well under the assumption that the Hund's rule coupling is much larger than the spin-

orbit interaction, since \mathbf{S} and \mathbf{L} are formed by the Hund's rule coupling prior to the inclusion of spin-orbit interaction. It is considered that this assumption is valid for insulating compounds with localized f electrons. However, when the spin-orbit interaction is not small compared with the Hund's rule coupling, the above assumption is not always satisfied. In addition, if the f electrons become itinerant owing to hybridization with the conduction electrons, the effect of Coulomb interactions would thereby be effectively reduced. In rough estimation, the effective size of the Coulomb interaction may be as large as the bandwidth of f electrons, leading to a violation of the assumption required for the LS coupling scheme.

Furthermore, even in the insulating state, we often encounter some difficulties to understand the complex magnetic phases of f -electron systems with active *multipole* degrees of freedom from a microscopic viewpoint. In a phenomenological level, it is possible to analyze a model for relevant multipoles obtained from the LS coupling scheme, in order to explain the phenomena of multipole ordering. However, it is difficult to understand the origin of the interaction between multipoles in the LS coupling scheme.

From these viewpoints, it seems to be rather useful to exploit the j - j coupling scheme for the purpose to understand magnetism and superconductivity of f -electron materials. Since individual f -electron states is clearly defined, it is convenient for including many-body effects using the standard quantum-field theoretical techniques. However, it is not the reason to validate to use the j - j coupling scheme for the model construction. In order to clarify how the j - j coupling scheme works, it is necessary to step back to the understanding of the local f -electron state. In the next subsection, let us consider this issue in detail.

5.2. Local f -electron state

In general, the local f -electron term is composed of three parts as

$$H_f = H_{\text{el-el}} + H_{\text{so}} + H_{\text{CEF}}, \quad (104)$$

where H_C is the Coulomb interaction term, written as

$$H_{\text{el-el}} = \sum_{\mathbf{i}} \sum_{m_1 \sim m_4} \sum_{\sigma_1, \sigma_2} I_{m_1, m_2, m_3, m_4}^f f_{\mathbf{i}m_1\sigma_1}^\dagger f_{\mathbf{i}m_2\sigma_2}^\dagger f_{\mathbf{i}m_3\sigma_2} f_{\mathbf{i}m_4\sigma_1}. \quad (105)$$

Here $f_{\mathbf{i}m\sigma}$ is the annihilation operator for f -electron with spin σ and angular momentum $m(=-3, \dots, 3)$ at a site \mathbf{i} . Similar to the d -electron case, the Coulomb integral I_{m_1, m_2, m_3, m_4}^f is given by

$$I_{m_1, m_2, m_3, m_4}^f = \delta_{m_1+m_2, m_3+m_4} \sum_{k=0}^6 F_f^k c^{(k)}(m_1, m_4) c^{(k)}(m_2, m_3), \quad (106)$$

where the sum on k includes only even values ($k=0, 2, 4,$ and 6), F_f^k is the Slater-Condon parameter for f electrons including the complex integral of the radial function, and c^k

is the Gaunt coefficient. It is convenient to express the Slater-Condon parameters as

$$\begin{aligned} F_f^0 &= A + 15C + 9D/7, \\ F_f^2 &= 225(B - 6C/7 + D/42), \\ F_f^4 &= 1089(5C/7 + D/77), \\ F_f^6 &= (429/5)^2 \cdot (D/462), \end{aligned} \quad (107)$$

where A , B , C , and D are the Racah parameters for f electrons [123].

The spin-orbit coupling term, H_{so} , is given by

$$H_{\text{so}} = \sum_{\mathbf{i}} \sum_{m,\sigma,m',\sigma'} \lambda_{\text{so}} \zeta_{m,\sigma,m',\sigma'} f_{\mathbf{i}m\sigma}^\dagger f_{\mathbf{i}m'\sigma'}, \quad (108)$$

where λ_{so} is the spin-orbit interaction and the matrix elements are explicitly given by

$$\begin{aligned} \zeta_{m,\sigma,m,\sigma} &= m\sigma/2, \\ \zeta_{m+1,\downarrow,m,\uparrow} &= \sqrt{12 - m(m+1)}/2, \\ \zeta_{m-1,\uparrow,m,\downarrow} &= \sqrt{12 - m(m-1)}/2, \end{aligned} \quad (109)$$

and zero for other cases.

The CEF term H_{CEF} is given by

$$H_{\text{CEF}} = \sum_{\mathbf{i},m,m',\sigma} A_{m,m'} f_{\mathbf{i}m\sigma}^\dagger f_{\mathbf{i}m'\sigma}, \quad (110)$$

where $A_{m,m'}$ can be evaluated in the same manner as has done in Sec. 2 for d electrons with $\ell=2$. However, there is no new information, if we repeat here lengthy calculations for f electrons with $\ell=3$. As already mentioned in Sec. 2, it is rather useful and convenient to consult with the table of Hutchings for angular momentum $J=3$ [120]. For cubic symmetry, $A_{m,m'}$ is expressed by using a couple of CEF parameters, B_4^0 and B_6^0 , as

$$\begin{aligned} A_{3,3} &= A_{-3,-3} = 180B_4^0 + 180B_6^0, \\ A_{2,2} &= A_{-2,-2} = -420B_4^0 - 1080B_6^0, \\ A_{1,1} &= A_{-1,-1} = 60B_4^0 + 2700B_6^0, \\ A_{0,0} &= 360B_4^0 - 3600B_6^0, \\ A_{3,-1} &= A_{-3,1} = 60\sqrt{15}(B_4^0 - 21B_6^0), \\ A_{2,-2} &= A_{-2,2} = 300B_4^0 + 7560B_6^0. \end{aligned} \quad (111)$$

Following the traditional notation, we define

$$\begin{aligned} B_4^0 &= Wx/F(4), \\ B_6^0 &= W(1 - |x|)/F(6), \end{aligned} \quad (112)$$

where x specifies the CEF scheme for O_h point group, while W determines an energy scale for the CEF potential. Although $F(4)$ and $F(6)$ have not been determined uniquely, we simply follow the traditional definitions as $F(4)=15$ and $F(6)=180$ for $J=3$ [120].

Here we note that the CEF potential is originally given by the sum of electrostatic energy from the ligand ions at the position of f -electron ion, leading to the one-electron potential acting on the charge distribution of f -orbitals, as expressed by Eq. (110).

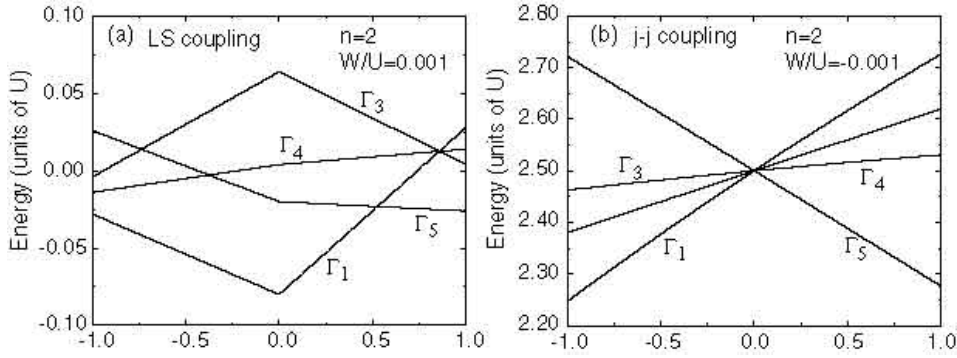


Figure 27. Energies of *f* electrons as functions of *x* for (a) the *LS* coupling and (b) the *j-j* coupling schemes for *n*=2. The magnitude of the CEF potential energy is fixed as $|W|/U=0.001$.

Thus, in principle, it is not necessary to change the CEF potential, depending on the *f*-electron number. As we will see later, the CEF schemes for *n*=1~13 are automatically reproduced by diagonalizing the local *f*-electron term H_{loc} , once we fix the CEF parameters in the form of one-electron potential Eq. (110).

Now we compare the electronic states of H_{loc} with those of *LS* and *j-j* coupling schemes. We believe that it is quite instructive to understand the meanings of the CEF potential in *f*-electron systems. We introduce “*U*” as an energy scale for the Racah parameters, *A*, *B*, *C*, and *D*. In this subsection, *U* is the energy unit, which is typically considered to be 1 eV. In *f*-electron compounds, the magnitude of the CEF potential is much smaller than both spin-orbit coupling and Coulomb interactions. Thus, it is reasonable to consider that *W* is always much smaller than λ_{so} and *U*. However, there occur two situations, depending on the order for taking the limits of $\lambda_{so}/W \rightarrow \infty$ and $U/W \rightarrow \infty$. When the limit of $U/W \rightarrow \infty$ is first taken and then, we include the effect of the spin-orbit coupling λ_{so} , we arrive at the *LS* coupling scheme. On the other hand, it is also possible to take first the infinite limit of λ_{so}/W . After that, we include the effect of Coulomb interaction, leading to the *j-j* coupling scheme. In the present local *f*-electron term H_{loc} , it is easy to consider two typical situations for *f*-electron problems, $|W| \ll \lambda_{so} < U$ and $|W| \ll U < \lambda_{so}$, corresponding to the *LS* and *j-j* coupling schemes, respectively.

Let us consider the case of *n*=2 as a typical example of the comparison between the two schemes. In the *LS* coupling scheme for the *f*²-electron system, we obtain the ground-state level as ³*H* with *S*=1 and *L*=5 from the Hund’s rules, where *S* and *L* denote sums of *f*-electron spin and angular momentum, respectively. Upon further including the spin-orbit interaction, the ground state is specified by *J*=4 expressed as ³*H*₄ in the traditional notation. Note that the total angular momentum *J* is given by $J=|L-S|$ and $J=L+S$ for *n*<7 and *n*>7, respectively. In order to consider further the CEF effect, we consult with the table of Hutchings for the case of *J*=4. In the *LS* coupling scheme, *W* is taken as $W/U=0.001$ and we set $F(4)=60$ and $F(6)=1260$ for

$J=4$ by following the traditional definitions [120]. Then, we easily obtain the nine eigenvalues, including Γ_1 singlet, Γ_3 doublet, and two kinds of triplets, Γ_4 and Γ_5 , as shown in Fig. 27(a). Note that for odd n , the eigenstate has odd parity, specified by “u” in Mulliken’s notation and “−” in Bethe’s notation, while the even n configuration has even parity, labeled by “g” and “+” [242]. When we use Bethe’s notation to specify the *f*-electron eigenstate, the “+” or “−” superscript is suppressed for convenience.

In the *j-j* coupling scheme, on the other hand, first we take the infinite limit of λ_{so} . Thus, we consider only the $j=5/2$ sextet, where j denotes the total angular momentum of one *f* electron. In the f^2 -electron system, two electrons are accommodated in the sextet, leading to fifteen eigen states including $J=4$ nontet, $J=2$ quintet, and $J=0$ singlet. Due to the effect of Hund’s rule coupling, $J=4$ nontet should be the ground state. When we further include the CEF potential, it is necessary to reconsider the accommodations of two electrons in the f^1 -electron potential with Γ_7 doublet and Γ_8 quartet. Thus, in the *j-j* coupling schemes, except for the energy scale W , only relevant CEF parameter is x , leading to the level splitting between Γ_7 doublet and Γ_8 quartet. For the *j-j* coupling scheme, we set $F(4)=60$ and $W/U=-0.001$. Note that the minus sign in W is added for the purpose of the comparison with the *LS* coupling scheme. As shown in Fig. 27(b), the $J=4$ nontet is split into Γ_1 singlet, Γ_3 doublet, Γ_4 triplet, and Γ_5 triplet. The ground state for $x>0$ is Γ_5 triplet composed of a couple of Γ_8 electrons, while for $x<0$, it is Γ_1 singlet which is mainly composed of two Γ_7 electrons. Note that for $x>0$, the first excited state is Γ_4 triplet, composed of Γ_7 and Γ_8 electrons.

At the first glance, the energy levels in the *j-j* coupling scheme seems to be different from those of the *LS* coupling scheme. How do we connect these different results? In order to answer to this question, let us directly diagonalize H_f by changing U and λ . Here it is convenient to introduce a new parameter to connect the *LS* and *j-j* coupling schemes as

$$k = \frac{\lambda_{\text{so}}/|W|}{U/|W| + \lambda_{\text{so}}/|W|}, \quad (113)$$

where we explicitly show $|W|$ in this formula, since both U and λ_{so} should be always very large compared with $|W|$ in actual *f*-electron compounds. Note that $k=0$ and 1 are corresponding to the limits of $\lambda_{\text{so}}/U=0$ and $\lambda_{\text{so}}/U=\infty$, respectively. Then, we can control the change of two schemes by one parameter k , by keeping $U/|W|\gg 1$ and $\lambda_{\text{so}}/|W|\gg 1$.

In Figs. 28(a)-(d), we show the energy levels of H_f for several values of k with both λ_{so} and U larger than $|W|$. Racah parameters are set as $A/U=10$, $B/U=0.3$, $C/U=0.1$, and $D/U=0.05$ in the units of U . As described above, the CEF potential is always small and here we set $W/U=-0.001$. In Fig. 28(a), results for $k=0.1$ are shown. In this case, $\lambda_{\text{so}}/U=0.11$, while the condition $\lambda_{\text{so}}/|W|\gg 1$ is still satisfied. Without the spin-orbit interaction, the ground-state level is expressed as 3H with $S=1$ and $L=5$ due to the Hund’s rules. When we increase λ_{so} , the multiplets labeled by J are well separated and the ground-state level is specified by $J=4$, as expected from the *LS* coupling scheme. Then, the energy levels in Fig. 28(a) are quite similar to those of Fig. 27(a), since we

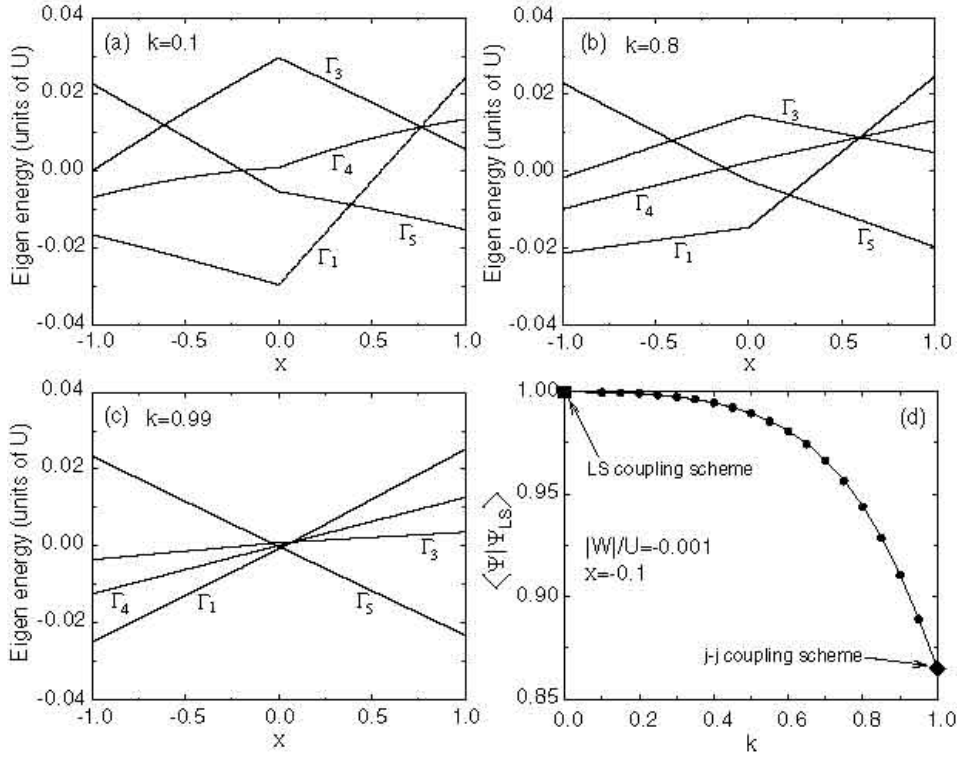


Figure 28. Eigen energies of H_f as functions of x for (a) $k=0.1$, (b) $k=0.8$, and (c) $k=0.99$. Racah parameters are set as $A/U=10$, $B/U=0.3$, $C/U=0.1$, and $D/U=0.05$. The energy scale for CEF potentials are given by $W/U=-0.001$. (d) Overlap integral between the eigenstate of H_f and that in the LS coupling scheme for the case of the Γ_1 ground state. Solid squares at $k=0$ and 1 are obtained separately from the LS and j - j coupling schemes, respectively.

are now in the region where the LS coupling scheme is appropriate.

Even when λ_{so} is further increased and k is equal to 0.5, the structure of the energy levels is almost the same as that of the LS coupling scheme (not shown here). However, when k becomes 0.8, as shown in Fig. 28(b), the energy level structure is found to be deviated from that of the LS coupling scheme. Rather, it becomes similar to the energy level structure of the j - j coupling scheme. To see the agreement with the j - j coupling scheme more clearly, we consider very large λ which gives $k=0.99$. As shown in Fig. 28(c), we can observe the energy level structure similar to Fig. 27(b). In particular, the region of the Γ_3 ground state becomes very narrow, as discussed later. Thus, it is concluded that H_f actually reproduces the energy levels both for the LS and j - j coupling schemes. We also stress that H_f provides correct results in any value of f -electron number.

A crucial point is that the structure of energy levels is continuously changed, as long as λ_{so} and U are large compared with the CEF potential. Namely, the states both in the LS and j - j coupling schemes are continuously connected in the parameter space. Thus, depending on the situation to consider the problem, we are allowed to use

either *LS* or *j-j* coupling scheme. In order to clarify this point, we evaluate the overlap $\langle \Psi | \Psi_{LS} \rangle$, where $|\Psi\rangle$ and $|\Psi_{LS}\rangle$ are the eigenstate of H_f and that in the *LS* coupling scheme, respectively. In Fig. 28(d), we show the overlap for the case of Γ_1 ground state for $x=-0.1$ and $W/U=-0.001$. For $k=0$, $\langle \Psi | \Psi_{LS} \rangle=1$ due to the definition. The overlap is gradually decreased with the increase of k , but it smoothly converges to the value at $k=1$, i.e., the *j-j* coupling scheme. Note that the overlap between the eigenstates of the *LS* and *j-j* coupling schemes is as large as 0.865, which seems to be larger than readers may naively anticipated from the clear difference between Figs. 27(a) and 27(b). It is not surprising, if we are based on the principle of adiabatic continuation, since the eigenstates of the *LS* and *j-j* coupling schemes are continuously connected.

Remark that we can observe the common structure around at the value of x , in which singlet and triplet ground states are interchanged. Namely, essential point of the singlet-triplet crossing can be captured both in the two schemes. However, the Γ_3 non-Kramers doublet cannot be the ground state in the *j-j* coupling scheme, since the doublet in the $J=4$ nontet is composed of degenerate two singlets formed by Γ_7 and Γ_8 electrons. As easily understood, such singlets are energetically penalized by the Hund's rule interaction and the energy for Γ_4 triplet composed of Γ_7 and Γ_8 electrons is always lower than that of the singlets. Thus, in the *j-j* coupling scheme, Γ_3 non-Kramers doublet does not appear as the ground state except for $x=0$.

Of course, if $j=7/2$ octet is explicitly included and λ is kept finite, it is possible to reproduce Γ_3 doublet. Namely, taking account of the effect of $j=7/2$ octet is equivalent to consider the local *f*-electron term H_f , as we have done in this subsection. If we simply expand the Hilbert space so as to include both $j=5/2$ sextet and $j=7/2$ octet, we lose the advantage of the *j-j* coupling scheme considering only $j=5/2$ sextet. However, for an actual purpose, it is enough to consider perturbatively such effect in the order of $1/\lambda_{so}$. In fact, quite recently, Hotta and Harima have shown that the result of the *LS* coupling scheme can be reproduced quantitatively even in the *j-j* coupling scheme, when the effect of $j=7/2$ octet is included as effective one- and two-body potentials up to the order of $1/\lambda_{so}$ [243].

One may claim that it is possible to reproduce the result of the *LS* coupling scheme even within the *j-j* coupling scheme, just by assuming that the CEF potential for $J=4$ in the *LS* coupling scheme also works on the $J=4$ f^2 -states composed of a couple of *f* electrons among $j=5/2$ sextet. However, such a procedure is *not* allowed due to the following two reasons. First it should be noted that the CEF potential is *not* determined only by the value of J . For instance, the results of the energy levels for $n=7$ and 13 are apparently different, even though both of the ground-state multiplets are characterized by $J=7/2$, since the CEF potential depends also on the values of L and S . Note that for $n=7$, $S=7/2$ and $L=0$, while for $n=13$, $L=3$ and $S=1/2$. For the case of $n=2$, even if the f^2 -state is characterized by $J=4$ in the *j-j* coupling scheme, we cannot simply validate the application of the CEF potential in the *LS* coupling scheme to the $J=4$ f^2 -state in the *j-j* coupling scheme.

Second we should note again that the CEF effect appears only as a one-electron

potential. The CEF potential working on the two-electron state should be given by the superimposition of the one-electron potential. Thus, when we use the basis which diagonalizes the spin-orbit interaction, it is necessary to consider that the CEF potential should work on the state labeled by the z -component of j . This is the only way to define the CEF potential in the j - j coupling scheme, even though the Γ_3 non-Kramers doublet is not reproduced. As mentioned in the above paragraph, in order to reproduce the results of the LS coupling scheme including the non-Kramers doublet, it is necessary to consider appropriately the effect of $j=7/2$ octet, leading to the effective potential among $j=5/2$ states.

5.3. Local *f*-electron term in the j - j coupling scheme

In the previous subsection, we have shown the relation between LS and j - j coupling schemes on the basis of the local term including correctly the Coulomb interaction, spin-orbit coupling, and CEF potential terms. In order to make further steps to the construction of a microscopic Hamiltonian, let us first discuss the local f -electron state on the basis of the j - j coupling scheme. For the purpose, it is necessary to define the one f -electron state, labelled by μ , but in the j - j coupling scheme, the meaning of μ is clear. In the case of $n < 7$, μ should be the label to specify the state in the $j=5/2$ sextet, namely, the z -component of the total angular momentum $j=5/2$ and takes the values of $\mu = -5/2, -3/2, \dots, 5/2$. Note that for $3 < n < 7$, $j=7/2$ octet is *not* occupied, since we presume that the effect of spin-orbit interaction is larger than that of the Hund's rule coupling in the j - j coupling scheme. On the other hand, for the case of $n \geq 7$, μ should be considered to specify the state in the $j=7/2$ octet, since $j=5/2$ sextet is fully occupied. Note again that spin-orbit interaction is larger than that of the Hund's rule coupling. In this paper, we concentrate only on the case of $n < 7$. Thus, in the following, μ indicates the z -component of the total angular momentum which specifies the state in the $j=5/2$ sextet.

In the j - j coupling scheme, the local f -electron term should be composed of two parts as

$$H_{\text{loc}} = H_{\text{CEF}} + H_{\text{el-el}}, \quad (114)$$

where $H_{\text{el-el}}$ and H_{CEF} are Coulomb interactions among f electrons and the CEF term, respectively. Note that the spin-orbit interaction has been already included, when we define the one f -electron state in the j - j coupling scheme. In order to express $H_{\text{el-el}}$ and H_{CEF} , it is useful to define the annihilation operator of f electron in the j - j coupling scheme, $a_{i\mu}$, which is related to $f_{im\sigma}$ with real-spin σ and orbital m ($= -3, \dots, 3$) as

$$a_{i\mu} = \sum_{\sigma} C_{\mu\sigma} f_{i,\mu-\sigma/2,\sigma}. \quad (115)$$

where $C_{\mu\sigma}$ is the Clebsch-Gordan coefficient, given by

$$C_{\mu\sigma} = -\sigma \sqrt{\frac{7/2 - \mu\sigma}{7}}, \quad (116)$$

with $\sigma=+1$ (-1) for up (down) real spin.

As mentioned in the the previous subsection, in the *j-j* coupling scheme, we should take into account the CEF effect as the one-electron potential. Multi-electron state is obtained by simply accommodating electrons due to the balance between the Coulomb interaction and the one-electron potential, as has been done in *d*-electron systems. Then, the CEF term is given by

$$H_{\text{CEF}} = \sum_{\mathbf{i}, \mu, \nu} B_{\mu\nu} a_{\mathbf{i}\mu}^\dagger a_{\mathbf{i}\nu}, \quad (117)$$

where $B_{\mu\nu}$ is expressed by the CEF parameters for $J=5/2$. For the case of cubic structure, we can easily obtain

$$\begin{aligned} B_{\pm 5/2, \pm 5/2} &= 60B_4^0, \\ B_{\pm 3/2, \pm 3/2} &= -180B_4^0, \\ B_{\pm 1/2, \pm 1/2} &= 120B_4^0, \\ B_{\pm 5/2, \mp 3/2} &= B_{\mp 3/2, \pm 5/2} = 60\sqrt{5}B_4^0, \end{aligned} \quad (118)$$

and zero for other μ and ν . For the case of tetragonal structure, we obtain

$$\begin{aligned} B_{\pm 5/2, \pm 5/2} &= 10B_2^0 + 60B_4^0, \\ B_{\pm 3/2, \pm 3/2} &= -2B_2^0 - 180B_4^0, \\ B_{\pm 1/2, \pm 1/2} &= -8B_2^0 + 120B_4^0, \\ B_{\pm 5/2, \mp 3/2} &= B_{\mp 3/2, \pm 5/2} = 12\sqrt{5}B_4^0, \end{aligned} \quad (119)$$

and zero for other μ and ν .

Note that the coefficients B_n^m are, in actuality, determined by the fitting of experimental results for physical quantities such as magnetic susceptibility and specific heat. Note also that the above formulae have been obtained from the case of $J=5/2$. In general, the CEF term is expressed in matrix form, depending on the value of J ; for J larger than $5/2$, higher terms in B_n^m should occur. However, as already mentioned above, since in this paper the effect of the CEF is considered as a one-electron potential based on the *j-j* coupling scheme, it is enough to use the CEF term for $J=5/2$.

Next we consider $H_{\text{el-el}}$ in the *j-j* coupling scheme. It is easy to understand that the Coulomb interaction term is given in the form of

$$H_{\text{el-el}} = \frac{1}{2} \sum_{\mathbf{i}, \mu, \nu, \mu', \nu'} I(\mu, \nu; \nu', \mu') a_{\mathbf{i}\mu}^\dagger a_{\mathbf{i}\nu}^\dagger a_{\mathbf{i}\nu'} a_{\mathbf{i}\mu'}, \quad (120)$$

where I is the Coulomb interactions. The point here is the calculation of I , which is the sum of two contributions, written as

$$I(\mu, \nu; \nu', \mu') = K_{\mu\nu, \nu'\mu'} - K_{\mu\nu, \mu'\nu'}, \quad (121)$$

with the Coulomb integral K . The former indicates the Coulomb term, while the latter denotes the exchange one. It should be noted that I vanishes unless $\mu+\nu=\mu'+\nu'$ due to the conservation of z -component of total angular momentum. The matrix element $K_{\mu_1\mu_2, \mu_3\mu_4}$ is explicitly given by

$$K_{\mu_1\mu_2, \mu_3\mu_4} = \sum_{\sigma, \sigma'} C_{\mu_1\sigma} C_{\mu_2\sigma'} C_{\mu_3\sigma'} C_{\mu_4\sigma} I_{\mu_1-\sigma/2, \mu_2-\sigma'/2, \mu_3-\sigma'/2, \mu_4-\sigma/2}^f, \quad (122)$$

where I^f is the Coulomb matrix element among f electrons, already defined in the previous subsection.

When two electrons are accommodated in the $j=5/2$ sextet, the allowed values for total angular momentum J are 0, 2, and 4 due to the Pauli principle. Thus, the Coulomb interaction term should be written in a 15×15 matrix form. Note that “15” is the sum of the basis numbers for singlet ($J=0$), quintet ($J=2$), and nontet ($J=4$). As is easily understood, this 15×15 matrix can be decomposed into a block-diagonalized form labeled by J_z , including one 3×3 matrix for $J_z=0$, four 2×2 matrices for $J_z=\pm 2$ and ± 1 , and four 1×1 for $J_z=\pm 4$ and ± 3 . We skip the details of tedious calculations for the matrix elements and here only summarize the results in the following by using the Racah parameters E_k ($k=0,1,2$) in the j - j coupling scheme [244], which are related to the Slater-Condon parameters F^k as

$$E_0 = F^0 - \frac{80}{1225}F^2 - \frac{12}{441}F^4, \quad (123)$$

$$E_1 = \frac{120}{1225}F^2 + \frac{18}{441}F^4, \quad (124)$$

$$E_2 = \frac{12}{1225}F^2 - \frac{1}{441}F^4. \quad (125)$$

For the sectors of $J_z=4$ and 3, we obtain

$$I(5/2, 3/2; 3/2, 5/2) = E_0 - 5E_2, \quad (126)$$

and

$$I(5/2, 1/2; 1/2, 5/2) = E_0 - 5E_2, \quad (127)$$

respectively. For $J_z=2$ and 1, we obtain

$$\begin{aligned} I(3/2, 1/2; 1/2, 3/2) &= E_0 + 4E_2, \\ I(5/2, -1/2; -1/2, 5/2) &= E_0, \\ I(3/2, 1/2; -1/2, 5/2) &= -3\sqrt{5}E_2, \end{aligned} \quad (128)$$

and

$$\begin{aligned} I(3/2, -1/2; -1/2, 3/2) &= E_0 - E_2, \\ I(5/2, -3/2; -3/2, 5/2) &= E_0 + 5E_2, \\ I(3/2, -1/2; -3/2, 5/2) &= -2\sqrt{10}E_2, \end{aligned} \quad (129)$$

Finally, for $J_z=0$ sector, we obtain

$$\begin{aligned} I(1/2, -1/2; -1/2, 1/2) &= E_0 + 2E_2 + E_1, \\ I(3/2, -3/2; -3/2, 3/2) &= E_0 - 3E_2 + E_1, \\ I(5/2, -5/2; -5/2, 5/2) &= E_0 + 5E_2 + E_1, \\ I(1/2, -1/2; -3/2, 3/2) &= -E_1 - 3E_2, \\ I(1/2, -1/2; -5/2, 5/2) &= E_1 - 5E_2, \\ I(3/2, -3/2; -5/2, 5/2) &= -E_1. \end{aligned} \quad (130)$$

Note here the following relations:

$$I(\mu, \nu; \nu', \mu') = I(\mu', \nu'; \nu, \mu), \quad (131)$$

and

$$I(\mu, \nu; \nu', \mu') = I(-\nu, -\mu; -\mu', -\nu'). \quad (132)$$

By using these two relations and Eqs. (126-130), we can obtain all the Coulomb matrix elements [245].

It is instructive to understand how the f^2 configuration is determined by the Coulomb interaction in the j - j coupling scheme. We will discuss later the local f -electron state determined by $H_{\text{CEF}} + H_{\text{el-el}}$. In the j - j coupling scheme, two electrons are accommodated in the $j=5/2$ sextet. When we diagonalize the 15×15 matrix for Coulomb interaction terms, we can easily obtain the eigen energies as $E_0 - 5E_2$ for the $J=4$ nontet, $E_0 + 9E_2$ for the $J=2$ quintet, and $E_0 + 3E_1$ for the $J=0$ singlet. Since the Racah parameters are all positive, the ground state is specified by $J=4$ in the j - j coupling scheme. In the LS coupling scheme, on the other hand, we obtain the ground-state level as 3H with $S=1$ and $L=5$ from the Hund's rules. On further inclusion of the spin-orbit interaction, the ground state becomes characterized by $J=4$, expressed as 3H_4 in the traditional notation. Note that we are now considering a two-electron problem. Thus, if we correctly include the effects of Coulomb interactions, it is concluded that the same quantum number as that in the LS coupling scheme is obtained in the j - j coupling scheme for the ground-state multiplet.

In order to understand further the physical meaning of Racah parameters, it is useful to consider a simplified Coulomb interaction term. In the above discussion, the expressions using Racah parameters are not convenient, since they depend on the orbitals in a very complicated manner, even though they keep the correct symmetry required by group theory. To clarify their meanings, let us step back to the following simplified interaction form among $\ell = 3$ orbitals:

$$\begin{aligned} H_{\text{int}} = & U \sum_{\mathbf{im}} \rho_{\mathbf{im}\uparrow} \rho_{\mathbf{im}\downarrow} + U' \sum_{\mathbf{i}, \sigma, \sigma', m > m'} \rho_{\mathbf{im}\sigma} \rho_{\mathbf{im}'\sigma'} \\ & + J \sum_{\mathbf{i}, \sigma, \sigma', m > m'} f_{\mathbf{im}\sigma}^\dagger f_{\mathbf{im}'\sigma'}^\dagger f_{\mathbf{im}\sigma'} f_{\mathbf{im}'\sigma}, \end{aligned} \quad (133)$$

where $\rho_{\mathbf{im}\sigma} = f_{\mathbf{im}\sigma}^\dagger f_{\mathbf{im}\sigma}$. In this equation, we include only three interactions; intra-orbital Coulomb interaction U , inter-orbital Coulomb interaction U' , and the exchange interaction J . We ignore the pair-hopping J' for simplicity. Since we set $J'=0$ in the relation of $U = U' + J + J'$, the relation $U = U' + J$ holds among Coulomb interactions to ensure rotational invariance in the orbital space.

By using Clebsch-Gordan coefficients, $f_{\mathbf{im}\sigma}$ with real-spin σ can be related to $a_{\mathbf{i}\mu}$ as

$$f_{\mathbf{im}\sigma} = -\sigma \sqrt{\frac{3 - \sigma m}{7}} a_{\mathbf{i}m + \sigma/2}. \quad (134)$$

Note here that we consider only the $j = 5/2$ sextet. The Coulomb interaction term for $j=5/2$ is given by

$$H_{\text{int}} = U_{\text{eff}} \sum_{\mathbf{i}\mu > \mu'} n_{\mathbf{i}\mu} n_{\mathbf{i}\mu'} - J_{\text{eff}} \mathbf{J}_{\mathbf{i}}^2 + (35J_{\text{eff}}/4) N_{\mathbf{i}}, \quad (135)$$

where $n_{i\mu}=a_{i\mu}^\dagger a_{i\mu}$, $N_i=\sum_\mu n_{i\mu}$, $U_{\text{eff}}=U'-J/2$, $J_{\text{eff}}=J/49$, and \mathbf{J}_i is the operator for total angular momentum with $j=5/2$. Explicitly, \mathbf{J}_i^2 is written as

$$\begin{aligned} \mathbf{J}_i^2 = & \sum_{\mu,\mu'} [\mu\mu' n_{i\mu} n_{i\mu'} \\ & + (\phi_\mu^+ \phi_{\mu'}^- a_{i\mu+1}^\dagger a_{i\mu} a_{i\mu'-1}^\dagger a_{i\mu'} + \phi_\mu^- \phi_{\mu'}^+ a_{i\mu-1}^\dagger a_{i\mu} a_{i\mu'+1}^\dagger a_{i\mu'})/2], \end{aligned} \quad (136)$$

with $\phi_\mu^\pm = \sqrt{j(j+1) - \mu(\mu \pm 1)} = \sqrt{35/4 - \mu(\mu \pm 1)}$.

For two electrons in the $j=5/2$ sextet, based upon the simplified Coulomb interaction term, we can easily obtain the energy levels as $U_{\text{eff}}-5J_{\text{eff}}/2$ for the $J=4$ nontet, $U_{\text{eff}}+23J_{\text{eff}}/2$ for the $J=2$ quintet, and $U_{\text{eff}}+35J_{\text{eff}}/2$ for the $J=0$ singlet. When we compare these energy levels with the results obtained using Racah parameters, we understand the correspondence such as $E_0 \sim U_{\text{eff}}$ and $E_2 \sim J_{\text{eff}}$. Namely, E_0 is the effective inter-orbital Coulomb interaction, while E_2 denotes the effective Hund's rule coupling. Note that E_1 does not appear, since it is related to the pair-hopping interaction which is not included here.

We also note the smallness of J_{eff} , given as $J_{\text{eff}}=J/49$. The origin of the large reduction factor $1/49$ is, in one word, due to the neglect of $j=7/2$ octet. In the Coulomb interaction term Eq. (133), the Hund's rule term is simply written as $-\mathbf{J}\mathbf{S}^2$. Note the relation $\mathbf{S}=(g_J-1)\mathbf{J}$ with g_J the Landé's g -factor. For $j=5/2$, we easily obtain $g_J=6/7$, indicating $\mathbf{S}=-\mathbf{J}$. Thus, the original Hund's rule term is simply rewritten as $-(J/49)\mathbf{J}^2$.

5.4. Level scheme in the j - j coupling scheme

Before proceeding to the exhibition of the model Hamiltonian obtained by further considering the kinetic term of f electrons, it is instructive to show how the j - j coupling scheme works to reproduce the local level scheme of actual f -electron materials. It is an important point that we can resort to the analogy with the d -electron-like configuration, as discussed in Sec. 2. As a typical example, here we consider the f -electron state for the case of cubic CEF potential.

After some algebraic calculations, we obtain two degenerate levels under the cubic CEF. One is Γ_7 doublet with Kramers degeneracy and another is Γ_8 quartet including two Kramers doublets. It is quite useful to define new operators with "orbital" degrees of freedom to distinguish two Kramers doublets included in Γ_8 as

$$\begin{aligned} f_{i\uparrow} &= \sqrt{5/6}a_{i-5/2} + \sqrt{1/6}a_{i3/2}, \\ f_{i\downarrow} &= \sqrt{5/6}a_{i5/2} + \sqrt{1/6}a_{i-3/2}, \end{aligned} \quad (137)$$

for "a"-orbital electrons and

$$f_{i\uparrow} = a_{i-1/2}, \quad f_{i\downarrow} = a_{i1/2}, \quad (138)$$

for "b"-orbital electrons, respectively. The Γ_7 state, defined as "c" orbital, is characterized by

$$\begin{aligned} f_{i\uparrow} &= \sqrt{1/6}a_{i-5/2} - \sqrt{5/6}a_{i3/2}, \\ f_{i\downarrow} &= \sqrt{1/6}a_{i5/2} - \sqrt{5/6}a_{i-3/2}. \end{aligned} \quad (139)$$

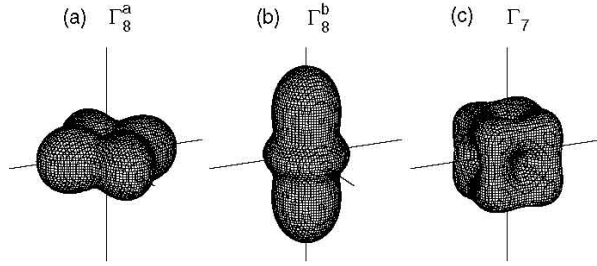


Figure 29. Views for (a) Γ_8^a , (b) Γ_8^b , and (c) Γ_7 orbitals. Γ_γ indicates the irreducible representation of point group in Bethe's notation [242].

For the standard time reversal operator $\mathcal{K} = -i\sigma_y K$, where K denotes an operator to take the complex conjugate, we can easily show the relation

$$\mathcal{K}f_{i\tau\sigma} = \sigma f_{i\tau-\sigma}. \quad (140)$$

Note that this has the same definition for real spin.

In Fig. 29, we show the shape of three orbitals. As intuitively understood from the shape of Γ_7 orbital, this keeps the cubic symmetry, indicating A-representation. In fact, in the group theory, it is characterized by a_u . Note that the subscript “u” indicates ungerade, since we consider f electron with $\ell=3$. On the other hand, degenerate Γ_8^a and Γ_8^b orbitals seems to be similar to $x^2 - y^2$ and $3z^2 - r^2$ orbitals of $3d$ electrons, respectively, indicating E-representation. In the group theoretical argument, these are classified into e_u . Concerning the similarity between Γ_8 and e_g orbitals, it is quite natural from a mathematical viewpoint, since we recall the fact that Γ_8 is isomorphic to $\Gamma_3 \times \Gamma_6$, where Γ_3 indicates E representation for the orbital part and Γ_6 denotes the spin part. This point is quite impressive when we consider the orbital physics for d - and f -electron systems. Namely, by exploiting this mathematical similarity, it is possible to understand the complex f -electron phenomena with the use of the microscopic Hamiltonian in common with that of the d -electron multiorbital model. We will see later this point in the construction of the model Hamiltonian.

Now we discuss the f -electron configuration in the Γ_7 and Γ_8 levels in the manner in which we have considered the d -electron configuration. First, we pick up the AuCu_3 -type cubic crystal structure. A typical AuCu_3 -type material with one f electron per site is CeIn_3 , in which Γ_7 and Γ_8 are the ground and first excited states, respectively [246]. If we accommodate one more electron to consider the f^2 configuration, immediately there appear two possibilities, “low” and “high” spin states, as we have discussed in the d -electron configuration. When the CEF splitting energy between Γ_7 and Γ_8 levels is smaller than the Hund's rule coupling, the second electron should be accommodated in the Γ_8 levels. In the situation in which one is in the Γ_7 and the other in the Γ_8 , a Γ_4 triplet appears for the f^2 state in the j - j coupling scheme. As mentioned in the previous subsection, Γ_3 non-Kramers doublet does not appear in the j - j coupling scheme. On the other hand, if the CEF splitting is larger than the Hund's rule interaction, then the f^2 ground state is formed from two Γ_7 electrons, leading to a Γ_1 singlet state. When we

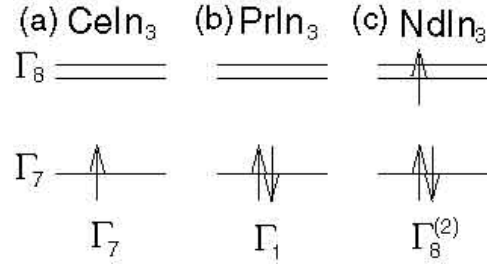


Figure 30. Electron configurations in the j - j coupling scheme for (a) CeIn_3 , (b) PrIn_3 , and (c) NdIn_3 . Γ_γ denotes the irreducible representation of point group in Bethe's notation [242].

compare this Γ_1 state with that in the LS coupling scheme, we notice that it is given by a mixture of $J=0$ and $J=4$ states, but the $J=4$ component is found to be dominant. Note also that Γ_1 is the antisymmetric representation of $\Gamma_7 \times \Gamma_7$.

Since we do not know the exact value of the Hund's rule interaction in f -electron compounds, it is difficult to determine the f^2 state by purely theoretical arguments. In this case, we have to refer to the data on actual materials. Fortunately, we have the example of PrIn_3 , a typical f^2 material with AuCu_3 -type crystal structure. From several experimental results, Γ_1 has been confirmed to be the ground level in PrIn_3 [247, 248]. Thus, the low-spin state should be taken for the AuCu_3 -type structure in the j - j coupling scheme.

Here the reader may pose a naive question: Is the Hund's rule interaction really so small in f -electron systems? However, we have already discussed this point in the previous subsection. Namely, the effective Hund's rule interaction J_{eff} is given by $J_{\text{eff}}=J/49$ in the j - j coupling scheme, where J is the original Hund's rule interaction among f electrons. Note again that the magnitude of the Hund's rule interaction is effectively reduced by the factor $1/49$ in the j - j coupling scheme. Even if $J=1\text{eV}$, J_{eff} is reduced to be about 200K , which is comparable with the CEF splitting energy. Thus, it is possible to have the low-spin state in the j - j coupling scheme.

Next, we take a further step to the f^3 state by adding one more f electron. Since Γ_7 is fully occupied to form Γ_1 , the next electron should be placed in the Γ_8 state, as shown in Fig. 30(c), clearly indicating that there exists an active orbital degree of freedom. The f^3 state composed of two Γ_7 and one Γ_8 electron is expressed as $\Gamma_8^{(2)}$ in the terminology of group theory. When we again consider actual materials, NdIn_3 is found to be a typical f^3 material with the AuCu_3 -type crystal structure. In experiments, it has been confirmed that $\Gamma_8^{(2)}$ is the ground level [249, 250, 251], as we have found with the present j - j coupling scheme.

Let us turn our attention to another crystal structure, in which Γ_8 is lower than Γ_7 in the f^1 configuration. Typical materials are the rare-earth hexaborides RB_6 with $\text{R}=\text{Ce}$, Pr , and Nd . As is well known, the ground level of CeB_6 is Γ_8 , indicating that the quadrupolar degree of freedom plays an active role in this material [252]. In

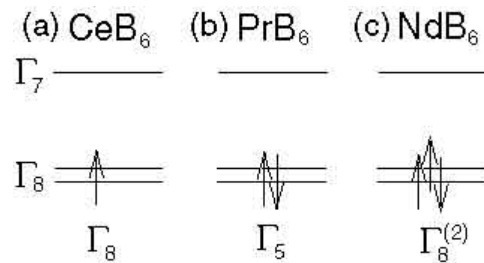


Figure 31. Electron configurations in the j - j coupling scheme for rare-earth hexaborides, (a) CeB_6 , (b) PrB_6 , and (c) NdB_6 . Γ_γ is the irreducible representation of point group in Bethe's notation [242].

fact, anomalous behavior related to quadrupolar ordering has been suggested by several experimental results.

First, we note that the level splitting between Γ_8 and Γ_7 is assumed to be larger than the Hund's rule interaction. When we accommodate two electrons in Γ_8 orbitals, the triplet (Γ_5), doublet (Γ_3), and singlet (Γ_1) states are allowed. Among these, owing to the effect of the Hund's rule interaction, even if it is small, the Γ_5 triplet should be the ground state. This has actually been observed in PrB_6 [253, 254]. Further, in order to consider NdB_6 , another electron is put into the Γ_8 orbital, making a total of three. Alternatively, we may say that there is one hole in the Γ_8 orbital. Such a state is found, again, to be characterized by $\Gamma_8^{(2)}$. Experimental results on NdB_6 have actually been reported which lead to the ground state of $\Gamma_8^{(2)}$ [253, 255, 256, 257]. Thus, when Γ_8 is the ground state for the one f -electron case, we obtain Γ_5 for the f^2 and $\Gamma_8^{(2)}$ for the f^3 configurations.

We have shown that the ground states deduced from the j - j coupling scheme are consistent with experimental results. However, in order to explain the experimental results quantitatively, it is unavoidable to analyze the CEF levels using the LS coupling scheme. As mentioned above, it is possible to reproduce the result of the LS coupling scheme by considering the effective potentials from the $j=7/2$ octet, but what we would like to stress here is that even in a localized system, the symmetry of the ground level can be understood via the simple j - j coupling scheme. We need to recognize the limitations of the simple j - j coupling scheme when we treat a local electronic state. For instance, to consider the f^3 state, we simply put three electrons into the CEF level scheme which is determined with the f^1 configuration. Thus, the wavefunction of the f^3 state is uniquely determined. However, in an actual situation, the dectet labeled by $J=9/2$ ($L=6$ and $S=3/2$) is split into two Γ_8 and one Γ_6 orbital. The ground-state wavefunctions will then depend on the two CEF parameters B_4^0 and B_6^0 [258]. In order to explain experimental results on localized f -electron materials, one should analyze the Hamiltonian which also includes the complex effective potentials from $j=7/2$ octet. In this paper, however, the electronic states are considered with an itinerant picture based on the simple j - j coupling scheme. Thus, it is important to check that the local electronic state formed

by *f* electrons in this way is consistent with the symmetry of the state obtained with the *LS* coupling scheme.

In summary, it has been shown that the ground states of the f^2 and f^3 configurations can be qualitatively reproduced by accommodating *f* electrons in the CEF levels of a corresponding f^1 material, provided that the CEF level splitting is larger than the Hund's rule interaction. Thus, the *j-j* coupling scheme works even in the localized case. Accordingly, we believe that a microscopic theory can be developed in which we discuss the magnetism and superconductivity of *f*-electron compounds in terms of the *j-j* coupling scheme.

5.5. Model Hamiltonian

In previous subsections, we have explained in detail that the *j-j* coupling scheme works for the local *f*-electron state. Now let us include the effect of kinetic motion of *f* electrons [72]. In this article, we are based on an itinerant picture for *f* electrons. From our experience, this picture seems to be valid, when we consider actinide compounds, in particular, heavy actinides. On the other hand, for rare-earth materials, it has been firmly believed to take the localized picture for *f* electrons. In particular, in order to consider the heavy fermion behavior, it is indispensable to consider the system including both the conduction electron with wide band and the almost localized *f* electron, which are hybridized with each other.

It is believed that the hybridization of *f* electrons with conduction electron band is important to understand the magnetism of *f*-electron systems. In fact, in the traditional prescription, first we derive the Coqblin-Schrieffer model from the periodic Anderson model by evaluating the *c-f* exchange interaction J_{cf} within the second-order perturbation in terms of the hybridization between *f*- and conduction electrons. Then, we derive the RKKY interactions again using the second-order perturbation theory with respect to J_{cf} . In general, the RKKY interactions are orbital dependent and interpreted as multipole interactions. Such orbital dependence originates from that of the hybridization. Note that the hybridization should occur only between *f*- and conduction band with the same symmetry. Here we emphasize that the symmetry of *f*-electron state is correctly included in our calculations. Thus, the structure in the multipole interactions will not be changed so much, even if we consider the effect of hybridization with conduction band, as long as we consider correctly the symmetry of *f* electron states.

In this paper, we consider the tight-binding approximation for *f*-electron hopping motion. The kinetic term can be written as

$$H_{\text{kin}} = \sum_{\mathbf{i}, \mathbf{a}, \mu, \nu} t_{\mu\nu}^{\mathbf{a}} a_{\mathbf{i}\mu}^{\dagger} a_{\mathbf{i}+\mathbf{a}\nu}, \quad (141)$$

where $t_{\mu\nu}^{\mathbf{a}}$ is the overlap integral between the μ - and ν -states connected by the vector \mathbf{a} .

Let us consider the hopping motion of *f* electrons based on the *j-j* coupling scheme. In order to evaluate $t_{\mu\nu}^{\mathbf{a}}$, which is hopping of *f* electrons between the μ -state at \mathbf{i} site

and the ν -state at $\mathbf{i} + \mathbf{a}$ site, again it is convenient to step back to f -electron operators in the $\ell=3$ multiplet, defined as $f_{i m \sigma}$. Since the real spin should be conserved in the hopping process, $t_{\mu\nu}^{\mathbf{a}}$ is given as

$$t_{\mu\nu}^{\mathbf{a}} = \sum_{\sigma} C_{\mu\sigma} C_{\nu\sigma} T_{3,\mu-\sigma/2;3,\nu-\sigma/2}^{\mathbf{a}}, \quad (142)$$

where $T_{\ell,m;\ell',m'}^{\mathbf{a}}$ is the hopping amplitude of electrons between (ℓ, m) - and (ℓ', m') -states along the \mathbf{a} -direction.

Now the problem is reduced to the evaluation of $T_{\ell,m;\ell',m'}^{\mathbf{a}}$. Although we can simply consult the paper of Slater and Koster [135, 259], a convenient formula has been obtained by Sharma for the overlap integral between two orbitals, (ℓ, m) and (ℓ', m') [260], connected by unit vector \mathbf{a} . It is expressed as

$$T_{\ell,m;\ell',m'}^{\mathbf{a}} = (\ell\ell'\sigma) \sqrt{\frac{4\pi}{2\ell+1}} \sqrt{\frac{4\pi}{2\ell'+1}} Y_{\ell m}^*(\theta, \varphi) Y_{\ell' m'}(\theta, \varphi), \quad (143)$$

where $(\ell\ell'\sigma)$ denotes Slater's two-center integral through the σ bond, for instance, it is $(ff\sigma)$ for $\ell=\ell'=3$ and $(fp\sigma)$ for $\ell=3$ and $\ell'=1$. θ and φ are polar and azimuth angles, respectively, to specify the vector \mathbf{a} as

$$\mathbf{a} = (\sin\theta \cos\varphi, \sin\theta \sin\varphi, \cos\theta). \quad (144)$$

Here we consider the hopping between f orbitals in nearest neighbor sites by putting $\ell=\ell'=3$. After some algebraic calculations, we obtain the hopping amplitudes as follows. For diagonal elements, we obtain

$$\begin{aligned} t_{\pm 5/2, \pm 5/2}^{\mathbf{a}} &= 5t_0 \sin^4 \theta, \\ t_{\pm 3/2, \pm 3/2}^{\mathbf{a}} &= t_0 \sin^2 \theta (1 + 15 \cos^2 \theta), \\ t_{\pm 1/2, \pm 1/2}^{\mathbf{a}} &= 2t_0 (1 - 2 \cos^2 \theta + 5 \cos^4 \theta), \end{aligned} \quad (145)$$

where the energy unit t_0 is given by

$$t_0 = (3/56)(ff\sigma). \quad (146)$$

Here $(ff\sigma)$ is the Slater-Koster two-center integral between adjacent f orbitals. Note that $t_{\mu, -\mu}^{\mathbf{a}} = 0$. For off-diagonal elements, we obtain

$$\begin{aligned} t_{\pm 5/2, \pm 1/2}^{\mathbf{a}} &= -t_0 \sqrt{10} e^{\mp 2i\varphi} \sin^2 \theta (1 - 3 \cos^2 \theta), \\ t_{\pm 5/2, \mp 3/2}^{\mathbf{a}} &= t_0 \sqrt{5} e^{\mp 4i\varphi} \sin^4 \theta, \\ t_{\pm 1/2, \mp 3/2}^{\mathbf{a}} &= -t_0 \sqrt{2} e^{\mp 2i\varphi} \sin^2 \theta (1 + 5 \cos^2 \theta), \end{aligned} \quad (147)$$

and

$$\begin{aligned} t_{5/2, -1/2}^{\mathbf{a}} &= -t_{1/2, -5/2}^{\mathbf{a}} = t_0 \sqrt{10} e^{-3i\varphi} \sin^2 \theta \sin 2\theta, \\ t_{5/2, 3/2}^{\mathbf{a}} &= -t_{-3/2, -5/2}^{\mathbf{a}} = -2t_0 \sqrt{5} e^{-i\varphi} \sin^2 \theta \sin 2\theta, \\ t_{1/2, 3/2}^{\mathbf{a}} &= -t_{-3/2, -1/2}^{\mathbf{a}} = t_0 \sqrt{2} e^{i\varphi} \sin 2\theta (1 - 5 \cos^2 \theta). \end{aligned} \quad (148)$$

Note that $t_{\nu\mu}^{\mathbf{a}} = t_{\mu\nu}^{\mathbf{a}*}$.

5.6. Γ_8 model

In the previous subsection, we have completed the construction of a model Hamiltonian, which is expected to be a basic model to investigate the microscopic aspects of magnetism and superconductivity of *f*-electron systems. Since it includes six states per site, i.e., three Kramers doublets, the analysis may be difficult. Of course, even if the calculations seem to be tedious, it is necessary to carry out analytical and/or numerical research on the basis of such a three orbital model. However, for practical purposes, it is convenient to simplify the model, if possible. In this subsection, as an effective model for actinide compounds, we introduce a Γ_8 model, by discarding Γ_7 orbital [72].

A simple explanation to validate the ignorance of Γ_7 is to assume large CEF splitting energy between Γ_7 and Γ_8 levels. This simplification is motivated by the fact that the possibility of exotic octupole ordering has been actively discussed in $\text{Ce}_x\text{La}_{1-x}\text{B}_6$ and NpO_2 with Γ_8 ground state. Here readers may be doubtful of the reality of our assumption, since the Coulomb interaction among *f* electrons is naively thought to be larger than the CEF level splitting in any case. However, it should be noted again that we are now considering the *f*-electron state in the *j-j* coupling scheme, not in the original *f*-electron state with angular momentum $\ell=3$. As already mentioned, the Hund's rule interaction in the *j-j* coupling scheme is effectively reduced to be 1/49 of the original Hund's rule coupling. Even when the original Hund's rule coupling among *f* electrons is 1 eV, it is reduced to 200 K in the *j-j* coupling scheme. For instance, the CEF level splitting in actinide dioxides is considered to be larger than 1000 K. We also recall that the CEF level splitting in CeB_6 is as large as 500 K. Thus, we safely conclude that our present assumption is correctly related to some actual materials. Of course, in order to achieve quantitative agreement with experimental results, it is necessary to include also Γ_7 level, since the magnitude of the CEF splitting is always finite, even if it is large compared with the effective Hund's rule interaction. However, we strongly believe that it is possible to grasp microscopic origin of unconventional superconductivity as well as spin and orbital, i.e., multipole, ordering in *f*-electron systems on the basis of the Γ_8 model, since this model is considered to be connected adiabatically from the realistic situation. It is one of future tasks to develop more general theory to include all the $j=5/2$ sextet in future.

Concerning the *f*-electron number, typically we treat the case with one *f* electron in the Γ_8 multiplet per site. However, this restriction does not simply indicate that we consider only the Ce-based compound. In the *j-j* coupling scheme, in order to consider f^n -electron systems, where *n* indicates local *f* electron number per site, we accommodate *f* electrons in the one-electron CEF levels due to the balance between Coulomb interactions and CEF level splitting energy, just as in the case of *d*-electron systems. Thus, as shown in Fig. 32(a), the Γ_8 model is applicable to the cases for $n = 1 \sim 4$ in the Γ_8 - Γ_7 system, where Γ_x - Γ_y symbolically denotes the situation with Γ_x ground and Γ_y excited states. Furthermore, we should note that due to the electron-hole

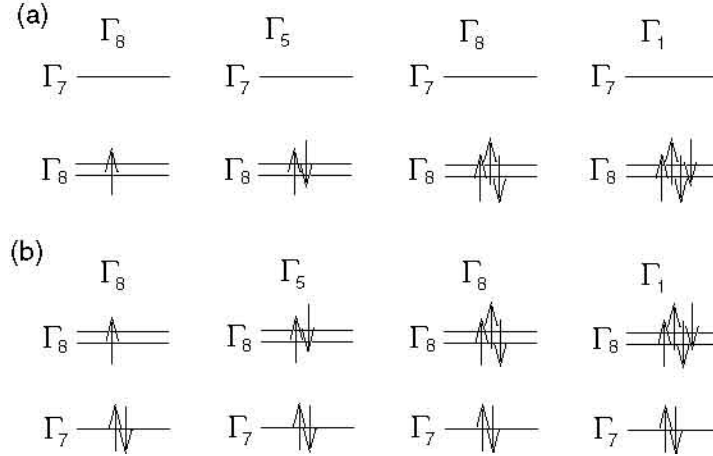


Figure 32. Electron configurations in the j - j coupling scheme to which the Γ_8 model is applicable. (a) $f^1 \sim f^4$ configuration when Γ_8 is lower. (b) $f^3 \sim f^6$ configuration when Γ_7 is lower,

symmetry in the Γ_8 subspace, the Γ_8 model is also applicable to the cases for $n = 3 \sim 6$ in the Γ_7 - Γ_8 system, as shown in Fig. 32(b).

Now let us define the Γ_8 model. First we consider the hopping part. For simplicity, here we set the cubic-based lattice. Later we will discuss the hopping amplitude of other lattice structures. We include the hopping in the xy plane and along the z -axis for $\mathbf{a}=\mathbf{x}=[1,0,0]$, $\mathbf{y}=[0,1,0]$, and $\mathbf{z}=[0,0,1]$, respectively. To evaluate the hopping amplitude, we simply set (θ, φ) to be $(\pi/2, 0)$, $(\pi/2, \pi/2)$, and $(0, 0)$ for x , y , and z directions. Then, by using the general results in the previous section, we easily obtain $t_{\mu\nu}^{\mathbf{a}}$ between neighboring f orbitals in the xy plane and along the z axis. Further we transform the basis by the above definitions for Γ_8 operators with orbital degrees of freedom. The results are given as

$$t_{\tau\tau'}^{\mathbf{x}} = t \begin{pmatrix} 3/4 & -\sqrt{3}/4 \\ -\sqrt{3}/4 & 1/4 \end{pmatrix}, \quad (149)$$

for the \mathbf{x} -direction,

$$t_{\tau\tau'}^{\mathbf{y}} = t \begin{pmatrix} 3/4 & \sqrt{3}/4 \\ \sqrt{3}/4 & 1/4 \end{pmatrix}, \quad (150)$$

for the \mathbf{y} direction, and

$$t_{\tau\tau'}^{\mathbf{z}} = t \begin{pmatrix} 0 & 0 \\ 0 & 1 \end{pmatrix}, \quad (151)$$

for the \mathbf{z} direction. Note that $t=8t_0=(3/7)(ff\sigma)$. Here we stress that the hopping amplitudes among Γ_8 orbitals are just the same as those for the e_g orbitals of $3d$ electrons. Intuitively, readers can understand this point due to the shapes of Γ_8 orbitals as shown in Fig. 29, which are similar to e_g orbitals.

After transforming the basis of the Coulomb interaction terms, the Hamiltonian for Γ_8 orbitals is given by

$$\begin{aligned}
H_{\Gamma_8} = & \sum_{\mathbf{i}, \mathbf{a}, \sigma, \tau, \tau'} t_{\tau\tau'}^{\mathbf{a}} f_{\mathbf{i}\tau\sigma}^\dagger f_{\mathbf{i}+\mathbf{a}\tau'\sigma} + U \sum_{\mathbf{i}, \tau} \rho_{\mathbf{i}\tau\uparrow} \rho_{\mathbf{i}\tau\downarrow} + U' \sum_{\mathbf{i}} \rho_{\mathbf{i}\mathbf{a}} \rho_{\mathbf{i}\mathbf{b}} \\
& + J \sum_{\mathbf{i}, \sigma, \sigma'} f_{\mathbf{i}\mathbf{a}\sigma}^\dagger f_{\mathbf{i}\mathbf{b}\sigma'}^\dagger f_{\mathbf{i}\mathbf{a}\sigma'} f_{\mathbf{i}\mathbf{b}\sigma} + J' \sum_{\mathbf{i}, \tau \neq \tau'} f_{\mathbf{i}\tau\uparrow}^\dagger f_{\mathbf{i}\tau\downarrow}^\dagger f_{\mathbf{i}\tau'\downarrow} f_{\mathbf{i}\tau'\uparrow}, \tag{152}
\end{aligned}$$

where $\rho_{\mathbf{i}\tau\sigma} = f_{\mathbf{i}\tau\sigma}^\dagger f_{\mathbf{i}\tau\sigma}$ and $\rho_{\mathbf{i}\tau} = \sum_{\sigma} \rho_{\mathbf{i}\sigma\tau}$. In the Coulomb interaction terms, U , U' , J , and J' denote intra-orbital, inter-orbital, exchange, and pair-hopping interactions among Γ_8 electrons, respectively, expressed by using the Racah parameters E_k as

$$\begin{aligned}
U &= E_0 + E_1 + 2E_2, \\
U' &= E_0 + (2/3)E_2, \\
J &= 5E_2, \\
J' &= E_1 - (11/3)E_2. \tag{153}
\end{aligned}$$

Note that the relation $U=U'+J+J'$ holds, ensuring rotational invariance in pseudo-orbital space for the interaction part. For d -electron systems, one also has another relation $J=J'$, as mentioned in Sec. 2. When the electronic wavefunction is real, this relation is easily demonstrated from the definition of the Coulomb integral. However, in the j - j coupling scheme, the wavefunction is complex, and J is not equal to J' , in general. For simplicity, we shall assume here that $J=J'$, noting that essential results are not affected. Since double occupancy of the same orbital is suppressed owing to the large value of U , pair-hopping processes are irrelevant in the present case.

We believe that this Γ_8 Hamiltonian provides a simple, but non-trivial model to consider superconductivity and magnetism in f -electron systems. Note again that it is essentially the same as the model for e_g electron systems such as manganites, although the coupling with Jahn-Teller distortion is not included in the present model. Due to the complex interplay and competition among charge, spin, and orbital degrees of freedom, a rich phase diagram has been obtained for manganites. Thus, it is definitely expected that a similar richness will also be unveiled for f -electron systems based on the Γ_8 model Hamiltonian.

6. Orbital physics in f -electron systems

We have constructed a microscopic model Hamiltonian for f -electron systems in the previous subsection. In particular, we could obtain the Γ_8 orbital degenerate model as an effective Hamiltonian for actinide compounds. In this section, we review the theoretical results of the spin and orbital structure, i.e., multipole order, based on the Γ_8 model.

6.1. Spin and orbital structure of actinide compounds

In this subsection, we review the theoretical effort to understand the magnetic structure of uranium and neptunium compounds with HoCoGa_5 -type tetragonal crystal structure

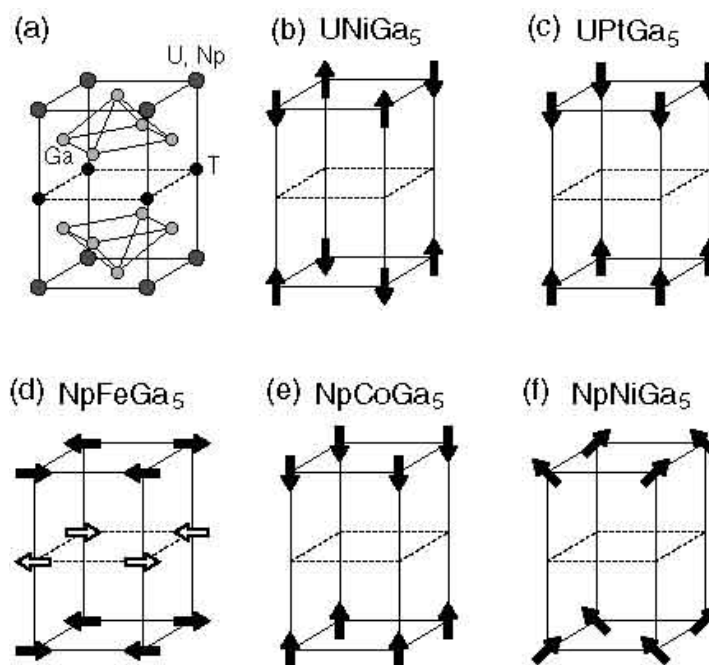


Figure 33. (a) Crystal structure of $AnTGa_5$. Schematic views of magnetic structures at low temperatures, composed of magnetic moments of U and Np ions for (b) $UNiGa_5$, (c) $UPtGa_5$, (d) $NpFeGa_5$, (e) $NpCoGa_5$, and (f) $NpNiGa_5$. For $NpFeGa_5$, magnetic moments at Fe sites are also depicted.

[82, 83]. The crystal structure is shown in Fig. 33(a). The varieties of magnetic structure of U-115 and Np-115 explained in Sec. 1 are summarized in Figs. 33(b)-33(f). In order to set up the microscopic model for actinide 115 materials, it is useful to consider UGa_3 and $NpGa_3$, which are the mother compounds of U-115 and Np-115. Among them, it has been reported that UGa_3 exhibits a G-type AF metallic phase in the low-temperature region [261], but a “hidden” ordering different from the magnetic one has been suggested by resonant X-ray scattering measurements [262]. Unfortunately, orbital ordering in UGa_3 is not yet confirmed experimentally, but it may be an interesting possibility to understand the result of resonant X-ray scattering experiment on UGa_3 based on the orbital-ordering scenario.

Although it is difficult to determine the valence of actinide ions in the solid state, for the time being, we assume that the valence is U^{3+} or Np^{3+} , including three or four *f* electrons per ion. By considering the CEF potential and Coulomb interactions, we then assign three or four electrons to the states in the $j=5/2$ sextet. In order to proceed with the discussion, it is necessary to know which is lower, Γ_7 or Γ_8 , in the one *f*-electron picture. For some crystal structures it is possible to determine the level scheme from intuitive discussions of *f*-electron wavefunctions and the positions of ligand ions. However, this is not the case for the $AuCu_3$ -type crystal structure. For this case, we again invoke experimental results on $CeIn_3$, a typical $AuCu_3$ -type Ce-based compound, where Γ_7 and Γ_8 have been reported as ground and excited states, respectively, with

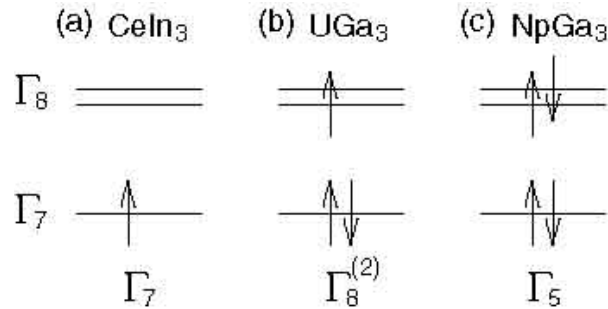


Figure 34. Level schemes for (a) CeIn_3 , (b) UGa_3 , and (c) NpGa_3 based on the j - j coupling scheme. Here we assume trivalent actinide ions as U^{3+} ($5f^3$) and Np^{3+} ($5f^4$). It should be noted that up and down arrows denote pseudospins to distinguish the states in the Kramers doublet. Note also that for NpGa_3 , a couple of electrons in Γ_8 orbitals form a local triplet, leading to Γ_5 .

an energy difference of 12meV [246]. Thus, we take Γ_7 to be lower for the present considerations, as shown in Fig. 34(a).

In the j - j coupling scheme for UGa_3 and NpGa_3 , we accommodate three or four electrons in the one-electron energy states Γ_7 and Γ_8 . We immediately notice that there are two possibilities, i.e., low- and high-spin states, depending on the Hund's rule interaction and the splitting between the Γ_7 and Γ_8 levels. As discussed in the previous subsection, the effective Hund's rule interaction can be small in the j - j coupling scheme and thus, the low-spin state should be realized, as shown in Figs. 34(b) and (c). We emphasize that this low-spin state is consistent with the LS coupling scheme. In fact, for NpGa_3 , the observed magnetic moment at Np ion has been found to be consistent with Γ_5 triplet [263].

In the electron configuration shown in Figs. 34(b) and (c), the Γ_7 level is fully occupied to form a singlet. If this Γ_7 level is located well below the Γ_8 , the occupying electrons will not contribute to the magnetic properties. Thus, we can ignore the Γ_7 electrons for our present purposes. In order to validate this simplification, it is useful to introduce the results of band-structure calculations for CeIn_3 [264] and UGa_3 [265]. Note that both results have been obtained assuming the system is in the paramagnetic state. In order to focus on the f electron components of the energy band, we concentrate on the bands around the Γ point near the Fermi level. For CeIn_3 , the energy band dominated by Γ_7 character is found to be lower than the Γ_8 -dominated band, consistent with the local level scheme in Fig. 34(a). An important point is that the Fermi level intersects the Γ_7 -dominant band, indicating that the Fermi surface is mainly composed of Γ_7 electrons hybridized with Ga-ion p electrons. On the other hand, for UGa_3 , the Γ_7 band is also lower than the Γ_8 band, but the Fermi level crosses the Γ_8 band. Thus, the Γ_7 band appears to be fully occupied, consistent with the j - j coupling level scheme, as shown in Fig. 34(b). Since the main contribution to the Fermi surface comes from Γ_8 electrons, it is natural to dwell on the Γ_8 bands and ignore the occupied Γ_7 bands in giving further consideration to many-body effects.

So far, we have considered the model in the cubic system, but as mentioned before, 115 materials exhibit tetragonal crystal structure. To include the effect of tetragonality, here we introduce two ingredients into the model Hamiltonian. One is non-zero Δ , which is the level splitting between two orbitals. Under the tetragonal CEF, the local electronic levels are given by two Γ_7 and one Γ_6 states. Among them, Γ_6 is just equal to Γ_8^b in the cubic system. Two Γ_7 states are given by the linear combinations of $a_{i\pm 3/2}^\dagger|0\rangle$ and $a_{i\mp 5/2}^\dagger|0\rangle$, which can be expressed also by the mixture of Γ_7 and Γ_8^a . Here for simplicity, we introduce Δ , splitting energy between Γ_8 orbitals, by ignoring the change of wavefunctions from cubic to tetragonal systems. Another is the change in the hopping amplitude along the z -axis. In AnTGa_5 (An=U and Np), AnGa_3 layer is sandwiched by TGa_2 blocks, as shown in Fig. 33(a), indicating that the hopping of f -electron along the z -axis should be reduced from that in AnGa_3 . However, it is difficult to estimate the reduction quantitatively, since it is necessary to include correctly the hybridization with d -electrons in transition metal ions and p -electrons in Ga ions. Thus, we change the hopping t as t_z in the definition of $t_{\tau\tau'}^z$.

Then, the Hamiltonian is the sum of H_{Γ_8} and the level splitting term, given by

$$H = H_{\Gamma_8} - \Delta \sum_{\mathbf{i}} (\rho_{i\mathbf{a}} - \rho_{i\mathbf{b}})/2. \quad (154)$$

Concerning the hopping amplitudes in the xy plane, they are given by Eqs. (149) and (150), but along the z -axis, it is necessary to include the change from cubic to tetragonal case. Namely, the effective hopping along the z axis is expressed as

$$t_{\tau\tau'}^z = t_z \begin{pmatrix} 0 & 0 \\ 0 & 1 \end{pmatrix}, \quad (155)$$

where t_z is the reduced hopping amplitude along the z -axis. The ratio t_z/t is less than unity. We note that in actuality, Δ should be related to the value of t_z , since both quantities depend on the lattice constant along the z axis. However, the relation between t_z and Δ is out of the scope at present and thus, here we simply treat them as independent parameters.

Among several methods to analyze the microscopic model, we resort to an exact diagonalization technique on a $2 \times 2 \times 2$ lattice. Although there is a demerit that it is difficult to enlarge the system size, we take a clear advantage that it is possible to deduce the magnetic structure by including the effect of electron correlation. In order to discuss the ground-state properties, it is useful to measure the spin and orbital correlations, which are, respectively, defined by

$$S(\mathbf{q}) = (1/N) \sum_{\mathbf{i}, \mathbf{j}} \langle \sigma_{\mathbf{i}}^z \sigma_{\mathbf{j}}^z \rangle e^{i\mathbf{q} \cdot (\mathbf{i} - \mathbf{j})}, \quad (156)$$

with $\sigma_{\mathbf{i}}^z = \sum_{\tau} (n_{i\tau\uparrow} - n_{i\tau\downarrow})/2$, and

$$T(\mathbf{q}) = (1/N) \sum_{\mathbf{i}, \mathbf{j}} \langle \tau_{\mathbf{i}}^z \tau_{\mathbf{j}}^z \rangle e^{i\mathbf{q} \cdot (\mathbf{i} - \mathbf{j})}, \quad (157)$$

with $\tau_{\mathbf{i}}^z = \sum_{\sigma} (n_{i\mathbf{a}\sigma} - n_{i\mathbf{b}\sigma})/2$. Here N is the number of sites.

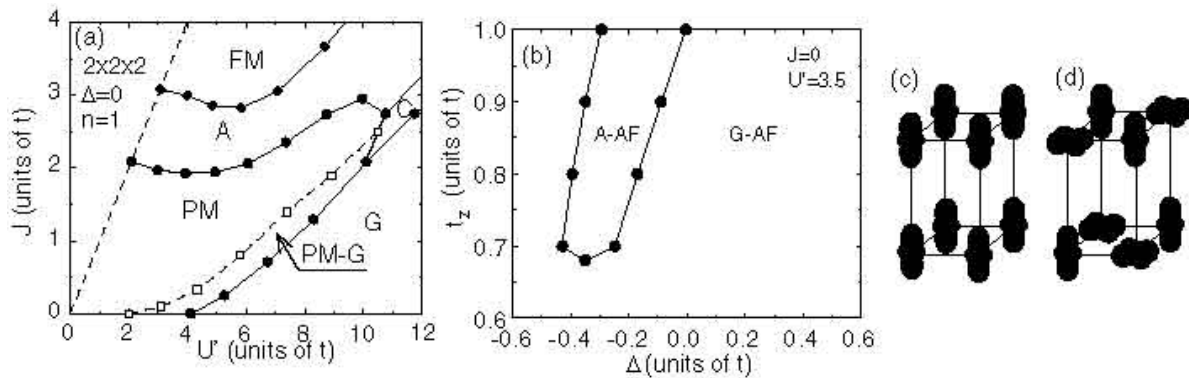


Figure 35. (a) Phase diagram for UGa_3 obtained by the exact diagonalization. The region of $J > U'$ is ignored, since it is unphysical. See Fig. 8(a) for the definitions of abbreviations. Here “PM-G” indicates the PM phase with enhanced (π, π, π) spin correlation. (b) Phase diagram of the magnetic structure in the (Δ, t_z) plane for $J=0$ and $U' = 3.5$. (c) Ferro orbital pattern in the A-type AF phase. (d) Antiferro orbital pattern in the G-type AF phase.

6.1.1. U-115 Let us review the results for $n=1$ [82], in which one electron is accommodated in Γ_8 orbital, corresponding to uranium compounds. First we consider the cubic case ($\Delta=0$ and $t_z/t=1$). After we evaluate spin and orbital correlations for several parameter sets, the ground-state phase diagram is completed on the (U', J) plane, as shown in Fig. 35(a). In the small- J region, the paramagnetic (PM) phase exists for large parameter space and in the boundary region between PM and G-type AF states, we can see the PM phase with dominant (π, π, π) spin correlation. Note that such a PM-G region is not specific to the case of $J=0$, since it appears even when we increase the Hund’s rule interaction.

Here we briefly discuss the phases in the large- J region. We observe an interesting similarity with the phase diagram for undoped manganites $RMnO_3$, in which mobile e_g -electrons are tightly coupled with the Jahn-Teller distortions and the background t_{2g} spins. Note that the present Hamiltonian is just equal to the e_g electron part of the model for manganites [72]. In the so-called double-exchange system with large Hund’s rule coupling between e_g and t_{2g} electrons, the Jahn-Teller distortion suppresses the probability of double occupancy and it plays a similar role as the interorbital Coulomb interaction U' . The AF coupling among t_{2g} spins, J_{AF} , controls the FM tendency in the e_g -electron phases. Roughly speaking, large (small) J_{AF} denotes small (large) J . Then, we see an interesting similarity between Fig. 35(a) and the phase diagram for manganites, except for the PM region. See Figs. 8(b) and 9(a). In particular, a chain of the transition, $FM \rightarrow A\text{-AF} \rightarrow C\text{-AF} \rightarrow G\text{-AF}$, occurs with decreasing J (increasing J_{AF}). Again we stress that the present Γ_8 model for f -electron systems is essentially the same as the e_g orbital model in the d -electron systems. It is interesting to observe common phenomena concerning orbital degree of freedom in f -electron systems.

Now we include the effect of tetragonality. Since the mother compound UGa_3 is AF

metal, in our phase diagram, it is reasonable to set the parameter region corresponding to “PM-G”. Then, we choose $U'=3.5$ and $J=0$. Again we evaluate spin and orbital correlations by changing Δ and t_z , and obtain the phase diagram in the (Δ, t_z) plane, as shown in Fig. 35(b) for $J=0$ and $U'=3.5$. Note that the ground state for $\Delta=0$ and $t_z=1$ is magnetic metallic, as seen in Fig. 35(a). It is found that an A-type AF phase appears in the negative Δ region for $t_z>0.68$. Note that the appearance of the A-AF phase is not sensitive to t_z as long as $t_z>0.68$. Rather, Δ seems to play a key role in controlling the change of the magnetic phase. Here we recall the experimental fact that UNiGa₅ exhibits a G-type AF phase, while UPtGa₅ shows an A-type. Thus, it is necessary to relate the effect of Δ to the difference in magnetic structure found between UNiGa₅ and UPtGa₅. Although t_z may differ among U-115 compounds, we focus here on the effect of Δ .

From the orbital correlation, we obtain the ferro-orbital and anti-ferro orbital patterns for A-AF and G-AF phases, respectively, as shown in Figs. 35(c) and 35(d). Let us now discuss the reasons for the appearance of an A-AF phase. For negative values of Δ , we easily obtain ferro-orbital (FO) pattern composed of Γ_8^b orbitals, as illustrated in Fig. 35(c). For electrons to gain kinetic energy of motion along the z -axis, it is necessary to place the AF spin arrangement along this same axis. In the FM spin configuration, electrons cannot move along the z -axis due to the Pauli principle, since hopping occurs *only* between Γ_8^b orbitals along the z -axis. On the other hand, in the xy plane b -orbital electrons can hop to neighboring a -orbitals with a significant amplitude, which is larger than that between neighboring b -orbitals. Thus, in order to gain kinetic energy, electrons tend to occupy a -orbitals even in the FO state composed of b -orbitals, as long as $|\Delta|$ is not so large. When we explicitly include the effects of the Hund’s rule interaction J , electron spins should have FM alignment between neighboring sites in order to gain energy in hopping processes from b - to a -orbitals. Consequently, a FM spin configuration is favored in the xy plane. In the case with antiferro orbital correlations, spin correlation tends in general to be FM, as has been widely recognized in orbitally degenerate systems.

Here we mention a relation of Δ to the magnetic anisotropy in U-115 materials. For UPtGa₅ with the A-AF phase, χ_a is larger than χ_c , whereas this anisotropy is not pronounced in UNiGa₅ with the G-AF phase [59]. An analysis for the high-temperature region based on LS coupling yields the $J_z=\pm 1/2$ Kramers doublet as the ground state among the dectet of $J=9/2$ ($L=6$ and $S=3/2$). The states with $J_z=\pm 1/2$ in the LS coupling scheme have significant overlap with $f_{ib\uparrow}^\dagger f_{ic\uparrow}^\dagger f_{ic\downarrow}^\dagger |0\rangle$ and $f_{ib\downarrow}^\dagger f_{ic\uparrow}^\dagger f_{ic\downarrow}^\dagger |0\rangle$ in the j - j coupling scheme. Accordingly, by the present definition Δ should be negative to place Γ_8^b below Γ_8^a . If the absolute value of $\Delta(<0)$ becomes large, Γ_8^b is well separated from Γ_8^a and the magnetic anisotropy will consequently become large. Thus, a change from G- to A-type AF phase is consistent with the trends of magnetic anisotropy in UNiGa₅ and UPtGa₅.

Finally, we make a brief comment about the effect of t_z . Following the above discussion, the A-AF phase should appear even for small t_z . However, in the present

calculation it disappears for $t_z < 0.68$, a critical value which seems to be rather large. Such a quantitative point depends on the system size, and we note that it is necessary to perform the calculation in the thermodynamic limit.

While such investigations are just beginning, we already see a number of opportunities for future work along this path. Concerning issues directly related to the present context, it is highly recommended that calculations be carried out in the thermodynamic limit, in order to confirm the present exact diagonalization results. For instance, the magnetic susceptibility should be evaluated in the random phase approximation or fluctuation-exchange method. With such an approach, the magnetic structure can be discussed by detecting the divergence in the magnetic susceptibility. This is one of our future tasks. Another problem is how to establish the effective reduction of t_z in considering the case of UTGa_5 . In such systems, TGa_2 blocks are interspersed between UGa_3 layers, but the main process may occur through the Ga ions. To analyze this, it is necessary to treat a three-dimensional *f-p* model with explicit consideration of U and Ga ions. This is another problem for future investigation.

6.1.2. Np-115 Now we review the theoretical results for magnetic structure of Np-115 [83]. First we consider the case of $n=2$, which is corresponding to the trivalent Np ion. At $t_z=1$ and $\Delta=0$ (cubic case), local triplet composed of a couple of *f* electrons is formed at each site and the G-type AF structure is stabilized due to the so-called superexchange interaction. Even when Δ is introduced as the tetragonal CEF effect, the G-AF structure remains robust for $|\Delta| < 1$. When $|\Delta|$ is larger than unity, two electrons simultaneously occupy the lower orbital, leading to the non-magnetic state composed of local Γ_1 , irrelevant to the present study to consider the magnetic phase. When we change t_z for $\Delta=0$, again the G-type AF structure is stabilized, but we find that the spin correlation of $\mathbf{q}=(\pi, \pi, 0)$ comes to be equivalent to that of $\mathbf{q}=(\pi, \pi, \pi)$ with the decrease of t_z , since the AF structure is stabilized in each *xy* plane due to superexchange interaction and the planes are decoupled for small t_z .

At the first glance, it seems difficult to understand the variety of magnetic phases observed in NpTGa_5 even in a qualitative level, when we consider only the trivalent Np ion. However, there is no *a priori* reason to fix the valence as Np^{3+} . In NpTGa_5 , *d*-electron band originating from transition metal ions may significantly affect the valence of Np ion [80]. In addition, we also stress that the actual compounds exhibit AF metallic behavior. In the band-structure calculation, the average number of *f* electrons at Np ion is easily decreased from four. Thus, we treat the local *f*-electron number as a parameter.

We may consider another reason to decrease effectively the number of *f* electron from $n=2$ in NpGa_3 . In the present two-orbital model, the G-AF structure is robust, which is natural from the theoretical viewpoint within the model. However, in the experimental result on NpGa_3 , the low-temperature ground state is ferromagnetic, although the AF phase has been observed around at $T \sim 60\text{K}$. In order to understand the occurrence of the FM phase in the two-orbital model, it is necessary to inject some amount of “hole” in the AF phase, since the double-exchange mechanism works to

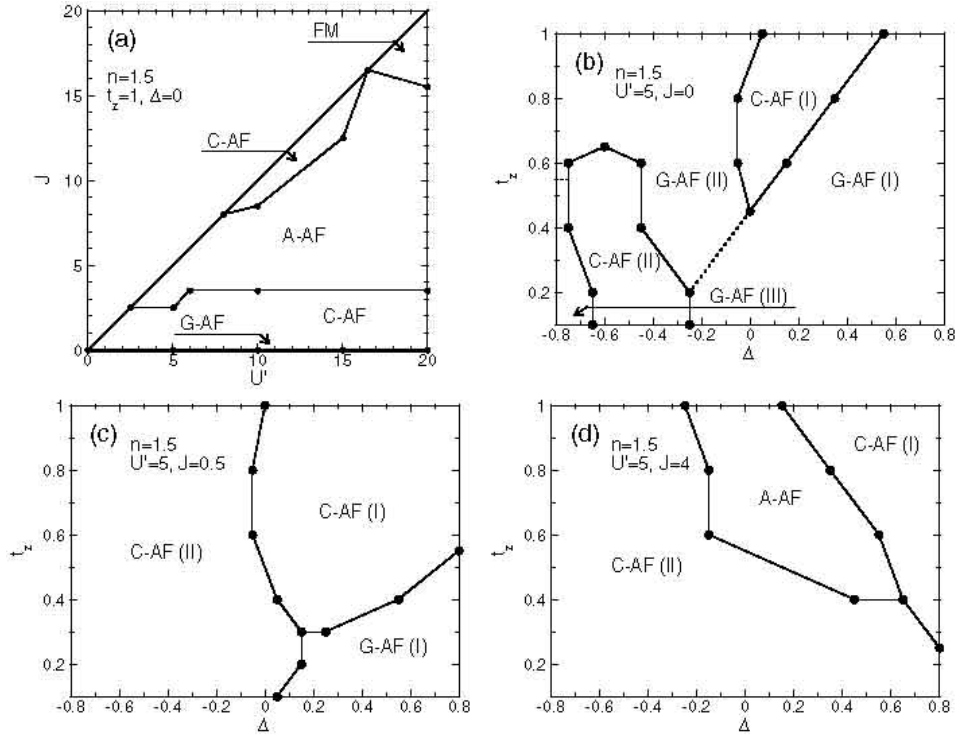


Figure 36. (a) Ground-state phase diagram in the (U', J) plane for $n=1.5$, $t_z=1$, and $\Delta=0$. Ground-state phase diagrams of the magnetic structure in the (Δ, t_z) plane for $n=1.5$, $U'=5$, (b) $J=0$, (c) $J=0.5$, and (d) $J=4$.

maximize the kinetic motion of electrons. It is difficult to determine the amount of doped holes to obtain the FM phase, but at least qualitatively, the effective decrease of n seems to be physically meaningful in NpGa_3 as well as NpTGa_5 .

Then, we consider the case of $n=1.5$. In Fig. 36(a), we show the ground-state phase diagram in the (U', J) plane at $n=1.5$ for the cubic case with $t_z=1$ and $\Delta=0$. At $J=0$, a G-type AF structure is stabilized due to superexchange interaction in the same way as the case of $n=2$. However, the G-AF structure is immediately changed to a C-AF structure only by a small value of the Hund's rule interaction. With increasing J , the magnetic phase changes in the order of G-AF, C-AF, A-AF, and FM phases, except for the C-AF phase in the large J region. Concerning the spin structures, see Fig. 8(a). This result is quite natural, since we are now considering the magnetic structure based on the two-orbital model, in which the FM tendency is due to the optimization of kinetic motion of electrons.

After calculations of the spin and orbital correlations for several parameter sets, we obtain the ground-state phase diagram in the (Δ, t_z) plane, as shown in Figs. 36(b), for $U'=5$ and $J=0$. In the region of large positive Δ , we find that G-AF(I) phase with ferro-type arrangement of Γ_g^g orbital extends in a wide range of the phase diagram. It is found that the C-AF(I) phase appears in the region for small positive Δ and $0.5 < t_z < 1$. The C-AF(I) phase exhibits the dominant component of $(\pi, \pi, 0)$ in the spin correlation.

When we further decrease Δ , we find G-AF(II) phase, which may be considered as orbital disordered, since there is no dominant component in the orbital correlation. For small t_z and small negative Δ , we find another C-AF phase, which we call C-AF(II), in which the spin correlation of $(\pi, 0, \pi)$ and $(0, \pi, \pi)$ are dominant. For small t_z and large negative Δ , there appears yet another G-AF phase, called G-AF(III) with ferro-type arrangement of Γ_8^b orbital. In any case, for $J=0$, we can observe several kinds of C- and G-AF phases, but A-AF phase does not occur.

Although we increase the value of J as $J=0.5$, no new phases appear in the phase diagram for $n=1.5$, as shown in Fig. 36(c). There are three phases, but they are two C-AF and one G-AF states. As labeled explicitly in the phase diagrams, C-AF(I), C-AF(II), and G-AF(I) are the same as those in the phase diagram of Fig. 36(b). Due to the effect of J , G-AF(II) and G-AF(III) disappear, since the number of FM bond should be increased to gain the kinetic energy. As shown in Fig. 36(d), when we further increase the value of J as $J=4$, the G-AF phase completely disappears and instead, we observe the A-AF phase sandwiched by two C-AF phases. By analogy with the various phases of manganites, the A-AF phase is considered to appear due to the double-exchange mechanism in the two-orbital model, when J is increased.

In the experiments for NpTGa₅, C-, A-, and G-AF magnetic phases have been found in NpFeGa₅, NpCoGa₅, and NpNiGa₅. Here we have a naive question: What is a key parameter to understand the change of the magnetic structure? In the case of UTGa₅, it has been claimed that the level splitting Δ is important to explain the difference in magnetic structure as well as the magnetic anisotropy for a fixed value of $n=1$. Roughly speaking, Δ is positive for T=Fe, small positive for T=Co, and negative for T=Ni. Among UTGa₅ with T=Ni, Pd, and Pt, when we assume that the absolute value of Δ is increased in the order of Ni, Pd, and Pt, it is possible to understand qualitatively the change in the magnetic anisotropy, in addition to the change in the magnetic structure of G-AF for T=Ni and A-AF for T=Pd and Pt. It has been found that the value of t_z is not so crucial to explain qualitatively the magnetic properties of U-115 based on the two-orbital model for $n=1$.

For $n=2$, we always obtain the G-AF phase. However, for $n=1.5$, we have observed three kinds of AF magnetic structure in the phase diagrams. Let us summarize the change in the magnetic structure for a fixed value of $t_z=0.8$. Note that this value is larger than $t_z=0.1$, which we have considered to reproduce two kinds of cylindrical Fermi-surface sheets of Np-115. However, in the small-sized cluster calculations, it is difficult to compare directly with the values in the thermodynamic limit. Thus, we do not discuss further the quantitative point on the values of t_z . As shown in Fig. 36(b), for $J=0$ and $t_z=0.8$, we see the change in the magnetic structure as G-AF ($\Delta < 0$), C-AF ($0 < \Delta < 0.4$), and G-AF ($\Delta > 0.4$). For $J=0.5$ and $t_z=0.8$, as shown in Fig. 36(c), the C-AF phases are always observed, but they have different orbital structures. Finally, for $J=4$ and $t_z=0.8$, we observe C-AF ($\Delta < -0.15$), A-AF ($-0.15 < \Delta < 0.3$), and C-AF ($\Delta > 0.3$), as shown in Fig. 36(d).

In order to understand the appearance of three types of the AF phases, we may

consider an explanation due to the combination of the changes in Δ and n . For instance, by assuming that $J=4$ for NpTGa_5 and the change in Δ for NpTGa_5 is just the same as that for UTGa_5 , we consider that $n \approx 2$ with $\Delta < 0$ for $\text{T}=\text{Ni}$, $n \approx 1.5$ with $\Delta \approx 0$ for $\text{T}=\text{Co}$, and $n \approx 1.5$ with $\Delta > 0$ for $\text{T}=\text{Fe}$. Then, it seems to be possible to relate our theoretical AF phases with the experimental observations in NpTGa_5 . However, it is difficult to claim that the above parameter assignment for three Np-115 materials is the best explanation for the magnetic structure of Np-115, since in actual compounds, there are other important ingredients which have not been included in the present model. For instance, we have never discussed the direction of the magnetic moment of Np ion. In particular, the canted AF structure cannot be considered at all for the G-AF phase of NpNiGa_5 . Thus, we need to recognize some distance between the actual magnetic states and the theoretically obtained phases. Our theory should be improved by taking into account other realistic ingredients of 115 structure.

Finally, let us remark a possible future direction of the research. In Fig. 36(b), we have explained the G-AF(II) as the orbital disordered phase, which is considered to be related to the metallic phase. Of course, we cannot conclude the metallicity only from the present calculations for small-size cluster. However, it seems to be an interesting concept that the *f*-electron state is controlled by orbital degeneracy. Quite recently, Onishi and Hotta has pointed out the orbital incommensurate state appearing between two kinds of localized AF phases, by using the density matrix renormalization group method to the model of the *j*-*j* coupling scheme [266]. We may throw new lights on the long-standing issue concerning the competition between localized and itinerant nature of *f*-electrons, when such competition is controlled by orbital degree of freedom.

6.2. Multipole ordering

In the previous subsection, we have discussed the spin and orbital structure of 115 materials on the basis of the Γ_8 model. Again we note that such “spin” and “orbital” are not real spin and orbital, but pseudo spin and orbital. In principle, in *f*-electron systems, real spin and orbital are not independent degrees of freedom, since they are tightly coupled with each other due to the strong spin-orbit interaction. Then, in order to describe such a complicated spin-orbital coupled system, it is rather appropriate to represent the *f*-electron state in terms of “multipole” degree of freedom, rather than using spin and orbital degrees of freedom as in *d*-electron systems. We show a table to summarize the multipole operators up to rank 3. The relation of the irreducible representation with pseudo spin and orbital are also shown. When we use the term of multipole degree of freedom, pseudo spin σ and pseudo orbital τ are Γ_{4u} dipole and Γ_{3g} quadrupole, respectively, from Table 3. Thus, in the previous section, we have considered the ordering tendencies of dipole and quadrupole degree of freedom. Note that it is important to show explicitly the parity of the multipole operator to complete its symmetry. In this section, for convenience, we use the subscripts “u” and “g” for odd and even parity, respectively.

Table 3. Multipole operators in the Γ_8 subspace, shown in Ref. [267]. The first, second, and third lines denote γ of the irreducible representation Γ_γ , multipole operator X^{Γ_γ} , and pseudospin representation, respectively. The multipole operators are represented by pseudospin operators as $\hat{\tau} = \sum_{\tau,\tau',\sigma} c_{\tau\sigma}^\dagger \sigma_{\tau\tau'} c_{\tau'\sigma}$ and $\hat{\sigma} = \sum_{\tau,\sigma,\sigma'} c_{\tau\sigma}^\dagger \sigma_{\sigma\sigma'} c_{\tau\sigma'}$, where σ are the Pauli matrices. We use notations $\hat{\eta}^\pm = (\pm\sqrt{3}\hat{\tau}^x - \hat{\tau}^z)/2$ and $\hat{\zeta}^\pm = -(\hat{\tau}^x \pm \sqrt{3}\hat{\tau}^z)/2$. For simplicity, we suppress the site label \mathbf{r} in this table.

$2u$	$3gu$	$3gv$	$4u1x$	$4u1y$	$4u1z$	$4u2x$	$4u2y$	$4u2z$
T_{xyz}	O_2^0	O_2^2	J_x^{4u1}	J_y^{4u1}	J_z^{4u1}	J_x^{4u2}	J_y^{4u2}	J_z^{4u2}
$\hat{\tau}^y$	$\hat{\tau}^z$	$\hat{\tau}^x$	$\hat{\sigma}^x$	$\hat{\sigma}^y$	$\hat{\sigma}^z$	$\hat{\eta}^+ \hat{\sigma}^x$	$\hat{\eta}^- \hat{\sigma}^y$	$\hat{\tau}^z \hat{\sigma}^z$

$5ux$	$5uy$	$5uz$	$5gx$	$5gy$	$5gz$
T_x^{5u}	T_y^{5u}	T_z^{5u}	O_{yz}	O_{zx}	O_{xy}
$\hat{\zeta}^+ \hat{\sigma}^x$	$\hat{\zeta}^- \hat{\sigma}^y$	$\hat{\tau}^x \hat{\sigma}^z$	$\hat{\tau}^y \hat{\sigma}^x$	$\hat{\tau}^y \hat{\sigma}^y$	$\hat{\tau}^y \hat{\sigma}^z$

In this article, we pick up octupole ordering in NpO_2 . First we briefly discuss the level scheme for actinide dioxides with CaF_2 cubic crystal structure. Due to the CEF effect, the sextet is split into Γ_8 quartet and Γ_7 doublet. In this case, due to the intuitive discussion on the direction of the extension of orbital and the position of oxygen ions, the Γ_7 state should be higher than the Γ_8 level. Here we define the splitting energy as Δ . As discussed in Sec. 5, in order to make the low-spin state, we accommodate two, three, and four electrons in the Γ_8 level. Then, the ground states are Γ_5 , $\Gamma_8^{(2)}$, and Γ_1 , respectively [72], consistent with the CEF ground states of UO_2 [268, 269], NpO_2 [270, 271], and PuO_2 [272, 273], respectively. Then, Δ is estimated from the CEF excitation energy in PuO_2 , experimentally found to be 123 meV [272, 273]. On the other hand, as mentioned repeatedly in this article, the Hund's rule coupling J_H between Γ_8 and Γ_7 levels is 1/49 of the original Hund's rule interaction among *f* orbitals. Namely, J_H is as large as a few hundred Kelvins. Thus, we validate our assumption that the Γ_7 state is simply ignored. From the qualitative viewpoint, unfortunately, this simplification is not appropriate to reproduce experimental results, since the ground-state wave-function is not exactly reproduced in the Γ_8 model. However, we believe that this approximation provides a qualitatively correct approach, in order to understand the complex multipole state from the microscopic viewpoint.

Let us here review the recent theoretical result on octupole order of NpO_2 [113, 116, 117, 118, 119]. We set the Hamiltonian for actinide dioxides as the Γ_8 model Eq. (152) on an fcc lattice. The form of the Hamiltonian is already given, but the hopping should be estimated on the fcc lattice. For instance, the hopping amplitudes between *f*-orbitals at $(0, 0, 0)$ and $(a/2, a/2, 0)$ (a is the lattice constant) are given by

$$t_{\tau\uparrow;\tau'\uparrow}^{(a/2,a/2,0)} = t_{\tau\downarrow;\tau'\downarrow}^{(a/2,a/2,0)*} = t \begin{pmatrix} 4 & 2\sqrt{3}i \\ -2\sqrt{3}i & 3 \end{pmatrix}. \quad (158)$$

Table 4. Coupling constants in the effective model. The energy unit is $(1/16)t^2/(U' - J)$.

a_1	a_3	a_4	b_8	b_9	b_{10}	$b_1^{(1)}$	$b_2^{(1)}$	$b_3^{(1)}$
12	$64\sqrt{3}$	192	195	-336	576	-196	-4	0
$b_4^{(1)}$	$b_5^{(1)}$	$b_6^{(1)}$	$b_1^{(2)}$	$b_2^{(2)}$	$b_3^{(2)}$	$b_4^{(2)}$	$b_5^{(2)}$	$b_6^{(2)}$
$224\sqrt{3}$	0	0	4	193	-336	$64\sqrt{3}$	$2\sqrt{3}$	$112\sqrt{3}$

and

$$t_{\tau\uparrow;\tau'\downarrow}^{(a/2,a/2,0)} = t_{\tau\downarrow;\tau'\uparrow}^{(a/2,a/2,0)} = 0, \quad (159)$$

where $t = (ff\sigma)/28$ and $t_{\tau\sigma;\tau'\sigma'}^{-\mu} = t_{\tau\sigma;\tau'\sigma'}^{\mu}$. Note that the hopping integrals depend on μ and they are intrinsically complex numbers in the fcc lattice. It is in sharp contrast to the previous model on a simple cubic lattice, in which the hopping integrals are real and the same form as for e_g orbitals of d electrons. In other words, there is no difference between the Γ_8 model for f electrons and the e_g orbital model for d electrons on the simple cubic lattice in the absence of a magnetic field. For e_g orbitals, we can always set the hopping integrals to be real irrespective of the lattice type, by selecting appropriate basis wave-functions, while Γ_8 orbitals on the fcc lattice appear to be complex in nature, specific to f -electron systems with strong spin-orbit coupling.

In order to discuss multipole ordering, we derive an effective multipole model in the strong-coupling limit using standard second-order perturbation theory with respect to t , which is exactly the same as that used in the derivation of the Heisenberg model from the Hubbard model in the research field of transition metal oxides. It is one of advantages of the f -electron model on the basis of the j - j coupling scheme that we can exploit the technique developed in the d -electron research. We consider the case of one electron per f ion in the Γ_8 orbitals, but the effective model is the same for the one-hole case, which corresponds to NpO_2 , due to an electron-hole transformation. Among the intermediate f^2 -states in the perturbation theory, we consider only the lowest-energy Γ_5 triplet states, in which the two electrons occupy different orbitals, assuming that other excited states are well separated from the f^2 ground states. In fact, the excitation energy from the Γ_5 ground state of f^2 in UO_2 is 152 meV [268, 269]. Note that the CEF excitation energy is considered to be larger than the triplet excitation one, since the Hund's rule interaction is effectively reduced in the j - j coupling scheme. Thus, it is reasonable to take only the Γ_5 states as the intermediate states.

After straightforward, but tedious calculations [113, 116], we arrive at an effective model in the form of

$$H_{\text{eff}} = \sum_{\mathbf{q}} (H_{1\mathbf{q}} + H_{2\mathbf{q}} + \mathcal{H}_{4u1\mathbf{q}} + H_{4u2\mathbf{q}}), \quad (160)$$

where \mathbf{q} is the wave vector. $H_{1\mathbf{q}}$ denotes the interactions between quadrupole moments, given by

$$H_{1\mathbf{q}} = a_1(O_{2,-\mathbf{q}}^0 O_{2,\mathbf{q}}^0 c_x c_y + \text{c.p.})$$

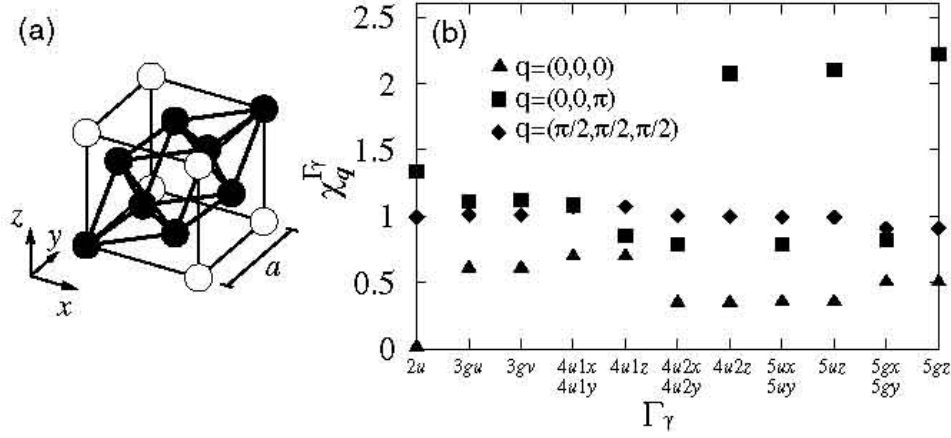


Figure 37. (a) The 8-site fcc cluster, shown by solid spheres, taken in the calculation of exact diagonalization. (b) Correlation functions for the 8-site cluster for $\mathbf{q} = (0, 0, 0)$ (triangles), $\mathbf{q} = (0, 0, 1)$ (squares), and $\mathbf{q} = (1/2, 1/2, 1/2)$ (diamonds) in units of $2\pi/a$.

$$\begin{aligned}
& + a_3(O_{2,-\mathbf{q}}^0 O_{xy,\mathbf{q}} s_x s_y + \text{c.p.}) \\
& + a_4(O_{xy,-\mathbf{q}} O_{xy,\mathbf{q}} c_x c_y + \text{c.p.}), \tag{161}
\end{aligned}$$

where c.p. denotes cyclic permutations, $c_\nu = \cos(q_\nu a/2)$, and $s_\nu = \sin(q_\nu a/2)$ ($\nu = x, y$, or z). The definitions of the multipole operators and values of the coupling constants a_i are given in Tables 3 and 4, respectively. Note that $O_{2\mathbf{q}}^0$ transforms to $(\sqrt{3}O_{2\mathbf{q}}^2 - O_{2\mathbf{q}}^0)/2$ and $(-\sqrt{3}O_{2\mathbf{q}}^2 - O_{2\mathbf{q}}^0)/2$ under c.p. $(x, y, z) \rightarrow (y, z, x)$ and $(x, y, z) \rightarrow (z, x, y)$, respectively. $\mathcal{H}_{2\mathbf{q}}$ and $H_{4un\mathbf{q}}$ ($n = 1$ or 2) are the interactions between dipole and octupole moments, given by

$$\begin{aligned}
H_{2\mathbf{q}} & = b_8 [T_{z,-\mathbf{q}}^{5u} T_{z,\mathbf{q}}^{5u} (c_y c_z + c_z c_x) + \text{c.p.}] \\
& + b_9 [T_{x,-\mathbf{q}}^{5u} T_{y,\mathbf{q}}^{5u} s_x s_y + \text{c.p.}] \\
& + b_{10} [T_{xyz,-\mathbf{q}} T_{xyz,\mathbf{q}} (c_x c_y + \text{c.p.})], \tag{162}
\end{aligned}$$

and

$$\begin{aligned}
H_{4un\mathbf{q}} & = b_1^{(n)} [J_{z-\mathbf{q}}^{4un} J_{z\mathbf{q}}^{4un} c_x c_y + \text{c.p.}] \\
& + b_2^{(n)} [J_{z-\mathbf{q}}^{4un} J_{z\mathbf{q}}^{4un} (c_y c_z + c_z c_x) + \text{c.p.}] \\
& + b_3^{(n)} [J_{x-\mathbf{q}}^{4un} J_{y\mathbf{q}}^{4un} s_x s_y + \text{c.p.}] \\
& + b_4^{(n)} [T_{xyz-\mathbf{q}} (J_{z\mathbf{q}}^{4un} s_x s_y + \text{c.p.})] \\
& + b_5^{(n)} [T_{z-\mathbf{q}}^{5u} J_{z\mathbf{q}}^{4un} c_z (c_x - c_y) + \text{c.p.}] \\
& + b_6^{(n)} [T_{z-\mathbf{q}}^{5u} (-J_{x\mathbf{q}}^{4un} s_z s_x + J_{y\mathbf{q}}^{4un} s_y s_z) + \text{c.p.}], \tag{163}
\end{aligned}$$

where values of the coupling constants b_i and $b_i^{(n)}$ are shown in Table 4. The above Eqs. (160)–(163) are consistent with the general form of multipole interactions on the fcc lattice derived by Sakai et al. [274]. We follow the notation in Ref. [274] for convenience.

When a mean-field theory is applied to the effective model, due care should be taken, since in an fcc lattice with geometrical frustration, the effect of fluctuations may

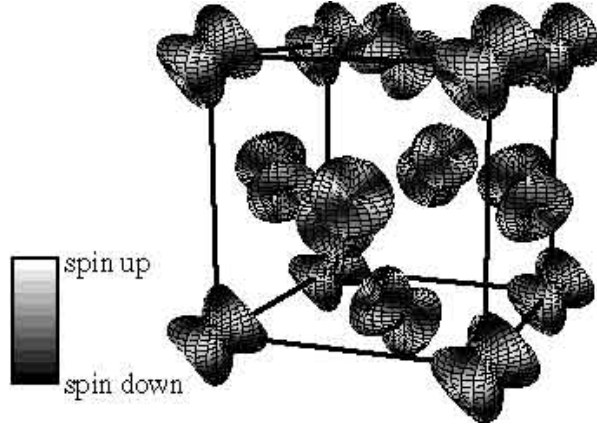


Figure 38. The triple- \mathbf{q} Γ_{5u} octupole state in the fcc lattice.

be strong enough to destroy the state obtained within the mean-field theory. Thus, we first evaluate the correlation function in the ground state using an unbiased method such as exact diagonalization on the N -site lattice. Here we set $N = 8$, as shown Fig. 37(a). The correlation function of the multipole operators is defined by

$$\chi_{\mathbf{q}}^{\Gamma\gamma} = (1/N) \sum_{\mathbf{r}, \mathbf{r}'} e^{i\mathbf{q}\cdot(\mathbf{r}-\mathbf{r}')} \langle X_{\mathbf{r}}^{\Gamma\gamma} X_{\mathbf{r}'}^{\Gamma\gamma} \rangle, \quad (164)$$

where $\langle \dots \rangle$ denotes the expectation value by the ground-state wave-function. Figure 37(b) exhibits the results for correlation functions. As shown in the Table 4, the absolute value of the interaction between Γ_{2u} moments (b_{10}) is the largest among multipole interactions, but the correlation function of the Γ_{2u} moment is not so enhanced, suggesting that the frustration effect is significant for an Ising-like moment such as Γ_{2u} . Rather, large values of correlation functions are found for J_z^{4u2} , T_z^{5u} , and O_{xy} moments at $\mathbf{q} = (0, 0, 1)$ in units of $2\pi/a$. Note that the effective model does not include the term which stabilizes O_{xy} quadrupole order at $\mathbf{q} = (0, 0, 1)$. The enhancement of this correlation function is due to an induced quadrupole moment in Γ_{4u2} or Γ_{5u} moment ordered states. Thus, the relevant interactions of the system should be $b_2^{(2)}$ and b_8 , which stabilize the J_z^{4u2} and T_z^{5u} order, respectively, at $\mathbf{q} = (0, 0, 1)$. In the following, then, we consider a simplified multipole model which includes only $b_2^{(2)}$ and b_8 .

Now we apply mean-field theory to the simplified model to specify the ordered state. As easily understood, the coupling constant b_8 is slightly larger than $b_2^{(2)}$, indicating that Γ_{5u} order has lower energy than Γ_{4u2} order. The interaction b_8 stabilizes longitudinal ordering of the Γ_{5u} moments, but their directions are not entirely determined by the form of the interaction. Here we point out that in the Γ_8 subspace, the Γ_{5u} moment has an easy axis along $[111]$ $[100, 101, 110]$. Thus, taking the moment at each site along $[111]$ or other equivalent directions, we find that a triple- \mathbf{q} state is favored, since it gains interaction energy in all the directions. In fact, as shown in Fig. 38, the ground state has longitudinal triple- \mathbf{q} Γ_{5u} octupole order with four sublattices, i.e., $(\langle T_{x\mathbf{r}}^{5u} \rangle, \langle T_{y\mathbf{r}}^{5u} \rangle, \langle T_{z\mathbf{r}}^{5u} \rangle) \propto (\exp[i2\pi x/a], \exp[i2\pi y/a], \exp[i2\pi z/a])$. Note that this triple- \mathbf{q}

structure does not have frustration even in the fcc lattice. The ground state energy is $-4b_8$ per site, and the transition temperature T_0 is given by $k_B T_0 = 4b_8$. Another important message of Fig. 38 is that both up- and down-spin densities are anisotropic with different distribution. It may be natural, if we consider octupole as the combined degree of freedom of spin and orbital, but such an intuitive explanation of octupole becomes possible from the microscopic viewpoint on the basis of the *j-j* coupling scheme.

Let us briefly introduce new experimental evidence of octupole ordering in NpO_2 . Quite recently, in order to clarify the nature of the ordered phase of NpO_2 , Tokunaga et al. have performed ^{17}O -NMR measurement of NpO_2 below T_0 [111]. Tokunaga et al. have observed the occurrence of two inequivalent oxygen sites below T_0 from the ^{17}O -NMR spectrum. They have also found that the hyperfine interaction at the oxygen sites are explained by invoking a hyperfine interaction with field-induced AF moments due to the longitudinal triple- \mathbf{q} octupole order. Thus, the NMR results strongly support the occurrence of the longitudinal triple- \mathbf{q} multipole structure in NpO_2 .

Here we briefly mention the physical properties of the phase in the high-temperature region. The magnetic susceptibility of UO_2 follows the standard Curie-Weiss law [275], while that of NpO_2 is significantly deviated from the Curie-Weiss behavior well above the transition temperature T_0 [276, 277]. As pointed out by Kubo and Hotta [278], the difference in the temperature dependence of magnetic susceptibilities in these materials is naturally explained due to the fact that dipole *and* octupole moments coexist in NpO_2 while only dipole exists in UO_2 . When the magnetic moment consists of two independent moments, it is intuitively understood that in such a situation, the magnetic susceptibility is given by the sum of two different Curie-Weiss relations, leading to non-Curie-Weiss behavior. It is one of characteristic issues of the system with active orbital degree of freedom.

We have not included the effect of oxygen in the model, but it has been already shown that the conclusion does not change [117], even if we analyze the so-called *f-p* model which include both $5f$ electrons of Np ion and $2p$ electrons of O ions. It is also possible to perform similar analysis for another lattice structure. In fact, we have found a Γ_{3g} antiferro-quadrupole transition for the simple cubic lattice and a Γ_{2u} antiferro-octupole transition for the bcc lattice [116, 118].

7. Conclusions

We have reviewed orbital ordering phenomena in *d*- and *f*-electron compounds starting from a basic level for the construction of the model. Since this subject includes so many kinds of materials such as transition metal oxides, rare-earth compounds, and actinide materials, it is almost impossible to cover all the results concerning the orbital-related phenomena in these compounds. Thus, we have picked up some typical materials and attempted to explain how and why the orbital ordering occurs.

In order to summarize this article, we would like to emphasize three points. One is the understanding of the orbital ordering from a band-insulating picture, which

beautifully explains the appearance of E- and CE-type spin structure. The heart of the explanation is the interference effect of electron phase originating from the anisotropic orbital. By including further the realistic effect of Jahn-Teller distortions and/or Coulomb interactions, it is possible to obtain spin, charge, and orbital ordering of transition metal oxides.

Second is the similarity between *d*- and *f*-electron orbital, when we consider the *f*-electron model on the basis of the *j*-*j* coupling scheme. In particular, we have remarked significant correspondence between e_g orbital degenerate model for *d* electrons and Γ_8 model for *f* electrons. The large variety of manganite-like magnetic structure observed in U-115 and Np-115 has been understood qualitatively on the basis of the Γ_8 model.

The third point is the understanding of multipole order in a microscopic level on the basis of the *j*-*j* coupling model. As a typical example, we have reviewed the octupole ordering in NpO₂. By applying the *d*-electron-like analysis on the Γ_8 model on the fcc lattice, it is possible to understand naturally the stability of octupole ordering. It is also remarkable that octupole is clearly understood by the anisotropic spin-dependent charge distribution.

Of course, there still remain more kinds of orbital ordering in *d*- and *f*-electron compounds, which cannot be explained in this review article. We could not cite lots of important papers of other authors on the issue of orbital ordering phenomena. However, it is not the main purpose of this article to introduce orbital order in *d*- and *f*-electron systems with complete references. We would like to convey the unique viewpoint that orbital ordering (including multipole ordering) is the common phenomenon in *d*- and *f*-electron systems. By developing further microscopic theory on orbital ordering using the orbital degenerate model, we hope that it is possible to understand complex magnetism among transition metal oxides, rare-earth compounds, and actinide materials, from a unified viewpoint.

Acknowledgments

The author would like to thank E. Dagotto, A. Feiguin, H. Koizumi, A. Malvezzi, M. Mayr, E. Moraghebi, A. Moreo, H. Onishi, Y. Takada, J. C. Xavier, and S. Yunoki for collaborations on orbital ordering in transition metal oxides. He is also grateful to K. Kubo, T. Maehira, H. Onishi, T. Takimoto, and K. Ueda for collaborations on novel magnetism and unconventional superconductivity of *f*-electron systems. The author expresses sincere thanks to M. Kubota for his kind offer of original figures used in Fig. 23. He also thanks D. Aoki, T. Fujimoto, T. Ito, Y. Haga, H. Harima, R. H. Heffner, W. Higemoto, Y. Homma, F. Honda, S. Ikeda, S. Jonen, S. Kambe, K. Kaneko, Y. Kuramoto, T. D. Matsuda, N. Metoki, A. Nakamura, Y. Ōnuki, H. Sakai, Y. Shiokawa, N. Tateiwa, Y. Tokunaga, R. E. Walstedt, E. Yamamoto, and H. Yasuoka for useful discussions on *f*-electron materials.

The work on manganites was supported by the Ministry of Education, Science, Sports, and Culture of Japan during my stay in the National High Magnetic Field

Laboratory, Florida State University. The author was supported by the Grant-in-Aid for Encouragement of Young Scientists under the contract Nos. 12740230 and 14740219 from the Ministry of Education, Culture, Sports, Science, and Technology (MEXT) of Japan. The work on *f*-electron systems has been also supported by a Grant-in-Aid for Scientific Research in Priority Area “Skutterudites” under the contract Nos. 16037217 and 18027016 from the MEXT. The author has been partly supported by a Grant-in-Aid for Scientific Research (C)(2) under the contract No. 16540316 from Japan Society for the Promotion of Science.

References

- [1] Imada M, Fujimori A and Tokura Y 1998 *Rev. Mod. Phys.* **70** 1039
- [2] Tokura Y and Nagaosa N 2000 *Science* **288** 462
- [3] Dagotto E, Hotta T and Moreo A 2001 *Phys. Rep.* **344** 1
- [4] Hotta T and Dagotto E 2004 *Colossal Magnetoresistive Manganites* ed Chatterji T K (Amsterdam: Kluwer) pp 207-262
- [5] Tokura Y 2000 *Colossal Magnetoresistance Oxides* ed Tokura Y (New York: Gordon & Breach) pp 1-52
- [6] Dagotto E 2002 *Nanoscale Phase Separation and Colossal Magnetoresistance* (Berlin: Springer)
- [7] Zener C 1951 *Phys. Rev.* **82** 403
- [8] Wollan E O and Koehler W C 1955 *Phys. Rev.* **100** 545
- [9] Matsumoto G 1970 *J. Phys. Soc. Japan* **29** 606
- [10] Murakami Y, Hill J P, Gibbs D, Blume M, Koyama I, Tanaka M, Kawata H, Arima T, Tokura Y, Hirota K and Endoh Y 1988 *Phys. Rev. Lett.* **81** 582
- [11] Mizokawa T and Fujimori A 1995 *Phys. Rev. B* **51** 12880
- [12] Mizokawa T and Fujimori A 1996 *Phys. Rev. B* **54** 5368
- [13] Solovyev I, Hamada N and Terakura K 1996 *Phys. Rev. Lett.* **76** 4825
- [14] Solovyev I, Hamada N and Terakura K 1996 *Phys. Rev. B* **53** 7158
- [15] Koshibae W, Kawamura Y, Ishihara S, Okamoto S, Inoue J and Maekawa S 1997 *J. Phys. Soc. Japan* **66** 957
- [16] Shiina R, Nishitani T and Shiba H 1997 *J. Phys. Soc. Japan* **66** 3159
- [17] Ishihara S, Inoue J and Maekawa S 1997 *Phys. Rev. B* **55** 8280
- [18] Sawada H, Morikawa Y, Terakura K and Hamada N 1997 *Phys. Rev. B* **56** 12154
- [19] Feinberg D, Germain P, Grilli M and Seibold G 1998 *Phys. Rev. B* **57** R5583
- [20] Maezono R, Ishihara S and Nagaosa N 1998 *Phys. Rev. B* **57** R13993
- [21] Feiner L F and Oleś A M 1999 *Phys. Rev. B* **59** 3295
- [22] Horsch P, Jaklič J and Mack F 1999 *Phys. Rev. B* **59** 6217
- [23] van den Brink J, Horsch P, Mack F and Oleś A M 1999 *Phys. Rev. B* **59** 6795
- [24] Benedetti P and Zeyher R 1999 *Phys. Rev. B* **59** 9923
- [25] Hotta T, Yunoki S, Mayr M and Dagotto E 1999 *Phys. Rev. B* **60** R15009
- [26] Allen P B and Perebeinos V 1999 *Phys. Rev. B* **60** 10747
- [27] Capone M, Feinberg D and Grilli M 2000 *Euro. Phys. J. B* **17** 103
- [28] Muñoz A, Casáis M T, Alonso J A, Martínez-Lope M J, Martínez J L and Fernández-Díaz M T 2001 *Inorg. Chem.* **40** 1020
- [29] Kimura T, Ishihara S, Takahashi K T, Shintani H and Tokura Y 2003 *Phys. Rev. B* **68** 060403
- [30] Hotta T, Moraghebi M, Feiguin A, Moreo A, Yunoki S and Dagotto E 2003 *Phys. Rev. Lett.* **90** 247203
- [31] Hotta T 2003 *Phys. Rev. B* **67** 104428
- [32] Yunoki S, Hotta T and Dagotto E 2000 *Phys. Rev. Lett.* **84** 3714

- [33] Hotta T, Feiguin A and Dagotto E 2001 *Phys. Rev. Lett.* **86** 4922
- [34] Loudon J C, Mathur N D and Midgley P A 2002 *Nature* **420** 797
- [35] Mathur N D and Littlewood P 2003 *Physics Today* **56** 25
- [36] Fiebig M 2005 *J. Phys. D: Appl. Phys.* **38** R123
- [37] Santini P, Lémanski R and Erdős P 1999 *Adv. Phys.* **48** 537
- [38] *Proceedings of the International Conference on Strongly Correlated Electrons with Orbital Degrees of Freedom* ed Hirota K, Aoki H and Kuramoto Y 2002 *J. Phys. Soc. Japan* **71** (Suppl.)
- [39] Hegger H, Petrovic C, Moshopoulou E G, Hundley M F, Sarrao J L, Fisk Z and Thompson J D 2000 *Phys. Rev. Lett.* **84** 4986
- [40] Petrovic C, Movshovich R, Jaime M, Pagliuso P G, Hundley M F, Sarrao J L, Fisk Z and Thompson J D 2001 *Europhys. Lett.* **53** 354
- [41] Petrovic C, Pagliuso P G, Hundley M F, Movshovich R, Sarrao J L, Thompson J D, Fisk Z and Monthoux P 2001 *J. Phys.: Condens. Matter* **13** L337
- [42] Sarrao J L, Morales L A, Thompson J D, Scott B L, Stewart G R, Wastin F, Rebizant J, Boulet P, Colineau E and Lander G H 2002 *Nature* **420** 297
- [43] Sarrao J L, Thompson J D, Moreno N O, Morales L A, Wastin F, Rebizant J, Boulet P, Colineau E and Lander G H 2003 *J. Phys.: Condens. Matter* **15** S2275
- [44] Wastin F, Boulet P, Rebizant J, Colineau E and Lander G H 2003 *J. Phys.: Condens. Matter* **15** S2279
- [45] Haga Y, Aoki D, Matsuda T D, Nakajima K, Arai Y, Yamamoto E, Nakamura A, Homma Y, Shiokawa Y and Ōnuki Y 2005 *J. Phys. Soc. Japan* **74** 1698
- [46] Sakai H, Tokunaga Y, Fujimoto T, Kambe S, Walstedt R E, Yasuoka H, Aoki D, Homma Y, Yamamoto E, Nakamura A, Shiokawa Y, Nakajima K, Arai Y, Matsuda T D, Haga Y and Ōnuki Y 2005 *J. Phys. Soc. Japan* **74** 1710
- [47] Curro N J, Caldwell T, Bauer E D, Morales L A, Graf M J, Bang Y, Balatsky A V, Thompson J D and Sarrao J L 2005 *Nature* **434** 622
- [48] Griveau J C, Boulet P, Colineau E, Wastin F and Rebizant J 2005 *Physica B* **359-361** 1093
- [49] Grin Y N, Rogl P and Hiebl K 1986 *J. Less-Common Met.* **121** 497
- [50] Sechovský V, Havela L, Schaudy G, Hilscher G, Pillmayr N, Rogl P and Fischer P 1992 *J. Magn. Mater.* **104-107** 11
- [51] Noguchi S and Okuda K 1992 *J. Magn. Mater.* **104-107** 57
- [52] Okuda K and Noguchi S 1993 *Physical Properties of Actinide and Rare Earth Compounds*, ed Kasuya T, Ishii T, Komatsubara T, Sakai S, Mōri N and Saso T, JJAP Series 8 (Tokyo: JJAP Publication Office) p 32
- [53] Ōnuki Y, Aoki D, Wiśniewski P, Shishido H, Ikeda S, Inada Y, Settai R, Tokiwa Y, Yamamoto E, Haga Y, Maehira T, Harima H, Higuchi M, Hasegawa A and Yamagami H 2001 *Acta Phys. Pol.* **B32** 3273
- [54] Tokiwa Y, Haga Y, Yamamoto E, Aoki D, Watanabe N, Settai R, Inoue T, Kindo K, Harima H and Ōnuki Y 2001 *J. Phys. Soc. Japan* **70** 1744
- [55] Tokiwa Y, Maehira T, Ikeda S, Haga Y, Yamamoto E, Nakamura A, Ōnuki Y, Higuchi M and Hasegawa A 2001 *J. Phys. Soc. Japan* **70** 2982
- [56] Tokiwa Y, Haga Y, Metoki N, Ishii Y and Ōnuki Y 2002 *J. Phys. Soc. Japan* **71** 725
- [57] Tokiwa Y, Ikeda S, Haga Y, Ōkubo T, Iizuka T, Sugiyama K, Nakamura A and Ōnuki Y 2002 *J. Phys. Soc. Japan* **71** 845
- [58] Kato H, Sakai H, Tokiwa Y, Kambe S, Walstedt R E and Ōnuki Y 2002 *J. Phys. Chem. Solids* **63** 1197
- [59] Ikeda S, Tokiwa Y, Haga Y, Yamamoto E, Ōkubo T, Yamada M, Nakamura N, Sugiyama K, Kindo K, Inada Y, Yamagami H and Ōnuki Y 2003 *J. Phys. Soc. Japan* **72** 576
- [60] Kaneko K, Metoki N, Bernhoeft N, Lander G H, Ishii Y, Ikeda S, Tokiwa Y, Haga Y and Ōnuki Y 2003 *Phys. Rev. B* **68** 214419
- [61] Colineau E, Javorský P, Boulet P, Wastin F, Griveau J C, Rebizant J, Sanchez J P and Stewart

- G R 2004 *Phys. Rev. B* **69** 184411
- [62] Aoki D, Yamamoto E, Homma Y, Shiokawa Y, Nakamura A, Haga Y, Settai R and Ōnuki Y 2004 *J. Phys. Soc. Japan* **73** 519
- [63] Aoki D, Homma Y, Shiokawa Y, Yamamoto E, Nakamura A, Haga Y, Settai R, Takeuchi T and Ōnuki Y 2004 *J. Phys. Soc. Japan* **73** 1665
- [64] Aoki D, Homma Y, Shiokawa Y, Yamamoto E, Nakamura A, Haga Y, Settai R and Ōnuki Y 2004 *J. Phys. Soc. Japan* **73** 2608
- [65] Aoki D, Yamagami H, Homma Y, Shiokawa Y, Yamamoto E, Nakamura A, Haga Y, Settai R and Ōnuki Y 2005 *J. Phys.: Condens. Matter* **17** L169
- [66] Honda F, Metoki N, Kaneko K, Aoki D, Homma Y, Yamamoto E, Shiokawa Y, Ōnuki Y, Colineau E, Bernhoft N and Lander G H 2005 *Physica B* **359-161** 1147
- [67] Yamamoto E, Aoki D, Homma Y, Shiokawa Y, Haga Y, Nakamura A and Ōnuki Y 2005 *Physica B* **359-161** 1099
- [68] Homma Y, Nasu S, Aoki D, Kaneko K, Metoki N, Yamamoto E, Nakamura A, Morimoto S, Yasuoka H, Ōnuki Y and Shiokawa Y 2005 *Physica B* **359-161** 1105
- [69] Metoki N, Kaneko K, Colineau E, Javorský P, Aoki D, Homma Y, Boulet P, Wastin F, Shokawa Y, Bernhoeft N, Yamamoto E, Ōnuki Y, Rebizant J and Lander G H 2005 *Phys. Rev. B* **72** 014460
- [70] Jonen S, Metoki N, Honda F, Kaneko K, Yamamoto E, Haga Y, Aoki D, Homma Y, Shiokawa Y and Ōnuki Y 2005 *Preprint*
- [71] Haga Y, Aoki D, Yamagami H, Matsuda T D, Nakajima K, Arai Y, Yamamoto E, Nakamura A, Homma Y, Shiokawa Y and Ōnuki Y 2005 *J. Phys. Soc. Japan* **74** 2889
- [72] Hotta T and Ueda K 2003 *Phys. Rev. B* **67** 104518
- [73] Hotta T and Ueda K 2003 *Acta Phys. Pol. B* **34** 443
- [74] Maehira T, Takimoto T, Hotta T, Ueda K, Higuchi M and Hasegawa A 2002 *J. Phys. Soc. Japan Suppl.* **71** 285
- [75] Maehira T, Hotta T, Takimoto T, Ueda K and Hasegawa A 2003 *Acta Phys. Pol. B* **34** 1023
- [76] Maehira T, Hotta T, Ueda K and Hasegawa A 2003 *Phys. Rev. Lett.* **90** 207007
- [77] Maehira T, Hotta T, Ueda K and Hasegawa A 2003 *J. Phys. Soc. Japan* **72** 854
- [78] Maehira T, Higuchi M and Hasegawa A 2003 *Physica B* **329-333** 574
- [79] Maehira T, Higuchi M and Hasegawa A 2003 *J. Phys.: Condens. Matter* **15** S2237
- [80] Maehira T, Hotta T, Ueda K and Hasegawa A 2006 *New J. Phys.* **8** 24
- [81] Maehira T and Hotta T *Preprint cond-mat/0507401*
- [82] Hotta T 2004 *Phys. Rev. B* **70** 054405
- [83] Onishi H and Hotta T 2004 *New J. Phys.* **6** 193
- [84] Takimoto T, Hotta T, Maehira T and Ueda K 2002 *J. Phys.: Condens. Matter* **14** L369
- [85] Takimoto T, Hotta T and Ueda K 2003 *J. Phys.: Condens. Matter* **15** S2087
- [86] Takimoto T, Hotta T and Ueda K 2004 *Phys. Rev. B* **69** 104504
- [87] Hotta T and Ueda K 2004 *J. Magn. Magn. Mater.* **272-276** e191
- [88] Hotta T and Ueda K 2004 *Phys. Rev. Lett.* **92** 107007
- [89] Sato H, Sugawara H, Namiki T, Saha S R, Osaki S, Matsuda T D, Aoki Y, Inada Y, Shishido H, Settai R and Ōnuki Y 2003 *J. Phys.: Condens. Matter* **15** S2063
- [90] Aoki Y, Sugawara H, Harima H and Sato H 2005 *J. Phys. Soc. Japan* **74** 209
- [91] Hotta T 2005 *Physica B* **359-361** 1003
- [92] Hotta T 2005 *Phys. Rev. Lett.* **94** 067003
- [93] Hotta T 2005 *J. Phys. Soc. Japan* **74** 1275
- [94] Hotta T 2005 *J. Phys. Soc. Japan* **74** 2425
- [95] Kuramoto Y and Kusunose H 2000 *J. Phys. Soc. Japan* **69** 671
- [96] Kusunose H and Kuramoto Y 2001 *J. Phys. Soc. Japan* **70** 1751
- [97] Sakakibara T, Tayama T, Tenya K, Yokoyama M, Amitsuka H, Aoki D, Ōnuki Y, Kletowski Z and Kunii S 2002 *J. Phys. Chem. Solids* **63** 1147 (2002)

- [98] Sakakibara T, Tenya K and Kunii S 2002 *Physica B* **312-313** 194
- [99] Morie T, Sakakibara T, Tayama T and Kunii S 2004 *J. Phys. Soc. Japan* **73** 2381
- [100] Kubo K and Kuramoto Y 2003 *J. Phys. Soc. Japan* **72** 1859
- [101] Kubo K and Kuramoto Y 2004 *J. Phys. Soc. Japan* **73** 216
- [102] Kobayashi S, Yoshino Y, Tsuji S, Tou H, Sera M and Iga F 2003 *J. Phys. Soc. Japan* **72** 2947
- [103] Iwasa K, Kuwahara K, Kohgi M, Fischer P, Dönni A, Keller L, Hansen T C, Kunii S, Metoki N, Koike Y and Ohoyama K 2003 *Physica B* **329-333** 582
- [104] Suzuki O, Nakamura S, Akatsu M, Nemoto Y, Goto T and Kunii S 2005 *J. Phys. Soc. Japan* **74** 735
- [105] Santini P and Amoretti G 2000 *Phys. Rev. Lett.* **85** 2188
- [106] Santini P and Amoretti G 2002 *J. Phys. Soc. Japan* **71** (Suppl.) 11
- [107] Paixão J A, Detlefs C, Longfield M J, Caciuffo R, Santini P, Bernhoeft N, Rebizant J and Lander G H 2003 *Phys. Rev. Lett.* **89** 187202
- [108] Caciuffo R, Paixão J A, Detlefs C, Longfield M J, Santini P, Bernhoeft N, Rebizant J and Lander G H 2003 *J. Phys.: Condens. Matter* **15** S2287
- [109] Lovesey S W, Balcar E, Detlefs C, van der Laan G, Sivia D S and Staub U 2003 *J. Phys.: Condens. Matter* **15**, 4511 (2003).
- [110] Kiss A and Fazekas P 2003 *Phys. Rev. B* **68** 174425
- [111] Tokunaga Y, Homma Y, Kambe S, Aoki D, Sakai H, Yamamoto E, Nakamura A, Shiokawa Y, Walstedt R E and Yasuoka H 2005 *Phys. Rev. Lett.* **94** 137209
- [112] Sakai O, Shiina R and Shiba H 2005 *J. Phys. Soc. Japan* **74** 457
- [113] Kubo K and Hotta T 2005 *Phys. Rev. B* **71** 140404(R)
- [114] Yoshizawa M, Nakanishi Y, Oikawa M, Sekine C, Shirotani I, Saha S R, Sugawara H and Sato H 2005 *J. Phys. Soc. Japan* **74** 2141
- [115] Hachitani K, Fukazawa H, Kohori Y, Watanabe I, Sekine C and Shirotani I 2006 *Phys. Rev. B* **73** 052408
- [116] Kubo K and Hotta T 2005 *Phys. Rev. B* **72** 144401
- [117] Kubo K and Hotta T 2005 *Phys. Rev. B* **72** 132411
- [118] Kubo K and Hotta T 2005 *Preprint cond-mat/0506041*
- [119] Kubo K and Hotta T 2005 *Preprint cond-mat/0512649*
- [120] Hutchings M T 1964 *Solid State Phys.* **16** 227
- [121] We refer the following literature written in Japanese. Kamimura H, Sugano S and Y Tanabe 1969 *Ligand Field Theory and Its Application* (Tokyo: Shokabo)
- [122] Gaunt J A 1929 *Phil. Trans. Roy. Soc.* **A228** 195
- [123] Racah G 1942 *Phys. Rev.* **62** 438
- [124] Slater J C 1960 *Theory of Atomic Structure* (New York: McGraw-Hill)
- [125] Yoshida K 1996 *Theory of Magnetism* (Berlin: Springer)
- [126] Slater J C 1929 *Phys. Rev.* **34** 1293
- [127] Condon E U and Shortley G H 1931 *Phys. Rev.* **37** 1025
- [128] Tang H, Plihal M and Mills D L 1998 *J. Magn. Magn. Mater.* **187** 23
- [129] Kanamori J 1963 *Prog. Theor. Phys.* **30** 275
- [130] Yunoki S, Hu J, Malvezzi A L, Moreo A, Furukawa N and Dagotto E 1998 *Phys. Rev. Lett.* **80** 845
- [131] Dagotto E, Yunoki S, Malvezzi A L, Moreo A, Hu J, Capponi S, Poilblanc D and Furukawa N 1998 *Phys. Rev.* **B58** 6414
- [132] Kanamori J 1960 *J. Appl. Phys. Suppl.* **31** 14S
- [133] Jahn H A and Teller E 1937 *Proc. Roy. Soc. London A* **161** 220
- [134] Struge M D 1967 *Solid State Phys.* **20** 91
- [135] Slater J C and Koster G F 1954 *Phys. Rev.* **94** 1498
- [136] Cieplak M 1978 *Phys. Rev. B* **18** 3470
- [137] Anderson P W and Hasegawa H 1955 *Phys. Rev.* **100** 675

- [138] Biedenharn L C, Blatt J M and Rose M E 1952 *Rev. Mod. Phys.* **24** 249
- [139] Goodenough J 1955 *Phys. Rev.* **100** 564
- [140] Müller-Hartmann E and Dagotto E 1996 *Phys. Rev.* B**54** R6819
- [141] Hotta T, Takada Y, Koizumi H and Dagotto E 2000 *Phys. Rev. Lett.* **84** 2477
- [142] van den Brink J, Khaliullin G and Khomskii D 1999 *Phys. Rev. Lett.* **83** 5118
- [143] Solovyev I V and Terakura K 1999 *Phys. Rev. Lett.* **83** 2825
- [144] Solovyev I V 2001 *Phys. Rev. B* **63** 174406
- [145] Longuet-Higgins H C, Öpik U, Pryce M H L and Sack R A 1958 *Proc. Roy. Soc.* **A244** 1
- [146] Ham F S 1987 *Phys. Rev. Lett.* **58** 725
- [147] Koizumi H, Hotta T and Takada Y 1998 *Phys. Rev. Lett.* **80** 4518
- [148] Koizumi H, Hotta T and Takada Y 1998 *Phys. Rev. Lett.* **81** 3803
- [149] Hotta T, Takada Y and Koizumi H 1998 *Int. J. Mod. Phys. B* **12** 3437
- [150] Wilczek F and Zee A 1984 *Phys. Rev. Lett.* **52** 2111
- [151] Takada Y, Hotta T and Koizumi H 1999 *Int. J. Mod. Phys. B* **13** 3778
- [152] Iliev M N, Abrashev M V, Lee H -G, Popov V N, Sun Y Y, Thomsen C, Meng R L and Chu C W *Phys. Rev. B* **57** 2872
- [153] Alonso J L, Fernández L A, Guinea F, Laliena V and Martín-Mayor V 2001 *Nucl. Phys. B* **596** 587
- [154] Motome Y and Furukawa N 1999 *J. Phys. Soc. Japan* **68** 3853
- [155] Motome Y and Furukawa N 2000 *J. Phys. Soc. Japan* **69** 3785
- [156] Hotta T, Malvezzi A L and Dagotto E 2000 *Phys. Rev. B* **62** 9432
- [157] Betouras J J and Fujimoto S 1999 *Phys. Rev. B* **59** 529
- [158] Yi H, Yu J and Lee S I 2000 *Phys. Rev. B* **61** 428
- [159] Maezono R, Ishihara S and Nagaosa N 1998 *Phys. Rev. B* **58** 11583
- [160] Efremov D V and Khomskii D I 2005 *Phys. Rev. B* **72** 012402
- [161] Kugel K I and Khomskii D I 1974 *Sov. Phys. JETP* **37** 725
- [162] Salafranca J and Brey L 2006 *Phys. Rev. B* **73** 024422
- [163] Hotta T 2005 *Progress in Ferromagnetism Research* Ed Murray V N (Nova Science Publishers Inc.: New York) pp 19-38
- [164] Hotta T, Takada Y, Koizumi H and Dagotto E 2000 *Phys. Rev. Lett.* **85** 2478
- [165] Moreo A, Mayr M, Feiguin A, Yunoki S and Dagotto E 2000 *Phys. Rev. Lett.* **84** 5568
- [166] Alonso J L, Fernández L A, Guinea F, Laliena V and Martín-Mayor V 2001 *Phys. Rev. B* **63** 64416
- [167] Alonso J L, Fernández L A, Guinea F, Laliena V and Martín-Mayor V 2001 *Phys. Rev. B* **63** 054411
- [168] Arima T and Tokura Y 1995 *J. Phys. Soc. Japan* **64** 2488
- [169] Mathieu R, Svedlindh P and Nordblad P 2000 *Europhys. Lett.* **52** 441
- [170] Mizokawa T and Fujimori A 1997 *Phys. Rev. B* **56** R493
- [171] Lee J D and Min B I 1997 *Phys. Rev. B* **55** R14713
- [172] Jackeli G, Perkins N B and Plakida N M 2000 *Phys. Rev. B* **62** 372
- [173] Anisimov V I, Elfimov I S, Korotin M A and Terakura K 1997 *Phys. Rev. B* **55** 15494
- [174] Mori S, Chen C H and Cheong S -W 1998 *Nature* **392** 473
- [175] Mori S, Chen C H and Cheong S -W 1998 *Phys. Rev. Lett.* **81** 3972
- [176] Kajimoto R, Yoshizawa H, Kawano H, Kuwahara H, Tokura Y, Ohoyama K and Ohashi M 1999 *Phys. Rev. B* **60** 9506
- [177] Radaelli P G, Cox D E, Capogna L, Cheong S -W and Marezio M 1999 *Phys. Rev. B* **59** 14440
- [178] Kimura T, Hatsuda K, Ueno Y, Kajimoto R, Mochizuki H, Yoshizawa H, Nagai T, Matsui Y, Yamazaki A and Tokura Y 2002 *Phys. Rev. B* **65** 020407(R)
- [179] Hotta T, Dagotto E, Koizumi H and Takada Y 2000 *Int. J. Mod. Phys. B* **14** 3494
- [180] Mizokawa T, Khomskii D I and Sawatzky G A 2000 *Phys. Rev. B* **61** R3776
- [181] Korotin M, Fujiwara T and Anisimov V 2000 *Phys. Rev. B* **62** 5696

- [182] Hotta T and Dagotto E 2000 *Phys. Rev. B* **61** R11879
- [183] Adams C P, Lynn J W, Mukovskii Y M, Arsenov A A and Shulyatev D A 2000 *Phys. Rev. Lett.* **85** 3954
- [184] Dai P, Fernandez-Baca J A, Wakabayashi N, Plummer E W, Tomioka Y and Tokura Y 2000 *Phys. Rev. Lett.* **85** 2553
- [185] Kubota M, Oohara Y, Yoshizawa H, Fujioka H, Shimizu K, Hirota K, Moritomo Y and Endoh Y 2000 *J. Phys. Soc. Japan* **69** 1986
- [186] Vasiliu-Doloc L, Rosenkranz S, Osborn R, Sinha S K, Lynn J W, Mesot J, Seeck O H, Preosti G, Fedro A J and Mitchell J F 1999 *Phys. Rev. Lett.* **83** 4393
- [187] Buhler C, Yunoki S and Moreo A 2000 *Phys. Rev. Lett.* **84** 2690
- [188] Moritomo Y, Tomioka Y, Asamitsu A, Tokura Y and Matsui Y 1995 *Phys. Rev. B* **51** 3297
- [189] Tranquada J M, Sternlieb B, Axe J D, Nakamura Y and Uchida S 1995 *Nature* **375** 561
- [190] Mook H A, Dai P, Hayden S M, Aeppli G, Perring T G and Dogan F 1998 *Nature* **395** 580
- [191] Cheong S -W, Aeppli G, Mason T E, Mook H, Hayden S M, Canfield P C, Fisk Z, Clausen K N and Martinez J L 1991 *Phys. Rev. Lett.* **67** 1791
- [192] Mason T E, Aeppli G and Mook H A 1992 *Phys. Rev. Lett.* **68** 1414
- [193] Thurston T R, Gehring P M, Shirane G, Birgeneau R J, Kastner M A, Endoh Y, Matsuda M, Yamada K, Kojima H and Tanaka I 1992 *Phys. Rev. B* **46** 9128
- [194] Yamada K, Lee C H, Kurahashi K, Wada J, Wakimoto S, Ueki S, Kimura H, Endoh Y, Hosoya S, Shirane G, Birgeneau R J, Greven M, Kastner M A and Kim Y J 1998 *Phys. Rev. B* **57** 6165
- [195] Matsuda M, Fujita M, Yamada K, Birgeneau R J, Endoh Y and Shirane G 2003 *Phys. Rev. B* **65** 134515
- [196] Tranquada J M, Buttrey D J, Sachan V and Lorenzo J E 1994 *Phys. Rev. Lett.* **73** 1003
- [197] Sachan V, Buttrey D J, Tranquada J M, Lorenzo J E and Shirane G 1995 *Phys. Rev. B* **51** 12742
- [198] Yoshizawa H, Kakeshita T, Kajimoto R, Tanabe T, Katsufuji T and Tokura Y 2000 *Phys. Rev. B* **61** R854
- [199] Kajimoto R, Ishizuka K, Yoshizawa H and Tokura Y 2003 *Phys. Rev. B* **67** 014511
- [200] Emery V J, Kivelson S A and Zachar O 1997 *Phys. Rev. B* **56** 6120
- [201] Malvezzi A L and Dagotto E 2001 *Phys. Rev.* **63** 140409
- [202] Hotta T and Dagotto E 2004 *Phys. Rev. Lett.* **92** 227201
- [203] Murakami Y, Kawada H, Kawata H, Tanaka M, Arima T, Moritomo Y and Tokura Y 1998 *Phys. Rev. Lett.* **80** 1932
- [204] Boothroyd A T, Freeman P G, Prabhakaran D, Hiess A, Enderle M, Kulda J and Altorfer 2003 *Phys. Rev. Lett.* **91** 257201
- [205] Tranquada J M, Lorenzo J E, Buttrey D J and Sachan V 1995 *Phys. Rev. B* **52** 3581
- [206] Takada K, Sakurai H, Takayama-Muromachi E, Izumi F, Dilanian R A and Sasaki T 2003 *Nature* **422** 53
- [207] Onishi H and Hotta T 2004 *Phys. Rev. B* **70** 100402(R)
- [208] Xavier J C, Onishi H, Hotta T and Dagotto E 2006 *Phys. Rev. B* **73** 014405
- [209] Maeno Y, Hashimoto H, Yoshida K, Nishizaki S, Fujita T, Bednorz J G and Lichtenberg F 1994 *Nature* **372** 532
- [210] Nakatsuji S and Maeno Y 2000 *Phys. Rev. Lett.* **84** 2666
Cao G, McCall S, Shepard M, Crow J E and Guertin R P 1997 *Phys. Rev. B* **56** R2916
- [211] Nakatsuji S, Ikeda S and Maeno Y 1997 *J. Phys. Soc. Japan* **66** 1868
- [212] Braden M, André G, Nakatsuji S and Maeno Y 1998 *Phys. Rev. B* **58** 847
- [213] Mizokawa T, Tjeng L H, Sawatzky G A, Ghiringhelli G, Tjernberg O, Brooks N B, Fukazawa H, Nakatsuji S and Maeno 2001 *Phys. Rev. Lett.* **87** 077202
- [214] Hotta T and Dagotto E 2002 *Phys. Rev. Lett.* **88** 017201
- [215] Anisimov V I, Nekrasov I A, Kondakov D E, Rice T M and Sigrist M 2002 *Eur. Phys. J. B* **25** 191

- [216] Fang Z, Nagaosa N and Terakura K 2004 *Phys. Rev. B* **69** 045116
- [217] Jung J H, Fang Z, He J P, Kaneko Y, Okimoto Y and Tokura Y 2003 *Phys. Rev. Lett.* **91** 056403
- [218] Kubota M, Murakami Y, Mizumaki M, Ohsumi H, Ikeda N, Nakatsuji S, Fukazawa H and Maeno Y 2005 *Phys. Rev. Lett.* **95** 026401
- [219] Zegkinoglou I, Strempler J, Nelson C S, Hill J P, Chakhalian J, Bernhard C, Lang J C, Srajer G, Fukazawa H, Nakatsuji S, Maeno Y and Keimer B 2005 *Phys. Rev. Lett.* **95** 136401
- [220] *Magnetic Systems with Competing Interaction* 1994 ed Diep H T (World Scientific: Singapore)
- [221] Majumdar C K and Ghosh D K 1969 *J. Math. Phys.* **10** 1388
- [222] Tonegawa T and Harada I 1987 *J. Phys. Soc. Japan* **56** 2153
- [223] Okamoto K and Nomura K 1992 *Phys. Lett. A* **169** 433
- [224] White S R and Affleck I 1996 *Phys. Rev. B* **54** 9862
- [225] Tsunetsugu H and Motome Y 2003 *Phys. Rev. B* **68** 060405(R)
- [226] Motome Y and Tsunetsugu H 2004 *Phys. Rev. B* **70** 184427
- [227] Lee S -H, Louca D, Ueda H, Park S, Sato T J, Isobe M, Ueda Y, Rosenkranz S, Zschack P, Íñiguez I, Qiu Y and Osborn R 2004 *Phys. Rev. Lett.* **93** 156407
- [228] Di Matteo S, Jackeli G, Lacroix C and Perkins N B 2004 *Phys. Rev. Lett.* **93** 077208
- [229] Khomskii D and Mizokawa T 2005 *Phys. Rev. Lett.* **94** 156402
- [230] Onishi H and Hotta T 2005 *Phys. Rev. B* **71** 180410(R)
- [231] Onishi H and Hotta T 2005 *Physica B* **359-361** 669
- [232] Onishi H and Hotta T 2005 *Preprint* cond-mat/0506242
- [233] Onishi H and Hotta T 2005 *Preprint* cond-mat/0508414
- [234] White S R 1992 *Phys. Rev. Lett.* **69** 2863
- [235] White S R 1993 *Phys. Rev. B* **48** 10345
- [236] Liang S and Pang H 1994 *Phys. Rev. B* **49** 9214
- [237] Laukamp M, Martins G B, Gazza C, Malvezzi A L, Dagotto E, Hansen P M, López A C and Riera J 1998 *Phys. Rev. B* **57** 10755
- [238] Nishino M, Onishi H, Roos P, Yamaguchi K and Miyashita S 2000 *Phys. Rev. B* **61** 4033
- [239] Barnes T, Dagotto E, Riera J and Swanson E S 1994 *Phys. Rev. B* **47** 3196
- [240] Greven M, Birgeneau R J and Wiese U -J 1996 *Phys. Rev. Lett.* **77** 1865
- [241] Onishi H and Hotta T *Preprint* cond-mat/0604076
- [242] Burns G 1977 *Introduction to Group Theory with Applications* (New York: Academic Press)
- [243] Hotta T and Harima H *Preprint* cond-mat/0602646
- [244] Norman M R 1994 *Phys. Rev. B* **50** 6904
- [245] Inglis D R 1931 *Phys. Rev.* **38** 862
- [246] Knafo W, Raymond S, Fak B, Lapertot G, Canfield P C and Flouquet J 2003 *J. Phys.: Condens. Matter* **15** 3741
- [247] Buschow K H J, de Wijn H W and van Diepen A M 1969 *J. Chem. Phys.* **50** 137
- [248] Groß W, Knorr K, Murani A P and Buschow K H J 1977 *Crystal Field Effects in Metals and Alloys* ed Furrer A (New York: Plenum) p 37
- [249] Czopnik A, Kowalewski J and Hackemer M 1991 *Phys. Status Solidi A* **127** 243
- [250] Amara M, Morin P and Rouchy J 1994 *J. Magn. Magn. Mater.* **130** 115
- [251] Amara M, Galéra R M, Morin P, Veres T and Burlet P 1994 *J. Magn. Magn. Mater.* **130** 127
- [252] Sera M and Kobayashi S 1999 *J. Phys. Soc. Japan* **68** 664
- [253] Loewenhaupt M and Prager M 1986 *Z. Phys. B* **62** 195
- [254] Kobayashi S, Sera M, Hiroi M, Nishizaki T, Kobayashi N and Kunii S 2001 *J. Phys. Soc. Japan* **70** 1721
- [255] Pofahl G, Zirngiebl E, Blumenröder S, Brenten H, Güntherodt G and Winzer K 1987 *Z. Phys. B* **66** 339
- [256] Uimin G and Brenig W 2000 *Phys. Rev. B* **61** 60
- [257] Kubo K and Kuramoto Y 2003 *J. Phys.: Condens. Matter* **15** S2251
- [258] Lea K R, Leask M J M and Wolf W P 1962 *J. Phys. Chem. Solids* **23** 1381

- [259] Takegahara K, Aoki Y and Yanase A 1980 *J. Phys. C, Solid St. Phys.* **13** 583
- [260] Sharma R R 1979 *Phys. Rev. B* **19** 2813
- [261] Dervenagas P, Kaczorowski D, Bourdarot F, Burlet P, Czopnik A and Lander G H 1999 *Physica B* **269** 368
- [262] Mannix D, Stunault A, Bernhoeft N, Paolasini L, Lander G H, Vettier C, de Bergevin F, Kaczorowski D and Czopnik A 2001 *Phys. Rev. Lett.* **86** 4128
- [263] Colineau E, Bourdarot F, Burlet P, Sanchez J P and Larroque J 1997 *Physica B* **230-232** 773
- [264] Betsuyaku K and Harima H 2004 *J. Magn. Magn. Mater.* **272-276** 187
- [265] Harima H 2003 private communications
- [266] Onishi H and Hotta T *Preprint cond-mat/0511276*
- [267] Shiina R, Shiba H and Thalmeier P 1997 *J. Phys. Soc. Japan* **66** 1741
- [268] Kern S, Loong C -K and Lander G H 1985 *Phys. Rev. B* **32** 3051
- [269] Amoretti G, Blaise A, Caciuffo R, Fournier J M, Hutchings M T, Osborn R and Taylor A D 1989 *Phys. Rev. B* **40** 1856
- [270] Fournier J M, Blaise A, Amoretti G, Caciuffo R, Larroque J, Hutchings M T, Osborn R and Taylor A D 1991 *Phys. Rev. B* **43** 1142
- [271] Amoretti G, Blaise A, Caciuffo R, Cola D Di, Fournier J M, Hutchings M T, Lander G H, Osborn R, Severing A and Taylor A D 1992 *J. Phys.: Condens. Matter* **4** 3459
- [272] Kern S, Loong C -K, Goodman G L, Cort B and Lander G H 1990 *J. Phys.: Condens. Matter* **2** 1933
- [273] Kern S, Robinson R A, Nakotte H, Lander G H, Cort B, Watson P and Vigil F A 1999 *Phys. Rev.* **59** 104
- [274] Sakai O, Shiina R and Shiba H 2003 *J. Phys. Soc. Japan* **72** 1534
- [275] Arrott A and Goldman J E 1957 *Phys. Rev.* **108** 948
- [276] Ross J W and Lam D J 1967 *J. Appl. Phys.* **38** 1451
- [277] Erdös P, Solt G, Zolnierok Z, Blaise A and Fournier J M 1980 *Physica* **102B** 164
- [278] Kubo K and Hotta T 2006 *J. Phys. Soc. Japan* **75** 013702